ORF
3TC
2.1.25

BELLCOMM INC.

NASA CR 70713

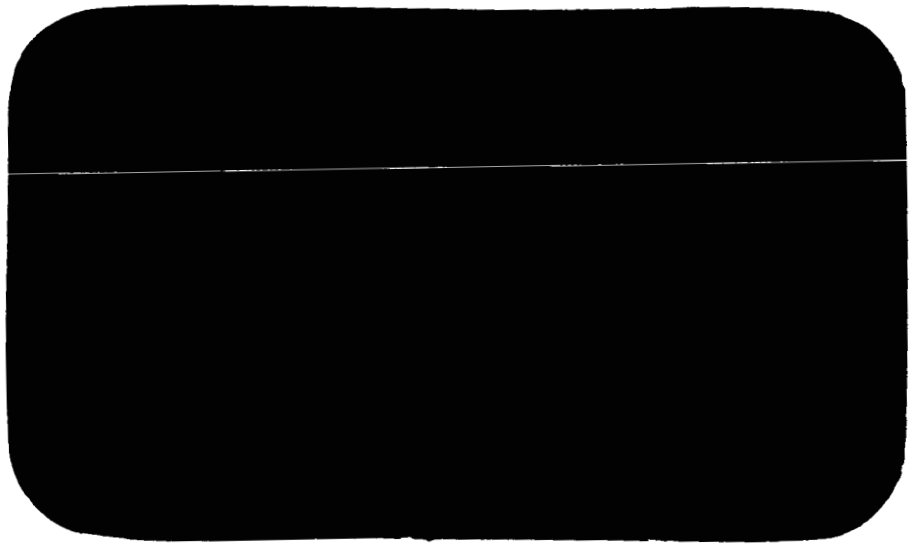

N66-19648

(ACCESSION NUMBER)	(THRU)
91	1
(PAGES)	(CODE)
CR 70713	30
(NASA CR OR TMX OR AD NUMBER)	(CATEGORY)

FACILITY FORM 602

GPO PRICE $ _____

CFSTI PRICE(S) $ _____

Hard copy (HC) 3.00

Microfiche (MF) .75

ff 653 July 65

PHOTOMETRY AND POLARIMETRY OF THE MOON AND THEIR RELATIONSHIP TO PHYSICAL PROPERTIES OF THE LUNAR SURFACE

August 23, 1963

(TR 63-211-6)

By C. A. Pearse

Bellcomm, Inc.
Washington, D. C.

TABLE OF CONTENTS

SUMMARY

This report is a review of the large body of experimental and theoretical information relating to the photometry of the moon, written, primarily, for those who have a direct interest in the subject matter.

In the report an attempt is made to display the salient lunar light reflecting properties which are controlled by the exact nature of the lunar surface microrelief. This summary presents a brief discussion of a currently favored model of the lunar surface covering layer and compares this model with the conclusions necessitated by photometric data. Subsequently a listing is given of factors excluded from the study and finally conclusions and recommendations are presented.

Description of the Lunar Covering Surface

From a consideration of the experimental lunar photometric and polarimetric data, laboratory experiments and theoretical models, the following lunar surface properties are necessitated:

(A) Nearly the entire lunar surface must have a uniform cover layer made up of nearly opaque material. This cover layer must have low surface reflectivity and possess an extremely porous and interconnected structure giving it complex shadow-casting properties in order to exhibit the characteristic lunar photometric behavior.

(B) In addition to these properties the layer-vacuum interface must be made up of highly irregular granule agglomerations, having mean dimensions of the order of a tenth of a millimeter and similar spacings in order that it exhibit the lunar polarization characteristics, especially the correct so-called negative polarization behavior.

Laboratory studies, at atmospheric pressures, have shown that it is possible to form a surface composed of complex overlapping dendritic structures of opaque grains having average dimensions of about 1/50 mm (if larger grain sizes are used to form the structure, consolidation results). This surface has been found experimentally to closely approximate the photometric properties of the lunar surface; however, this artificial surface does not display the same polarimetric behavior as the lunar surface.

A complex low-density matrix results when the bonding forces between the contact faces of grains are larger than the gravitational body forces acting on the grains. When the bonding forces are small, consolidation or a tight packing of grains results. On the moon, the bonding forces between grains may result from a cementing process, where such a process could be due to the grains being sprayed with hot vapors from micrometeorite explosions on the surface, volatile materials being slowly evolved from the lunar interior, or sputtering. The intergranular bonding forces also may result simply from ultra-clean grain faces being in close proximity. The density as a function of depth and the bearing strength properties of such a poorly organized matrix will depend primarily upon the exact nature of the bonding forces.

Information Not Obtainable From Present Study

It should be stressed that certain types of information cannot be obtained from an analysis of lunar photometric, polarimetric, and colorimetric data:

(1) Essentially no information relating to the correlation distances of lunar surface irregularities smaller than about 660 feet can be obtained since this is the lower limit of earth-based telescopic resolution.

(2) No information concerning the nature of the underlying structure of the lunar surface can be obtained, since visible light can penetrate at most a few millimeters into even a quite porous surface layer.

(3) Although the reflection coefficients of terrestrial materials are helpful in determining terrestrial material types, this has not been found to be true in the case of the moon.

(4) Even though different lunar regions have slight color differences, these small differences have been of little value in searching for terrestrial analogues of lunar materials. Furthermore, any original color of lunar materials probably has been drastically modified due to bombardment by solar x-rays, solar flare protons, the solar wind, micrometeoroids, etc.

(5) No information concerning albedo differences on a scale less than about 660 feet (lower limit on telescopic resolving power) can be obtained. Hence, the lunar photometric function does not take into account local albedo differences or gross shadowing.

Conclusions

One can reasonably conclude, on the basis of the previous considerations, that the lunar surface is not covered with loose dust, in any ordinary sense, but in fact is covered, to at least millimeter depths, with an intricate matrix made up of small adhesive grains, probably resulting from pulverization of lunar surface material by micrometeoroid bombardment. The strength properties of such a matrix on the lunar environment can only be poorly estimated at this time.

Recommendations

It is recommended that serious attempts be made to simulate, under ultra-high vacuum conditions (10^{-11} mm of Hg), an artificial surface matrix having lunar photometric and polarimetric properties.

Such an artificial surface layer would be of great value to Project Apollo in two ways:

(A) Lunar surface lighting condition simulators could be made more realistic.
(B) The bearing strength properties of such a layer could be analyzed in detail, both experimentally and theoretically.

PHOTOMETRY AND POLARIMETRY OF THE MOON AND THEIR RELATIONSHIP TO PHYSICAL PROPERTIES OF THE LUNAR SURFACE

I. INTRODUCTION

By observing the variation of brightness of the moon under varying conditions of illumination, one is able to obtain information about the lunar surface which at present cannot be obtained by any other means. However, complete information requires observation over the entire visible spectrum and in two planes of polarization. Integrated photometry is the study of the total radiation from the moon and detailed photometry is the study of an area so small that it may be considered to be located at a point on the lunar surface.

II. HISTORICAL BACKGROUND

For a long period of time it has been known that the moon is characterized by certain remarkable photometric properties, which are dependent evidently on the detailed structure of its surface. For instance, at full moon the distribution of brightness over the disc is nearly uniform. This peculiar property (lack of limb darkening) of the moon was considered as long ago as the seventeenth century by Galileo in his well known "Dialogues on Two Systems of the World." He explained this peculiarity by assuming that the lunar surface was covered by a very rough microrelief as well as by very steep mountains which cast shadows that were easily seen by the telescope. Modern photometric observations have fully confirmed this conclusion and have enabled us to unravel many peculiarities of the microrelief; in particular, the lunar surface has been found to reflect strongly in the direction of the sun, regardless of surface orientation, which is a very unusual reflection property.

Another remarkable feature of the lunar surface consists in the uniformity of the microrelief. Although visual observations of the moon have been made for over 300 years and photometric measurements for more than 50 years, no quasi-specular reflecting areas have been found. This indicates that the microrelief is uniform over the entire visible surface of the lunar sphere and is independent of the morphology and the albedo of the different areas.

The first systematic studies of the photometric properties of the moon were carried out by Herschel (1847) who studied the variation of the integral brightness of the moon over the lunar cycle. Later Bond (1861) observed the brightness of the moon during the lunar cycle, using the reduced image of the moon as formed by reflection from a small silvered sphere. He was the first to realize that the extant theories did not describe correctly the variation of the integral brightness of the moon throughout the lunar cycle. One of the major deficiencies in all of the early observations of the moon was the lack of knowledge concerning atmospheric extinction. To Russell (1916) must go the credit for re-examination of all previous data taking atmospheric extinction into account and consequently being able to reduce the mean errors in the variation of the integral brightness to reasonable values.

More recently a careful determination of integral brightness variation has been made by Rougier (1933). He pointed a photocell, without a telescope, toward the moon and matched the signal with that from a standard incandescent lamp. The integral brightness versus lunar phase angle, g, curves of Rougier and of Russell are shown in Figure 1. It should be noted that the brightness is sharply peaked at g = 0 or at full moon. For a definition of the angle g consult Figure 2.

III. MODERN PHOTOMETRIC MEASUREMENTS

Detailed photometry of individual regions on the moon is a comparatively recent branch of astrophysics. The first reliable measurements were made visually by Wisliscenus (1895) and published by Wirtz in (1915) and by Barabashev (1922). The visual method of photometry has been used even in recent times (Sytinskaya and Sharonov, 1952) due to the fact that the eye is well known to be superior to any instrument in distinguishing small detail and in having a large dynamic range.

Most modern investigations, however, make use of photographic photometry and measure the density of a photographic plate with a microphotometer. The dynamic range of the light signals to be measured is in general so great that diaphragms have to be introduced during the various lunation phases. Special corrections also have to be made for the veil which is always found around lunar photographs which is probably due collectively to atmospheric scattering, to photographic effects, and to diffracted or multiply reflected light inside the telescope.

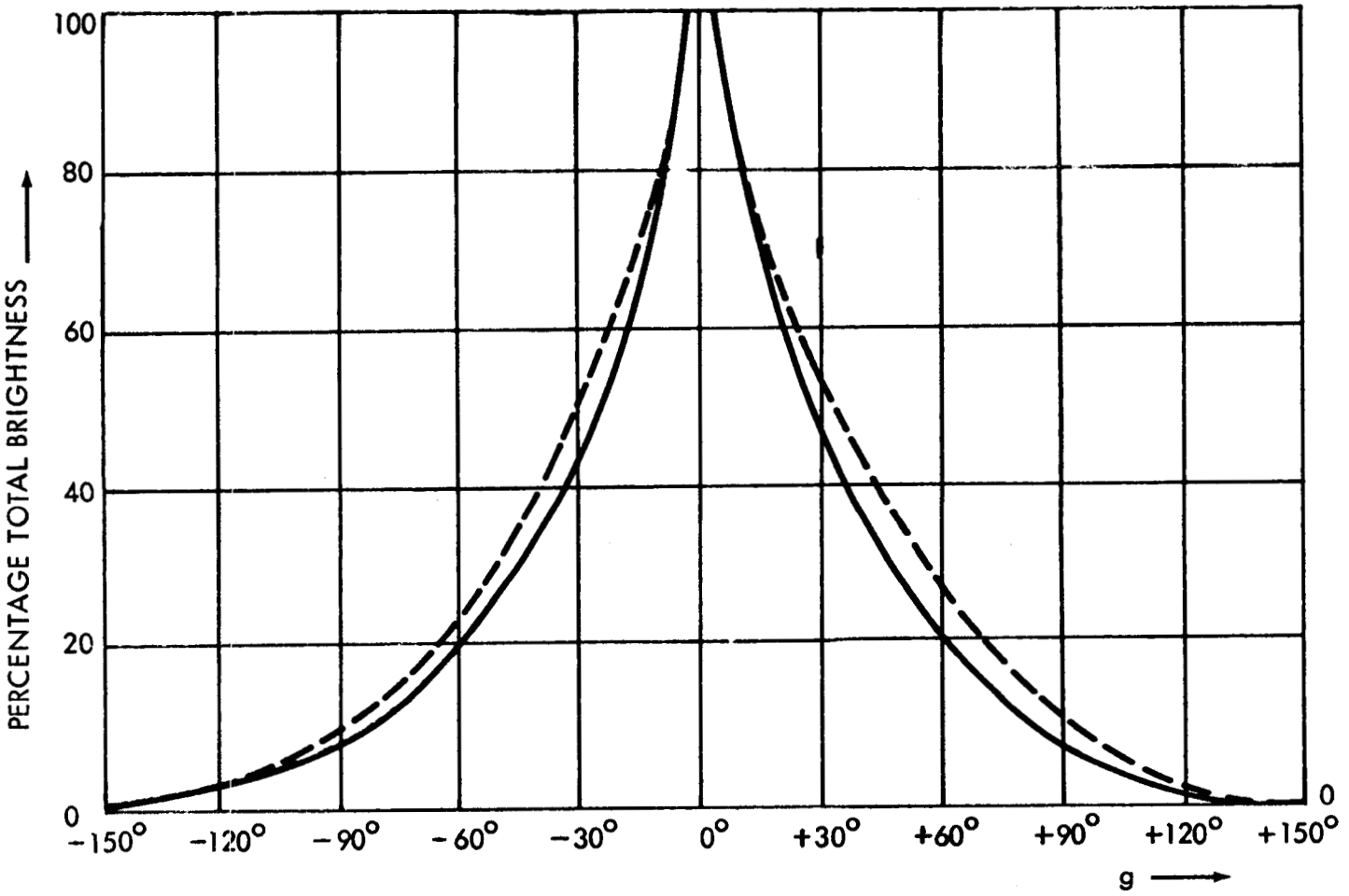

FIGURE 1 THE TOTAL BRIGHTNESS OF THE MOON AS A FUNCTION OF THE PHASE ANGLE, g. AFTER ROUGIER (Full Line) AND RUSSELL (Dashed Line).

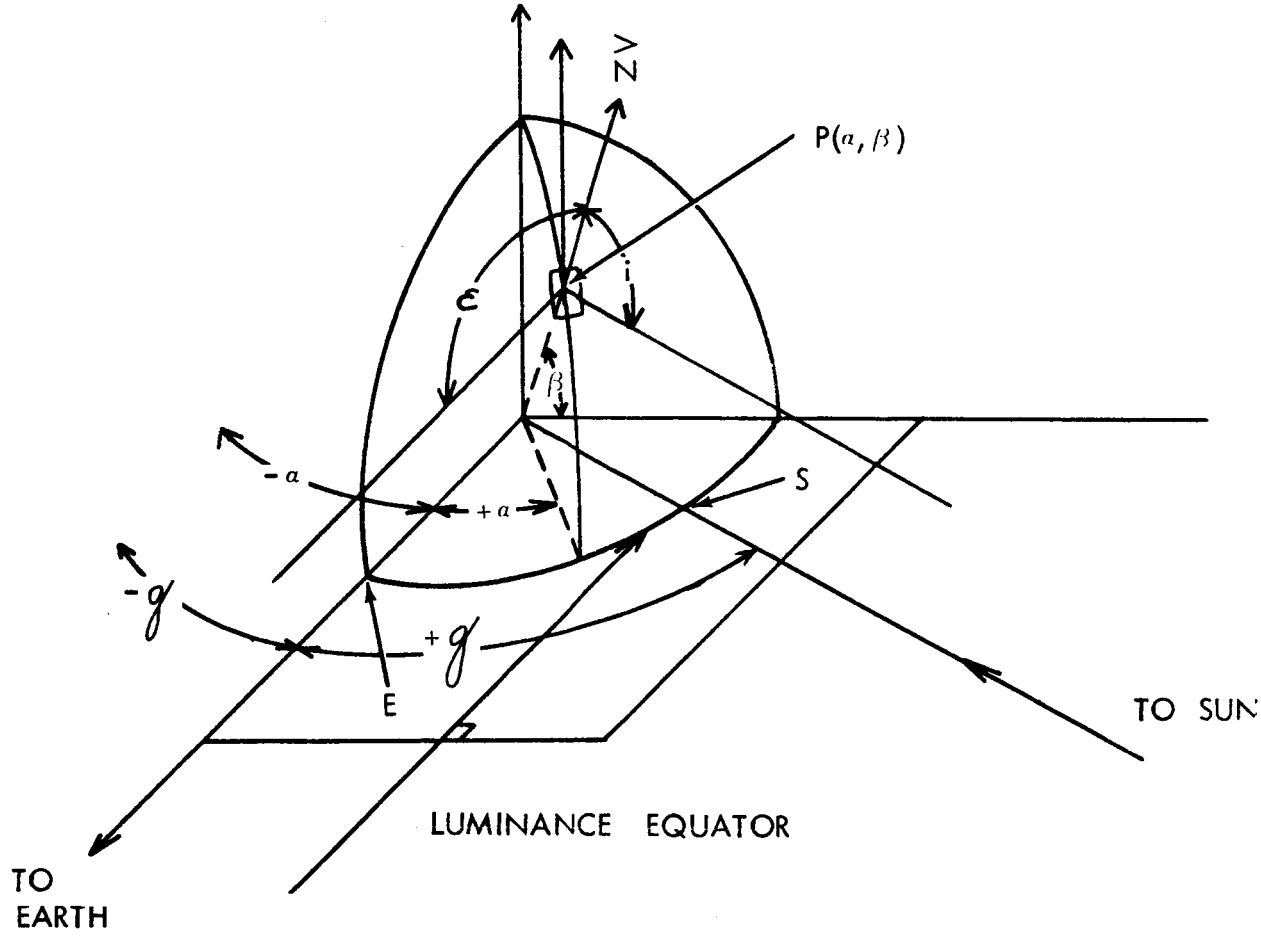

Figure 2 LUNAR PHOTOMETRIC COORDINATE SYSTEM

Since the advent of the photomultiplier, lunar photometric measurements have been made with this valuable instrument. Markov (1948) was the first to use it to study the integral brightness of successive annular regions of the lunar surface by putting a diaphragm in the focal plane of the telescope and screening off successive rings. In 1950 he observed the brightness of 18 points on the lunar surface during an entire lunation; taking various stars as standards he could determine atmospheric extinction for each night.

One of the most complete experimental studies of the moon was carried out in the years 1948, 1949 at the Karkov Observatory by Fedorets (1952). Photographs of the moon were taken by means of a lunar camera mounted on a 160 millimeter refracting telescope. In order to record the large range of brightness of the same feature at different phases of the moon, diaphragms with apertures of different diameter were placed in front of the telescopic objective lens. All of the photographs were connected with one another in the following fashion: for each phase of the moon two plates were exposed on which there were already photographs of the preceding phase, and two plates were exposed on which photographs would be taken for the next day's observation. In all, 160 photographs of the moon were made at 40 different phases. These photographic plates were then measured with a microphotometer, for 172 lunar regions, distributed almost uniformly over the entire surface of the moon. From the analysis of these measurements, tables were constructed in which the angle of incidence i, the angle of emergence ϵ, and the relative brightness were given for each feature and for each lunar phase angle g. Fedorets also constructed curves of brightness versus angle of the measured regions, and brightness versus angles of incidence and emergence of the same features. Fedorets' results are especially valuable because she obtained measurements very near full moon ($|g| = 1.5°$) by observing just before a lunar eclipse.

A very careful investigation of the photometric properties of several homogeneous objects on the moon was recently made by Van Diggelen (1959). Photometric measurements of 38 crater floors were obtained by analyzing photographs that were exposed in 1946, by Minnaert at the Yerkes Observatory, for five different phase angles of the moon. This investigation contains a thorough discussion and analysis of the many previous photometric measurements of the moon. It also critically discusses each of the

several reflection theories which have been proposed to account for the observed photometric properties of the moon.

IV. EXPERIMENTAL PHOTOMETRIC RESULTS

The coordinates of a point on the surface of the moon can be described in terms of a luminance longitude, α, and a luminance latitude, β, (Figure 2). In photometric investigations, the natural great circle to employ is the one which passes through the sub-solar point, S, and the sub-terrestrial point, E. Luminance longitude is measured positively along this intensity equator from left to right from the sub-terrestrial point while latitude is measured in the usual manner along meridians perpendicular to this equator. The longitude of the sub-solar point is the solar phase angle, g.

For any point on the lunar surface, $P(\alpha,\beta)$, we have $\cos\varepsilon = \cos\beta \cos\alpha$. $\cos i = \cos\beta \cos(g-\alpha)$, where i and ε are the angles of incidence and emergence. It can be seen that when the angle of incidence is equal to the angle of emergence, which occurs at full moon, the phase angle, g, must be zero.

In order to display over-all lunar photometric results we shall now discuss the most recent survey of this field which is found in the paper of Van Diggelen (1959). Van Diggelen has established four standard points as being representative of the moon. Their coordinates P_j (α,β) are: P_1 $(0°,0°)$, P_2 $(0°,\pm60°)$, P_3 $(-60°,0°)$, P_4 $(-60°,\pm60°)$. Points 2 and 4 have $\beta = \pm60°$ so each "point" is in actuality two points and an average of the two photometric functions is taken in each case.

Van Diggelen has also divided the moon into four crescents for purposes of analysis which are characterized as follows:

CRESCENT	PHOTOMETRIC LONGITUDE	
I. Central	(0° to +10°)	with 10 craters
II. Second	(+10° to +30°)	" 12 "
III. Third	(+30° to +50°)	" 10 "
IV. Limb	(+50° to +90°)	" 10 "

Each of the four crescents were further sub-divided into three latitude strips, having latitudes between 0°-20°, 20°-40°, 40°-90°, in both the north and south directions.

The USAF Lunar Reference Mosaic which has been taken as the standard coordinate system for this report, on which the four crescents and four standard points of Van Diggelen have been located, is shown in Figure 3.

Individual albedo differences of the craters have been normalized in such a way that the brightness of each crater floor has a value of 1.00 at full moon. The mean brightness was then found from all points within the area determined by a given strip and crescent. In this manner a mean brightness curve was determined for each of the areas. From an examination of Figure 4 it can easily be seen that there is no systematic variation of the brightness curve with latitude, and there is only a variation with longitude as Tschunko (1949) had concluded. Averaging the brightness of the three different strips of latitude of a given crescent, Van Diggelen then obtained a mean brightness curve for the four crescents. His brightness curves are reproduced here as Figure 5 for the four crescents. It can be seen from an examination of these curves that the brightness of each crescent is sharply peaked at exactly zero phase. Let us next examine brightness curves of four craters (Figure 6) near Van Diggelen's four standard points. It can be seen that all craters reach their peak intensity at exactly zero phase angle, as did the crescents.

In contradistinction to these four craters, let us now examine (Figure 7) four craters which are near the standard points but are characterized by being bright-rayed craters. It is clearly seen that maximum brightness of each of these craters occurs at about 12° <u>after</u> full moon.

It should be noted in Figure 6 that the experimental points have been roughly characterized by two straight lines, which tell one in first approximation the values of g at which the brightness is a maximum and at which it goes to zero (location of the terminator). This "triangle" representation of brightness was first introduced by Tschunko (1949) and is used extensively in Van Diggelen's lunation curves (i.e., brightness versus lunar phase angle).

Thus far we have examined only the change of brightness due to a change in phase angle. It is very instructive to examine the brightness or

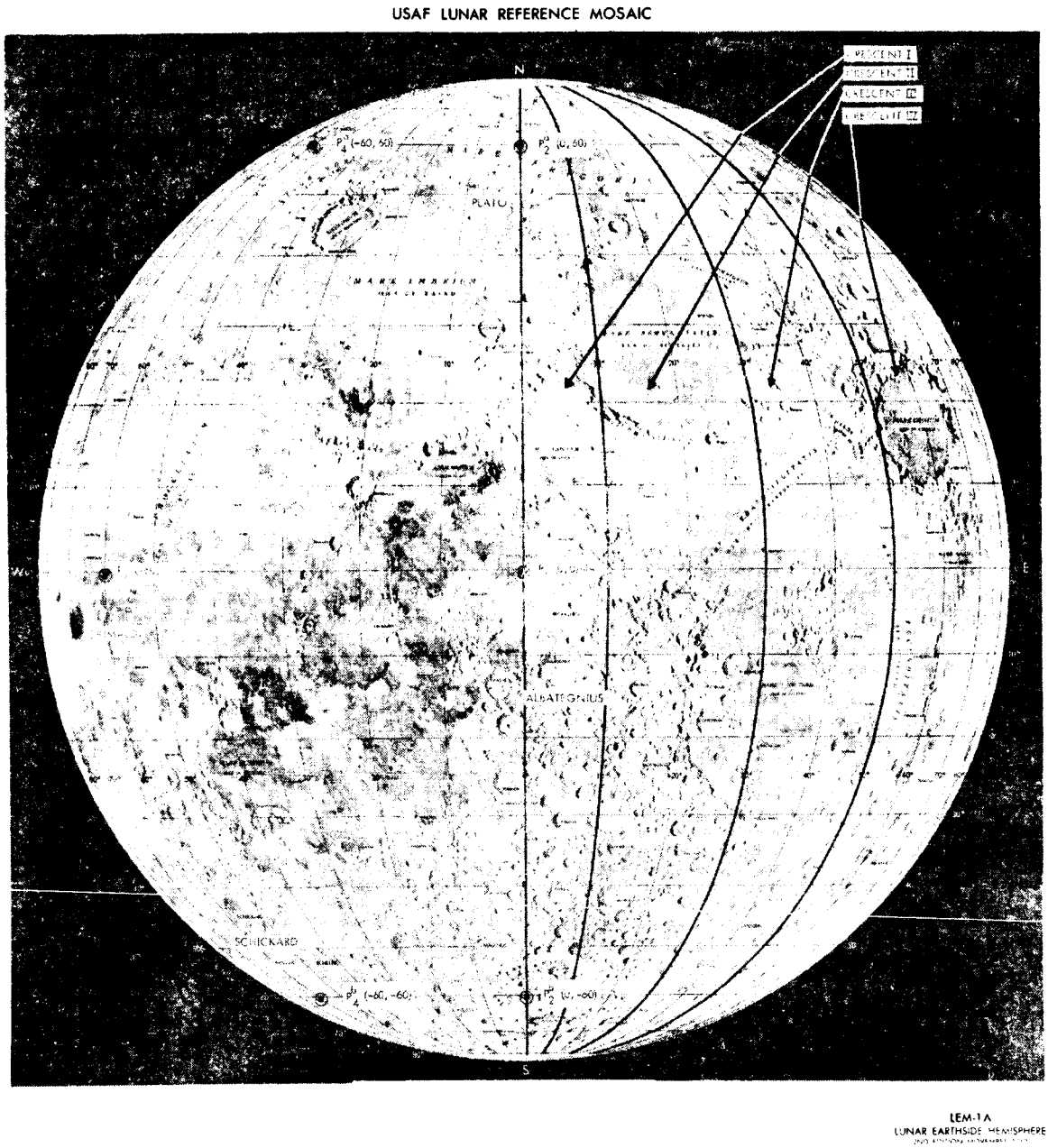

FIGURE 3 LOCATION OF THE FOUR STANDARD CRESCENTS AND POINTS.

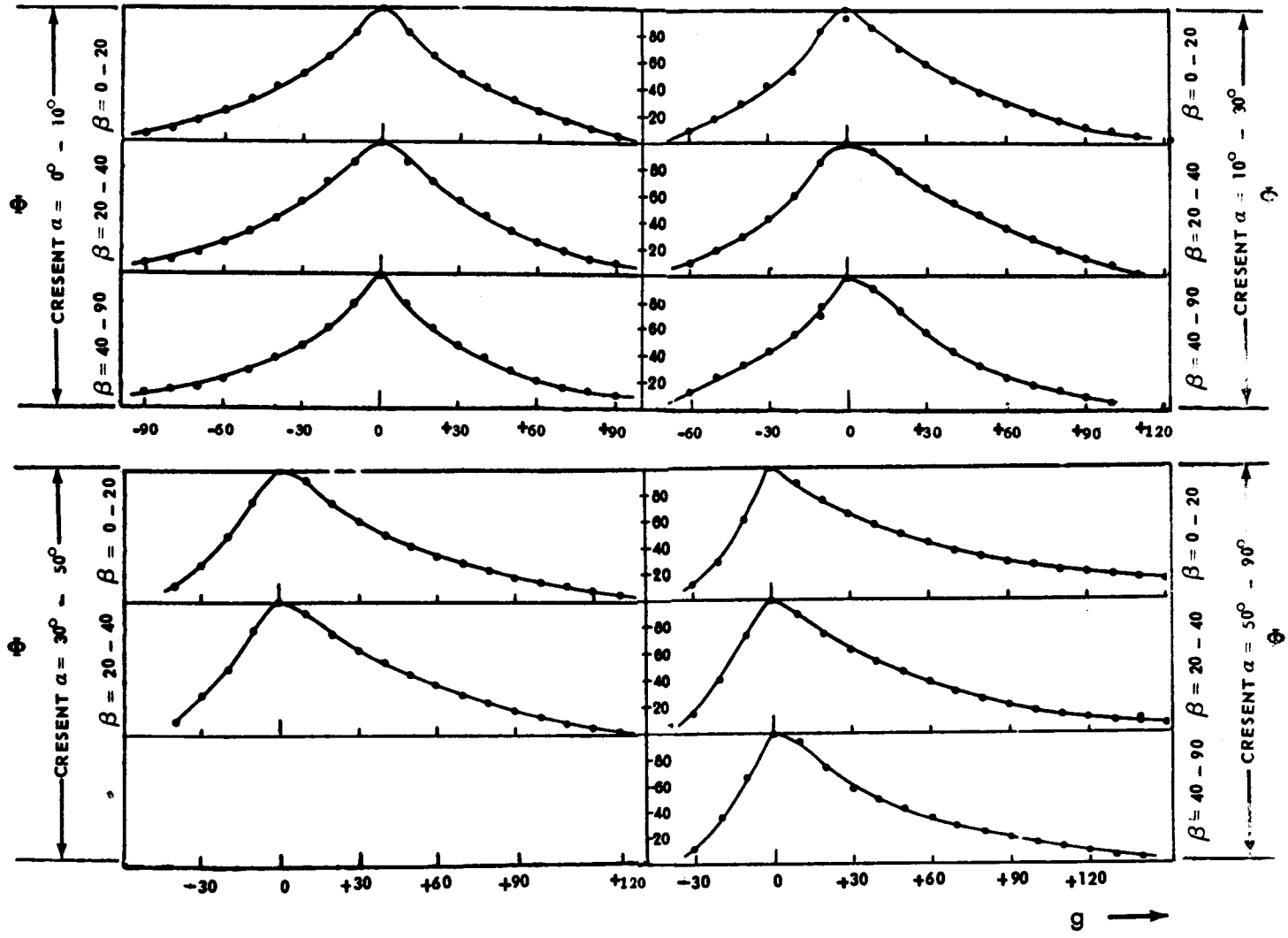

FIGURE 4 LUNATION CURVES OF FOUR CRESCENTS OF DIFFERENT PHOTOMETRIC LONGITUDE, SHOWING THAT THE BRIGHTNESS IS A FUNCTION OF THE LONGITUDE. EACH CRESCENT IS DIVIDED INTO THREE STRIPS OF LATITUDE, WHICH DO NOT SHOW SYSTEMATIC DIFFERENCES. MEAN LUNATION CURVES ARE COMPUTED FOR EACH CRESCENT.

(after Van Diggelen, 1959)

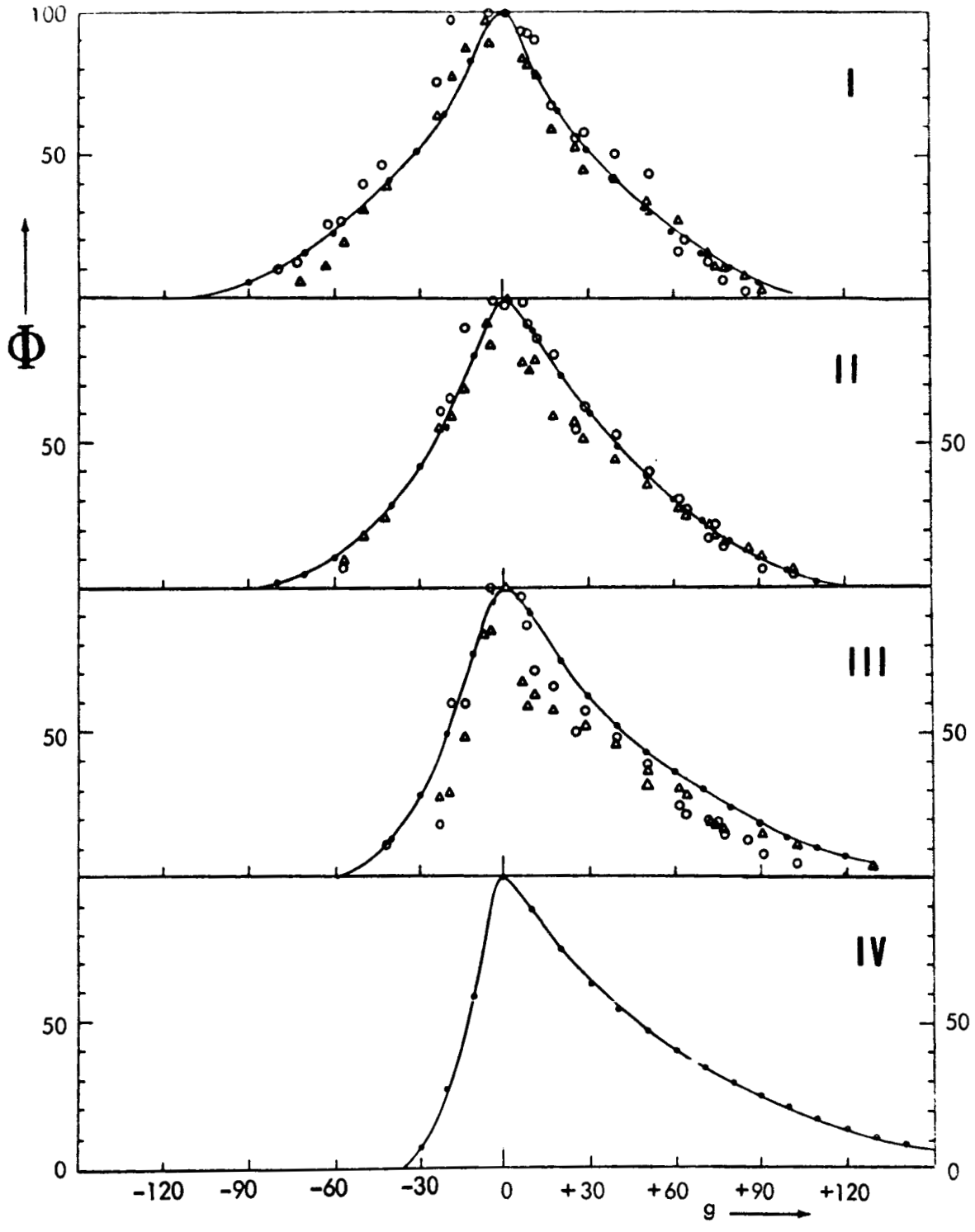

FIGURE 5 MEAN LUNATION CURVES OF CRATER FLOORS FOR THE FOUR CRESCENTS. MEASUREMENTS ARE COMPARED WITH THOSE OF FEDORETZ FOR INDIVIDUAL PLAINS (△) AND HIGHLANDS (○) IN THE SAME CRESCENT. THE FOUR FIGURES ARE RELATED WITH:

1) crescent α 0–10, β 0–90, △ Fedoretz 49, ○ Fedoretz 155;
2) crescent α 10–30, β 0–90, △ Fedoretz 16, ○ Fedoretz 153;
3) crescent α 30–50, β 0–90, △ Fedoretz 33, ○ Fedoretz 151;
4) crescent α 50–90, β 0–90.

(after Van Diggelen, 1959)

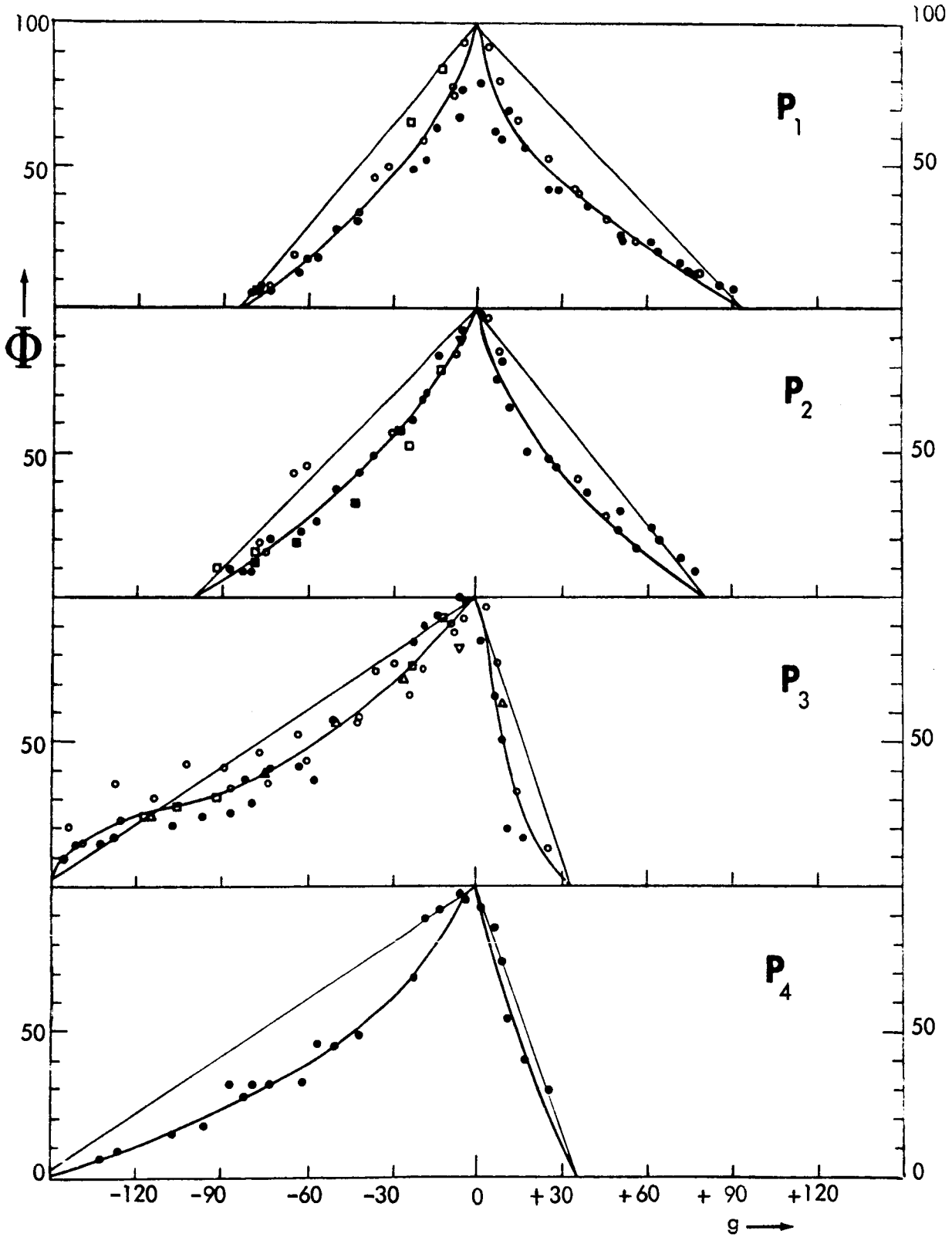

Figure 6 Lunation curves of four craters near the standard points. Albategnius, Plato, Grimaldi and Schikhard. The observations are made by Markov (1927), (▽), Markov - Sharonov (○), Öpik (■), Bennett (△), Fedoretz (•) and van Diggelen (□). (after Van Diggelen, 1959)

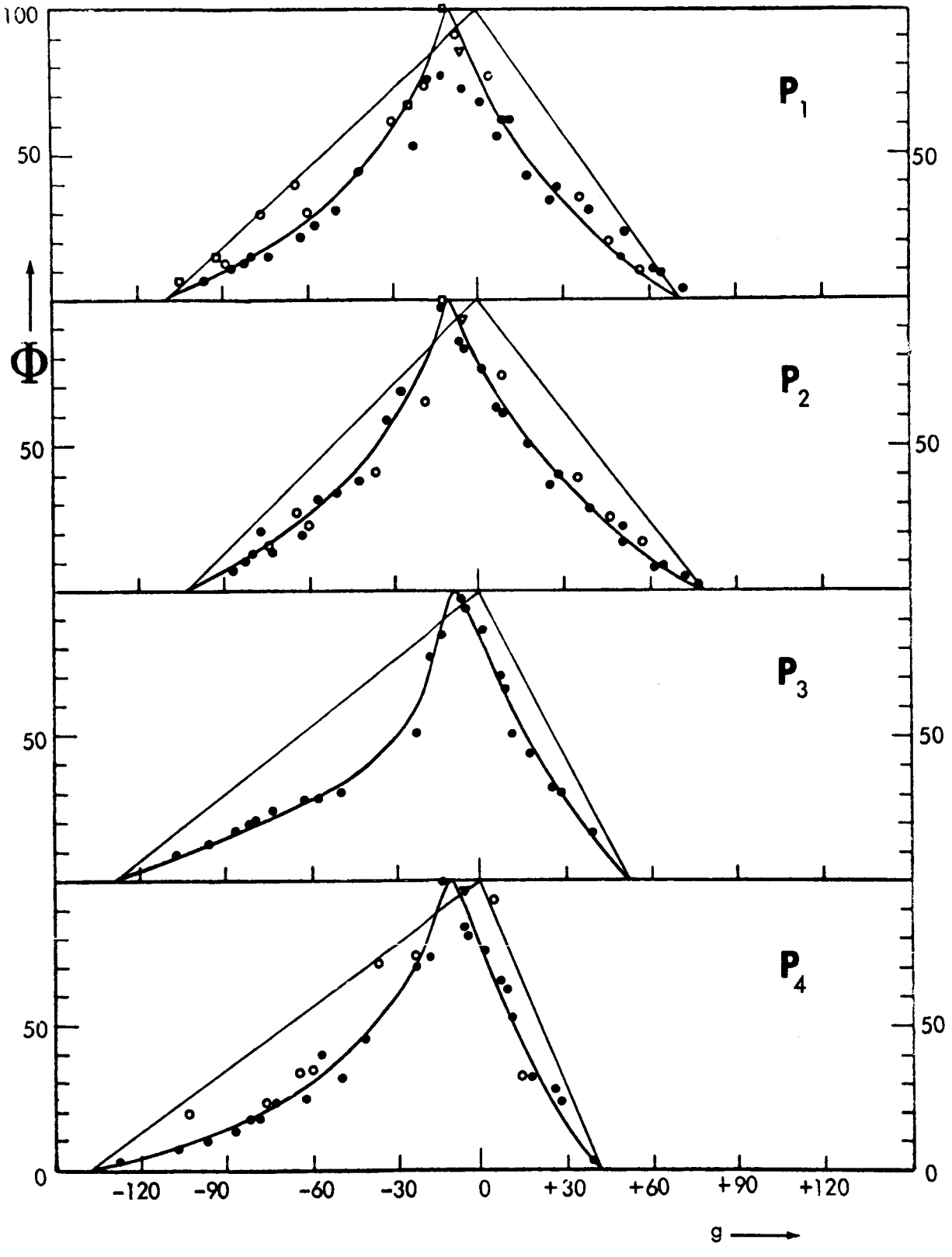

FIGURE 7 LUNATION CURVES OF FOUR RAY CRATERS NEAR THE STANDARD POINTS: COPERNICUS, TYCHO, KEPLER AND ARISTARCHUS. MAXIMAL BRIGHTNESS OCCURS AFTER FULL PHASE. (after Van Diggelen, 1959)

photometric function* as a function of the luminance longitude, α, for fixed values of the phase angle g.

If we use the experimental observation that the photometric function is essentially independent of luminance latitude, we can express the brightness of the surface in terms of only the longitude, α, and the phase angle g. Herriman, Washburn, and Willingham (1963) have made an examination of the data of Fedorets (1952), mentioned previously, and after hand-smoothing this data, have constructed curves showing the dependence of the photometric function, $\mathfrak{F}$, upon lunar phase angle and photometric longitude. From examining their photometric function (Figure 8) one can see, for instance, the rapid variation of the photometric function near $\alpha = 90^\circ$ for small values of the phase angle g. This, of course, is the circumstance in which one is looking at the lunar surface near the terminator. From this figure one can also see that when g = 0 (i.e., at full moon) the brightness is constant with longitude, as it should be.

Byrne (1963) has used the photometric functions of Herriman, Washburn, and Willingham to construct a photometric surface from which one can easily obtain the brightness of any point on the moon at a given lunar phase. This surface has been found to be particularly useful in analyzing the lunar lighting conditions under which an orbiting satellite would be required to take pictures.

This photometric surface was constructed by making panels, the outlines of which were the various $\mathfrak{F}(\alpha, g = \text{const})$ curves. By setting these panels parallel to each other along a phase angle axis for both halves of the visible moon the surface comes into being. Because there is a small number of panels, wires to indicate sample profiles were used. Different photographic views of this photometric surface are shown in Figures 9, 10, and 11. From an examination of Figure 11, one can easily determine the brightness versus phase angle g of a point on the moon by following a wire profile running over the surface.

* The terms brightness versus phase angle, lunation curve, photometric function versus phase angle are used somewhat indiscriminately in the literature. We shall primarily use the term photometric function.
(see Appendix A, page 4)

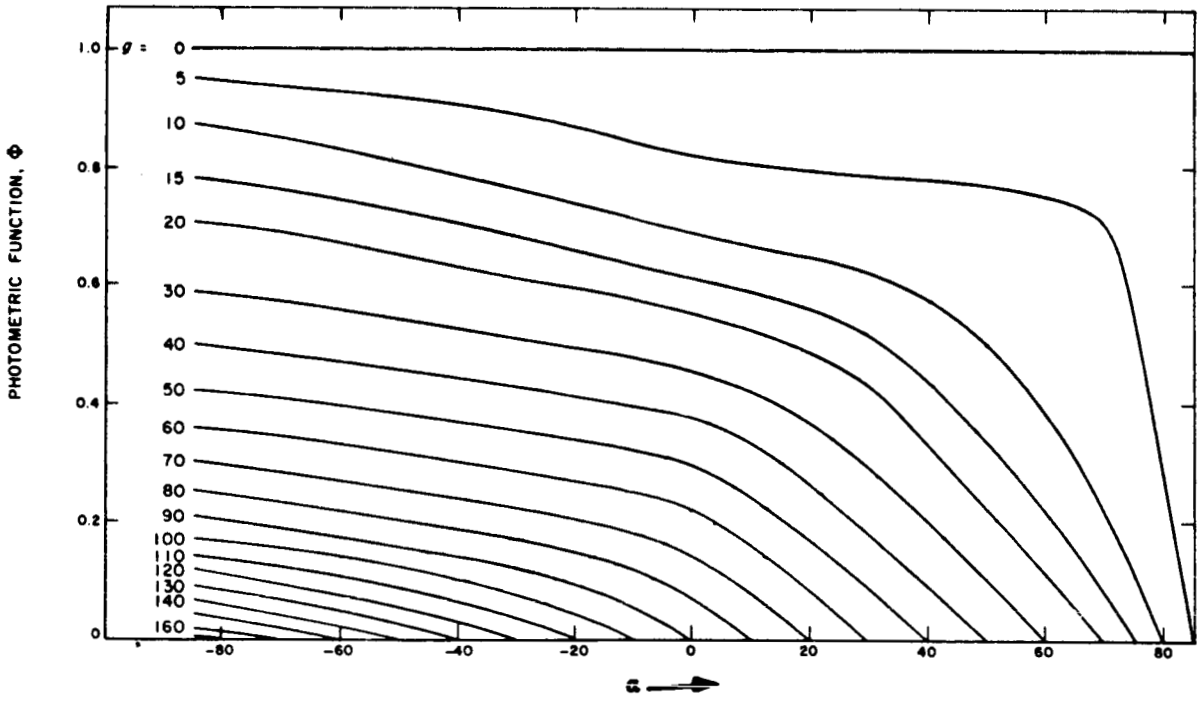

Figure 8 The photometric function vs. α

(After Herriman, Washburn, Willingham 1963)

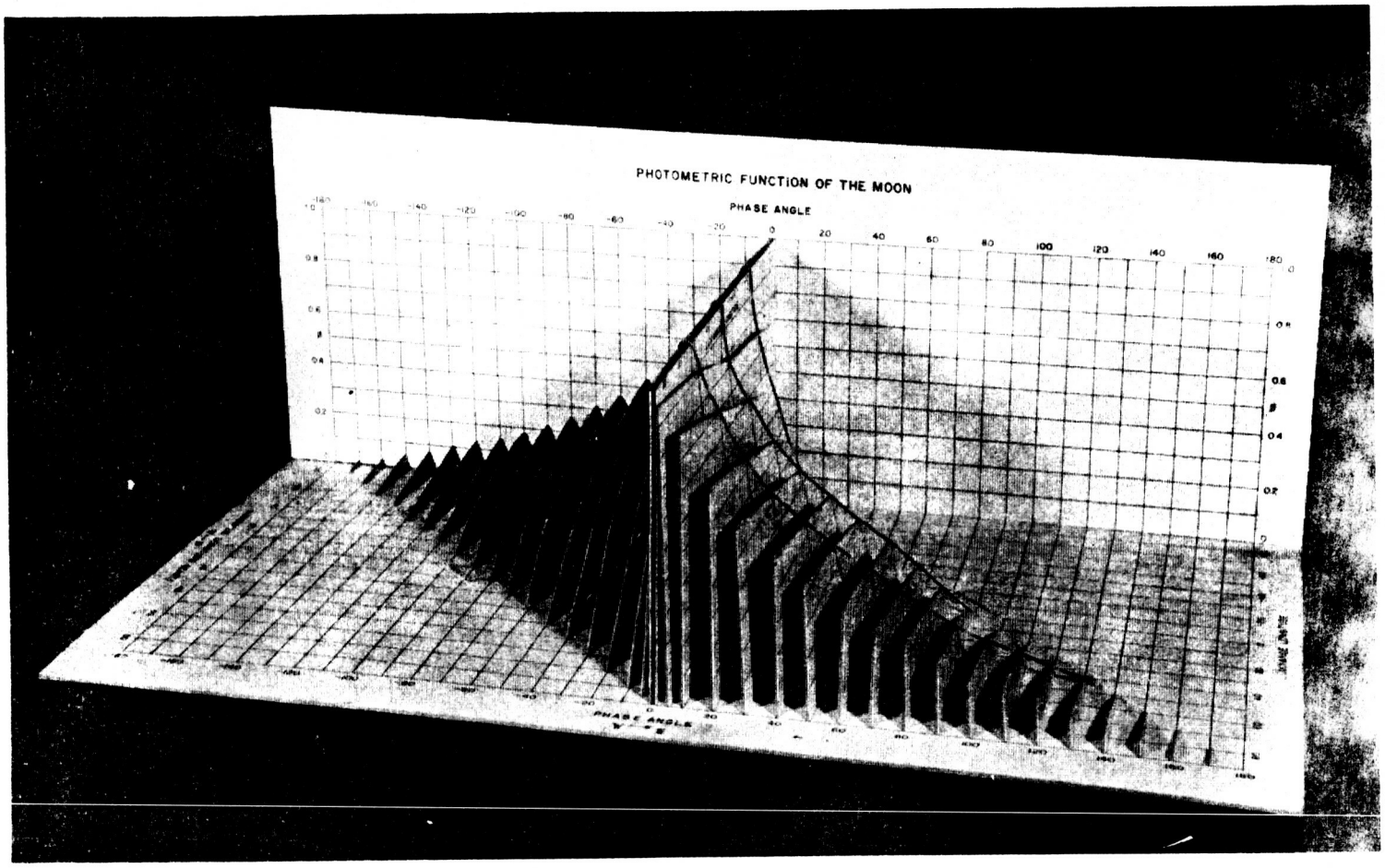

(After Byrne, 1963)

Figure 9

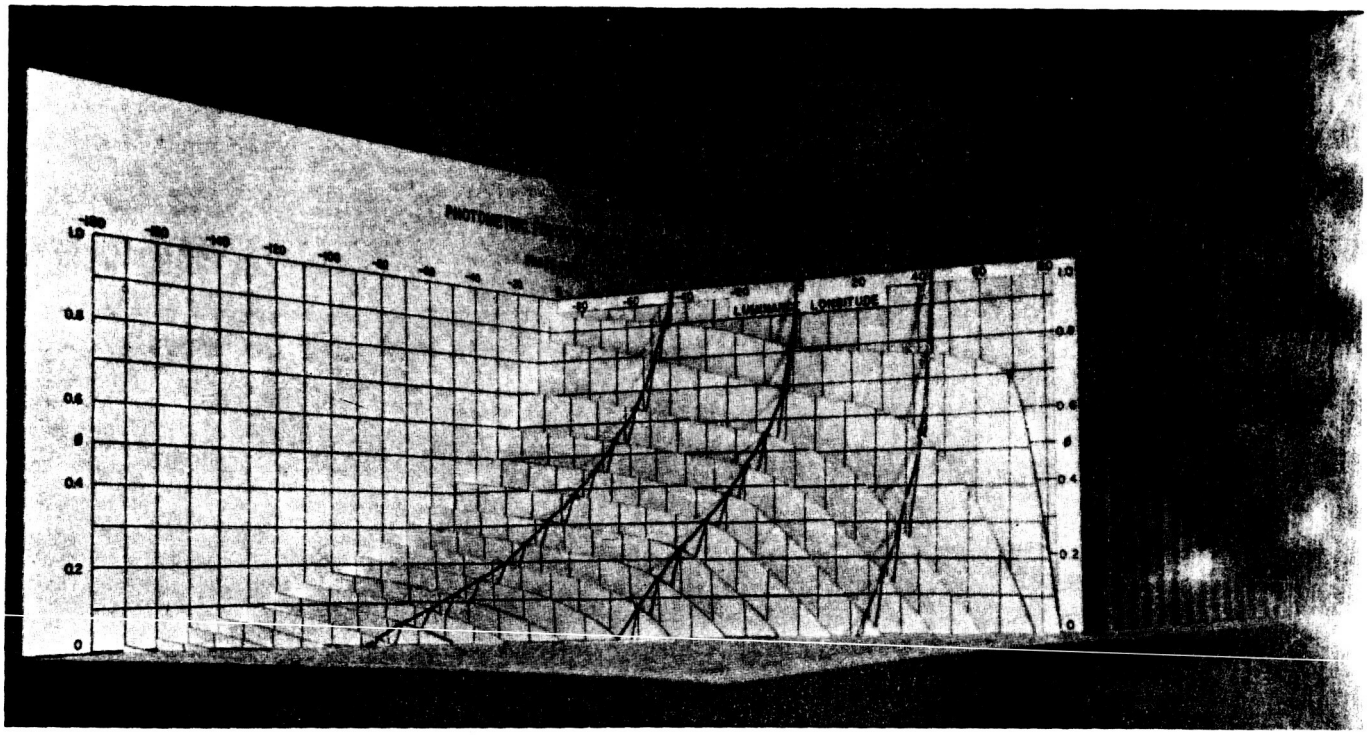

(After Byrne, 1963)

Figure 10

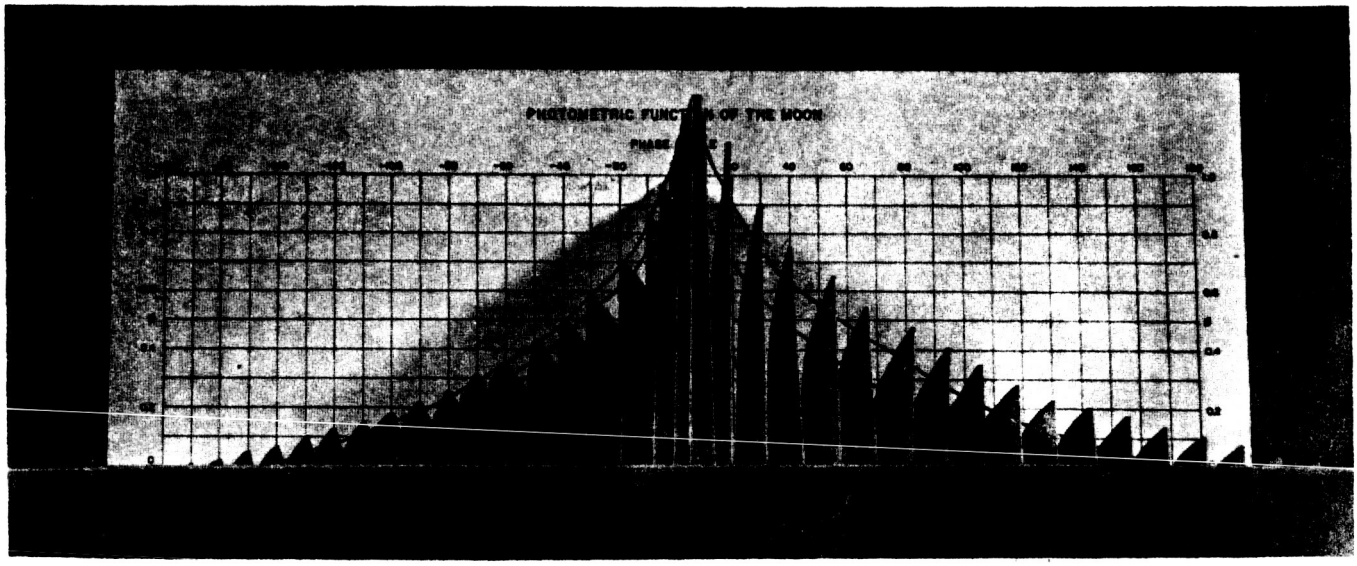

(After Byrne, 1963)

Figure 11

Since the sun travels from east to west around the moon (right to left in Figure 11) we can see by examining the wire profile closest to us, which represents a point at +45° (east) longitude, that the brightness at lunar morning rises relatively slowly to a maximum at full moon and then very quickly drops, becoming zero when the phase angle has reached -45°. On the other hand, by examining the wire profile which is farthest from us which applies to a point at -45° (west) longitude, we can see that the brightness at lunar morning rises rapidly beginning at a phase angle of +45°, reaching its maximum at full moon, and then decreases slowly to zero at a phase angle of -135°. These two asymmetric profiles, of course, can be seen to be mirror images of each other. A point located at zero longitude, as can be seen from the center wire profile, has a completely symmetric photometric function.

We have observed that the lunar brightness versus g for points on the eastern limb of the moon has a slow rise and a fast descent and vice versa for points on the western limb. This observation is easily explained, once given that the brightness of all points on the moon is a strong function of the phase angle g, having its maximum value at g = 0. Consider a point on the extreme eastern limb at say $\alpha = 85°$. At g = 175° (grazing incidence, hence small scattering) illumination of the point first occurs (i.e., new moon). It is clear that as the phase angle decreases from 175° to 0°, that the brightness will monotonically increase to its maximum value. On the other hand, when g approaches -5°, which is the condition that the point be at the terminator (again grazing incidence), the brightness must approach zero. Hence the "average" slope of brightness must be larger in the interval g = 0° to g = -5°, when compared with the interval g = 175° to g = 0. Of course, any serious moon-watcher will have observed this phenomenon many times.

V. OLDER THEORETICAL PHOTOMETRIC FUNCTIONS

Many theoretical attempts have been made to derive the lunation curve from physical theories which are concerned with the penetration and scattering of light inside of a plane surface layer made up of solid diffusing material. The simplest reflection laws are those of Lambert and Lommel-Seeliger, which are a function only of the angles of incidence and emergence. The Lommel-Seeliger law has the advantage of having a

theoretical basis, while that of Lambert does not (see Appendix A for derivations). As is shown in the Appendix A, the Lommel-Seeliger law represents correctly the appearance of a full moon, since it gives a uniformly bright surface. However, at all other phase angles it agrees very poorly with the observational data. Neither the Lambert or the Lommel-Seeliger law satisfies the condition that the brightness of all lunar areas reaches maximum brightness at full moon, rather than when the angle of incidence has its minimum value.

It might be thought that a more satisfactory lunar theory of the diffuse reflection could be obtained by carefully analyzing the scattering processes in a solid body, taking into account second order and non-isotropic scattering. However, the results of such considerations have entirely failed to describe the lunar observations.

There have been several attempts to obtain empirical expressions for the photometric function, among which the more successful were those obtained by Opik (1924) and Fessenkov (1926). Van Diggelen has compared the results of four different photometric functions with the Tschunko triangles for his four standard points in Figure 12. Of all of these curves, it can be seen that only the formula of Opik could be said to reasonably represent the experimental data, and it only in the case of points at zero longitude.

The visible part of the moon has a very rough structure, with a great number of large and small irregularities, craters and mountains. These irregularities cast shadows which grow larger as the angle of incidence of the solar radiation increases. Since the best resolution that one can obtain with telescopic observation of the moon is about 660 feet, it is quite possible that the major photometric effects one observes are due essentially to the formation of shadows which are much too small to be seen separately. The scattering function for individual surface particles may be relatively unimportant when compared with the effects of geometrical shadowing. A surface which is partially occupied by pits or clefts, too small to be seen directly with a telescope, but which cast shadows nevertheless, gives much better agreement with the integral brightness versus phase angle, as has been shown by Schoenberg (1925). Barabashev (1922) has elaborated a theory of clefts in which he calculated the intensity of light reflected by a plane surface, crossed by infinitely deep parallel clefts with perpendicular walls. Markov (1924) then extended

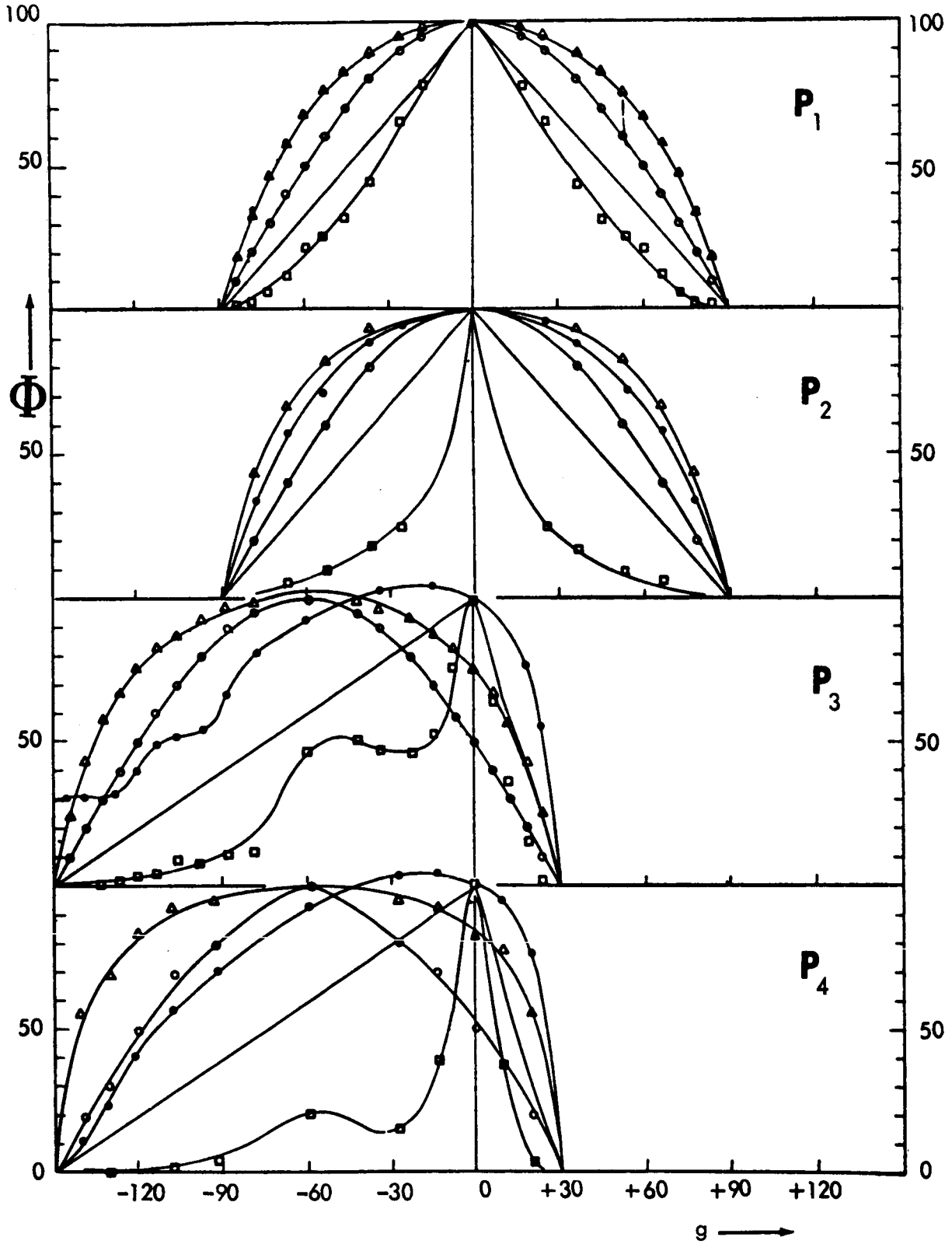

FIGURE 12 REFLECTION LAWS OF LAMBERT (○), ÖPIK (□), LOMMEL-SEELIGER (△), AND FESSENKOFF (●), COMPARED WITH THE TSCHUMKO TRIANGLES AT OUR FOUR STANDARD POINTS. (after Van Diggelen, 1959)

this theory to grooves located arbitrarily on the lunar disc. He made his calculations for three forms of reflection laws for the surface itself: First, he assumed the law of Lambert; second, that of Lommel-Seeliger; and third, the Fessenkov law. The Fessenkov law was used in comparing his theory with observations of the crater Grimaldi and Figure 13 shows the comparison between this theoretical calculation and the experimental points. As can be seen, the theoretical curve agrees fairly well with the data points near zero phase angle, however, it deviates widely otherwise. Since the macroscopic structure of the lunar surface shows us a great number of circular and hemispherical pits as compared with only a small number of clefts, one is not too surprised to find a lack of agreement of this type.

The theory of Bennett (1938) assumed that the lunar surface was a surface layer covered by a great number of hemispherical pits or cups similar to the porous surface of pumice. He made very simple assumptions about the reflection law of these pits or cups: namely, that brightness varies directly with the fraction of the visible area of the illuminated inner surface. For the plane surface between the cups he assumed Lambert's law to apply. Van Diggelen has compared the results of the theory of Bennett with observations at his four standard points, and the results are shown in Figure 14. Though the agreement between the experimental triangles and the theory is fair, it leaves something to be desired, especially in the cases of larger longitudes.

VI. SUMMARY OF PHOTOMETRIC RESULTS

A summary of the salient features of lunar photometric observations thus far discussed is:

(a) Except for individual differences in albedo (see Table I), the brightness at full moon is the same for all points on the lunar disc. Markov (1924); Markov and Barabashev (1926).

(b) The brightness of all points increases up to full moon and then decreases after full moon independently of their position on the lunar disc. This important effect for maria was discovered by Barabashev (1922) and generalized to all lunar formations by Markov (1924) on the basis of rather primitive measurements which have subsequently been verified for the great majority of the regions studied. Maximum brightness for most regions occurs at the smallest measured phase angle (1.5°);

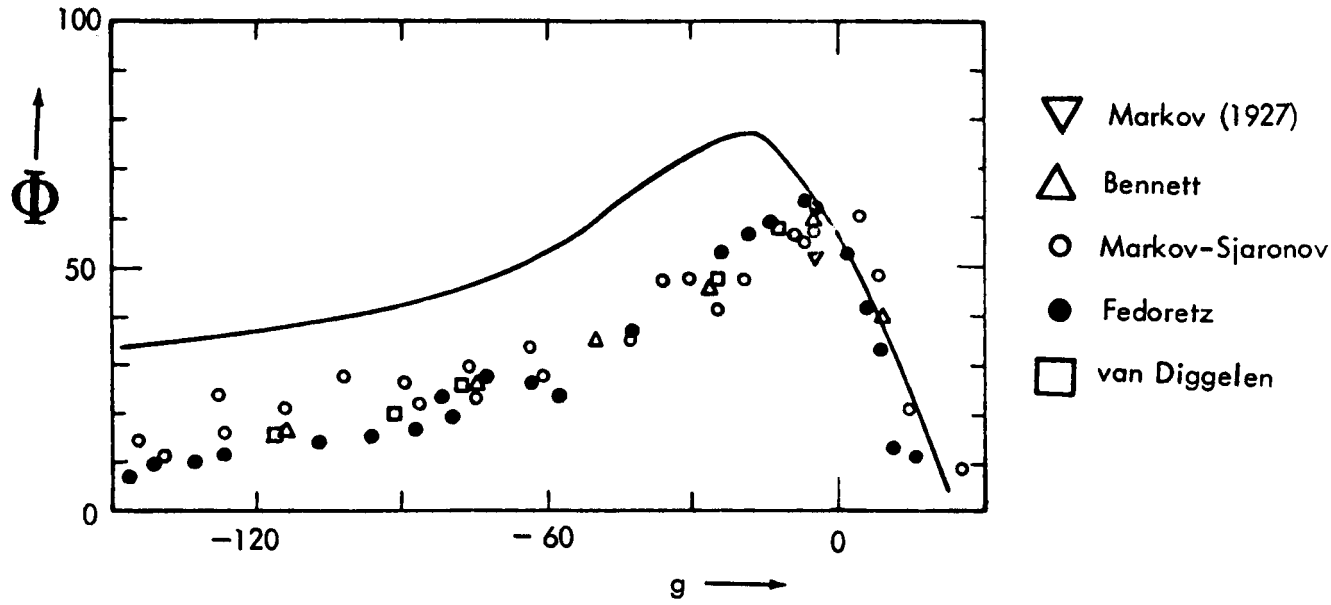

FIGURE 13 LUNATION CURVE OF GRIMALDI CALCULATED BY MARKOV COMPARED WITH THE THEORY OF CLEFTS.
(after Van Diggelen, 1959)

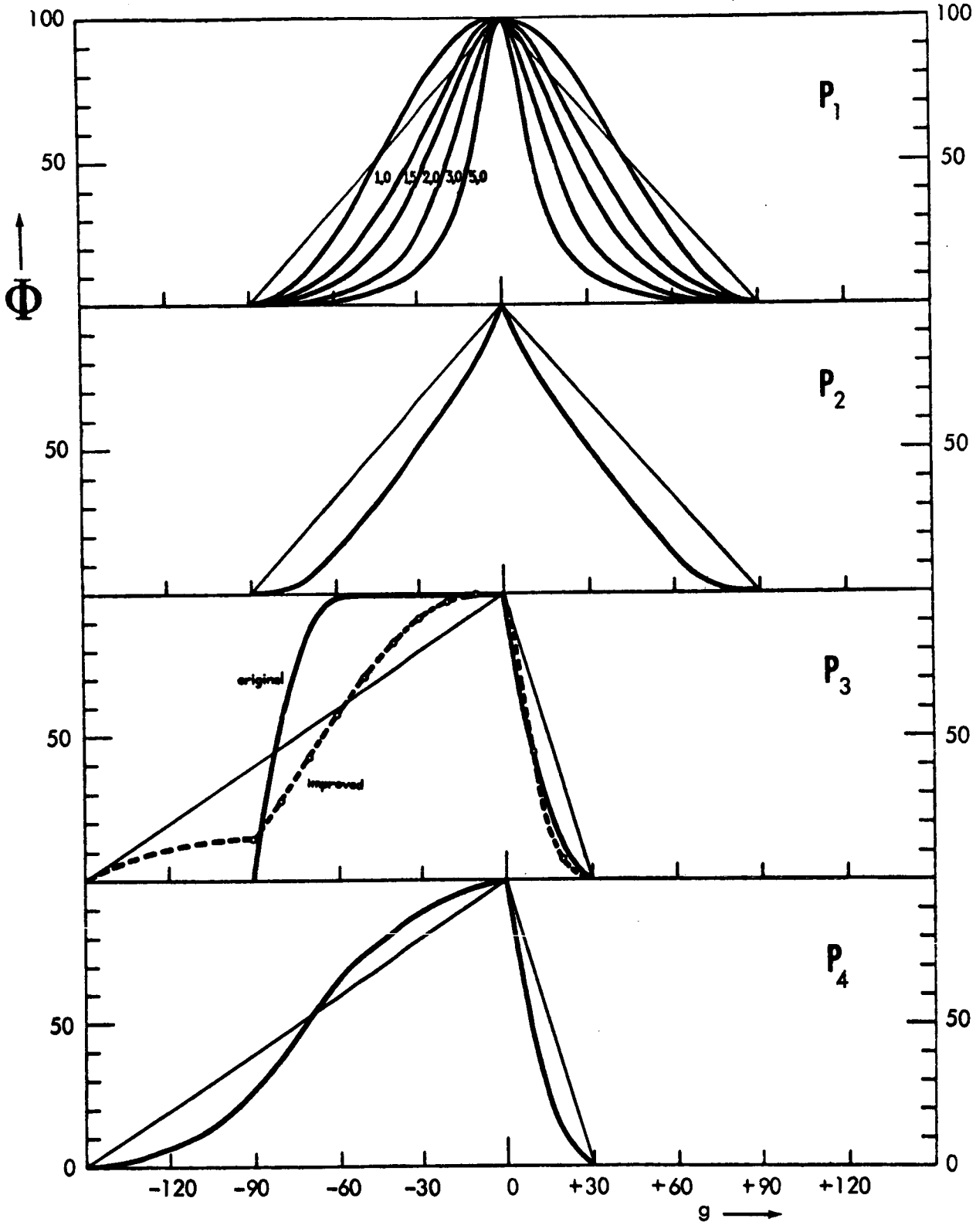

FIGURE 14 LUNATION CURVES OF A THEORETICAL SURFACE OCCUPIED 100% WITH HEMI-SPHERICAL CUPS (Theory of Bennett) LOCATED AT THE FOUR STANDARD POINTS. THE FIVE CURVES REFER TO RATIOS OF DEPTH TO RADIUS; 1; 1.5; 2; 3; 5.

(after Van Diggelen, 1959)

TABLE I

Type of object or material	Albedo a			Color Excess D		
	Aver.	Extreme		Aver.	Extreme	
Moon, maria and floors of dark cirques	0.065	0.05	0.08	+0.339	+0.29	+0.40
Moon, pali	0.091	0.09	0.10	+0.349	+0.31	+0.37
Moon, continents and floors of craters with normal colouring	0.105	0.08	0.12	+0.347	+0.31	+0.38
Bright rays and craters with bright floors	0.140	0.10	0.18	+0.352	+0.31	+0.39
All parts of Moon together	0.090	0.05	0.18	+0.344	+0.29	+0.40
Volcanic slag, scories	0.060	0.02	0.14	+0.11	-0.013	+1.28
Volcanic tuff	0.193	0.06	0.43	+0.29	-0.15	+1.10
Pumice	0.354	0.13	0.55	+0.43	+0.05	+0.81
Dunite, periodotite	0.104	0.06	0.16	-0.01	-0.17	+0.25
Gabbro, norite	0.155	0.08	0.21	-0.04	-0.17	+0.12
Basalt	0.133	0.06	0.28	-0.05	-0.31	+0.15
Diabase	0.151	0.11	0.19	-0.02	-0.19	+0.13
Andesite	0.139	0.08	0.31	-0.02	-0.12	+1.10
Granite	0.244	0.04	0.70	+0.39	-0.09	+1.23
Metamorphic rocks	0.281	0.08	0.78	+0.26	-0.25	+0.99
Clays and schist	0.251	0.12	0.50	+0.33	-0.24	+1.53
Sand	0.240	0.10	0.40	+0.49	+0.06	+1.22
Sandstone	0.222	0.06	0.54	+0,66	+0.03	+1.54
Limonite, ortstein	0.131	0.05	0.35	+0.69	0.00	+1.24
Limestone, marl	0.325	0.06	0.80	+0.38	-0.13	+1.52
Stone meteorites	0.183	0.04	0.48	+0.10	-0.16	+0.36
Fusion crust of meteorites	0.052	0.02	0.17	+0.11	-0.10	+0.38

(After Sharonov, 1962)

however, certain regions (craters, continents, and rays) attain maximum brightness at about 5-1/2° after full moon. Some features attain maximum brightness as late as 12° after full moon. This anomalous behavior remains a mystery and apparently is to be explained by some very peculiar orientation characteristic of the microrelief of these regions.

(c) The maxima of the brightness of the bright rays are higher and sharper than the maxima of the regions adjacent to them. This more rapid increase in brightness of the bright rays relative to the surrounding surface is evidently to be explained by some difference in the material composition of these regions.

(d) All objects which have the same photometric longitude have the same brightness (i.e., there is essentially no latitude dependence) after albedo differences of individual objects have been taken into account. This observation was first made by Tschunko (1949), and greatly simplifies the analysis of large quantities of data, since the photometric function, Φ, depends only upon the luminance longitude and phase angle.

(e) The scattering function of the lunar surface is characterized by having very strong back-scattering as was found by Orlova (1955, 1956).

VII. EXPERIMENTAL PHOTOMETRIC STUDIES OF TERRESTRIAL MATERIALS

A great many experimental studies have been made which have attempted to simulate the photometric properties of the moon's surface with terrestrial materials. Outstanding among these studies were those that have been carried out by Barabashev and Chekirda (1945) for different terrestrial rocks both in their natural state and in a pulverized state. They then compared the laws of reflection found for them with that of the lunar surface. This made it possible for the authors to conclude that the surface of the moon is extremely porous and that possibly it is covered with fragments of volcanic rock. A useful quantity in such studies is the albedo which is defined to be the ratio of the brightness of an object to that of an "ideal white screen" under the same conditions of illumination (see Appendix A). Comparing lunar albedo values (found in Table I, taken from Sharonov (1962)), it is seen that only very dark substances such as volcanic slag and the crust of meteorites

have values of albedo as low as those of the moon. Substances such as pumice, sandstone, clay, as well as granite, are found to have much too large values of albedo.

Sytinskaya (1953) has constructed a statistical distribution function of the lunar albedo values over the complete lunar surface, which is found in Figure 15.

Van Diggelen (1959) has made experimental investigations of the reflecting powers of various terrestrial substances, as well as surfaces on which there were placed pits and cups as well as glass beads. Especially interesting among his experimental investigations is the measurement of the photometric function of different volcanic ashes, the results of which are compared with his four standard points in Figure 16. As can be seen, the lunation curves of volcanic ashes deviate widely from the lunar curves, represented by the triangles, especially at the larger longitudes. In Figure 17 is displayed the results of Van Diggelen's measurements of the photometric function obtained with a surface which was 36% occupied with cups. As can be seen, agreement is by no means exact. In Figure 18, we see Van Diggelen's results for a plate that is 100% occupied with cups and covered with magnesium oxide as well as with a black powder. Again, the results are seen to be not too satisfactory. In Figure 19 we see his results for a plate which is occupied 100% with humps, which is again not satisfactory.

Two more cases will be discussed which are somewhat amusing, perhaps, but in fact seem to point to the correct solution of the problem. Van Diggelen investigated a surface covered by seeds and also a surface covered by lichen - in particular, 'Cladonia Rangiferina'. The measured properties of these surfaces compared with the four standard points is given in Figures 20 and 21. By comparing Figure 21 carefully with the experimental data from the four standard points, it can be seen that the photometric properties of the lichen surface are a very good approximation to the lunar surface. A comment by Minnaert (1961) on this agreement may be in order. He says: "Van Diggelen's attempt to reproduce the optical properties of the lunar surface by a thick layer of the loosely ramified lichen 'Cladonia Rangiferina' was particularly successful. As a result of the smallness of the lunar gravitation

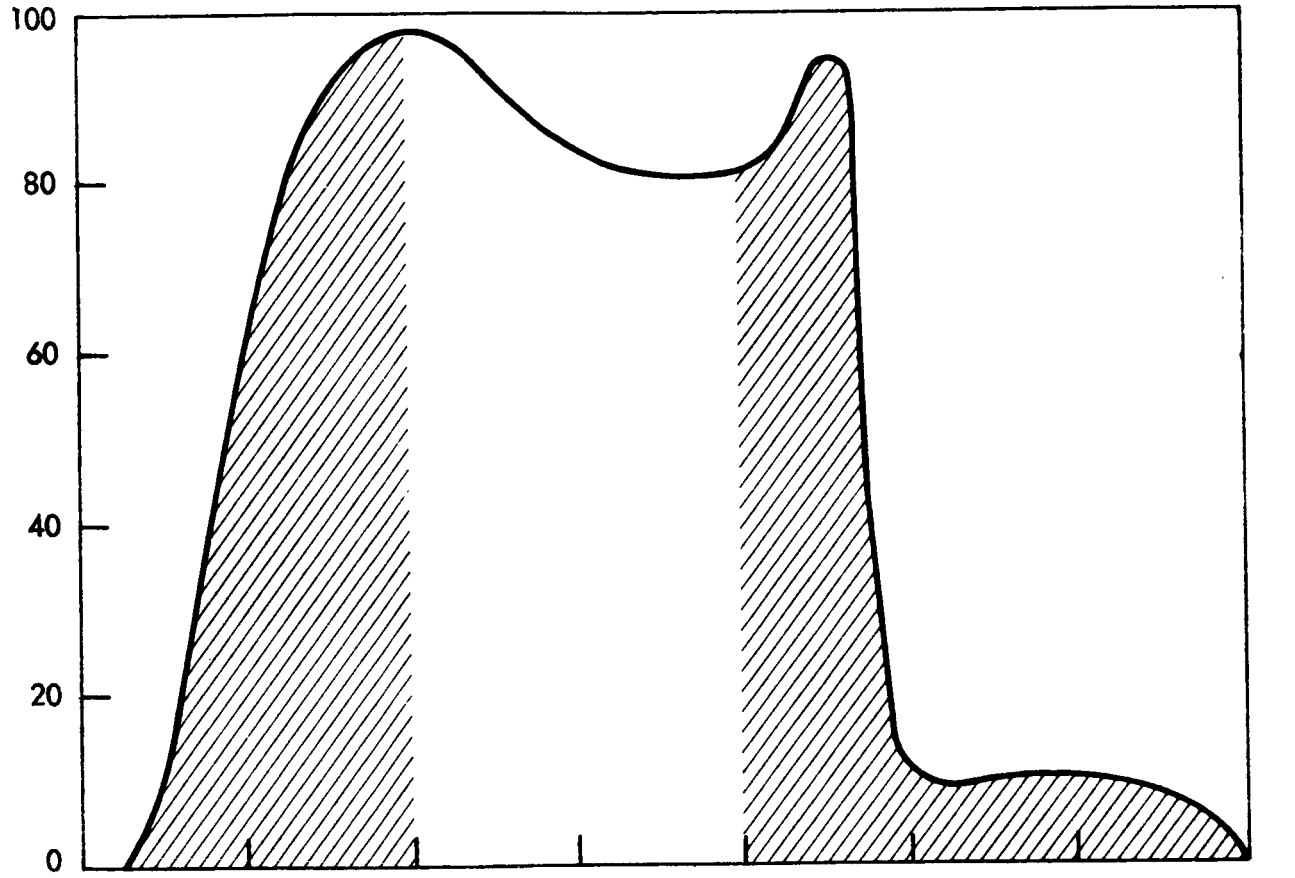

STATISTICAL DISTRIBUTION OF
LUNAR ALBEDO VALUES
(AFTER SYTINSKAYA, 1953)

Figure 15

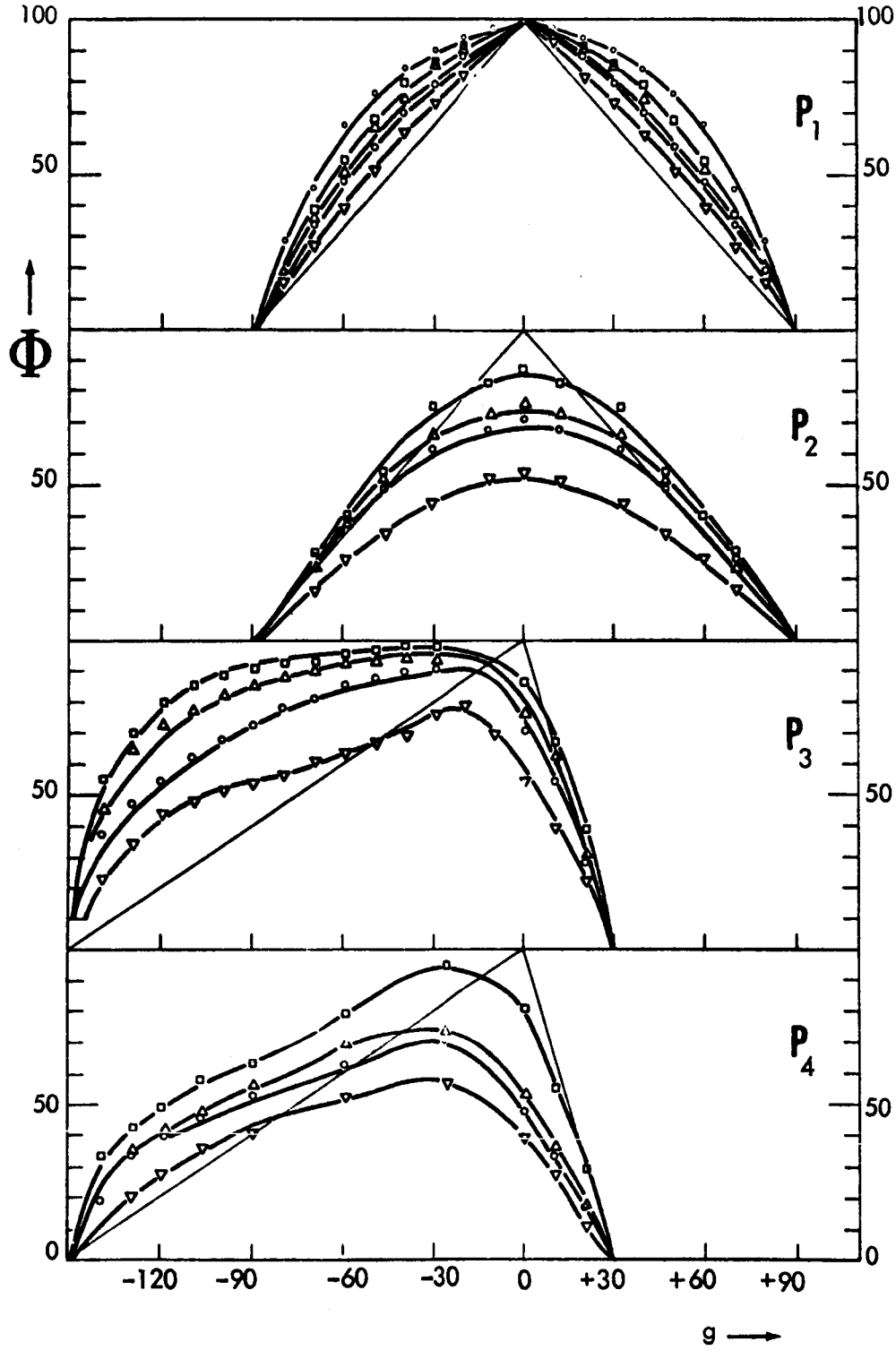

FIGURE 16 LUNATION CURVES FOR DIFFERENT VOLCANIC ASHES LOCATED AT THE FOUR STANDARD POINTS.

- □ Vesuvius sand 1830.
- △ Vesuvius sand 1894.
- ○ Vesuvius ashes 1906 coarse.
- ▽ ashes Asama Yama 1901.
- ● ashes Vesuvius 1906 fine.

(after Van Diggelen, 1959)

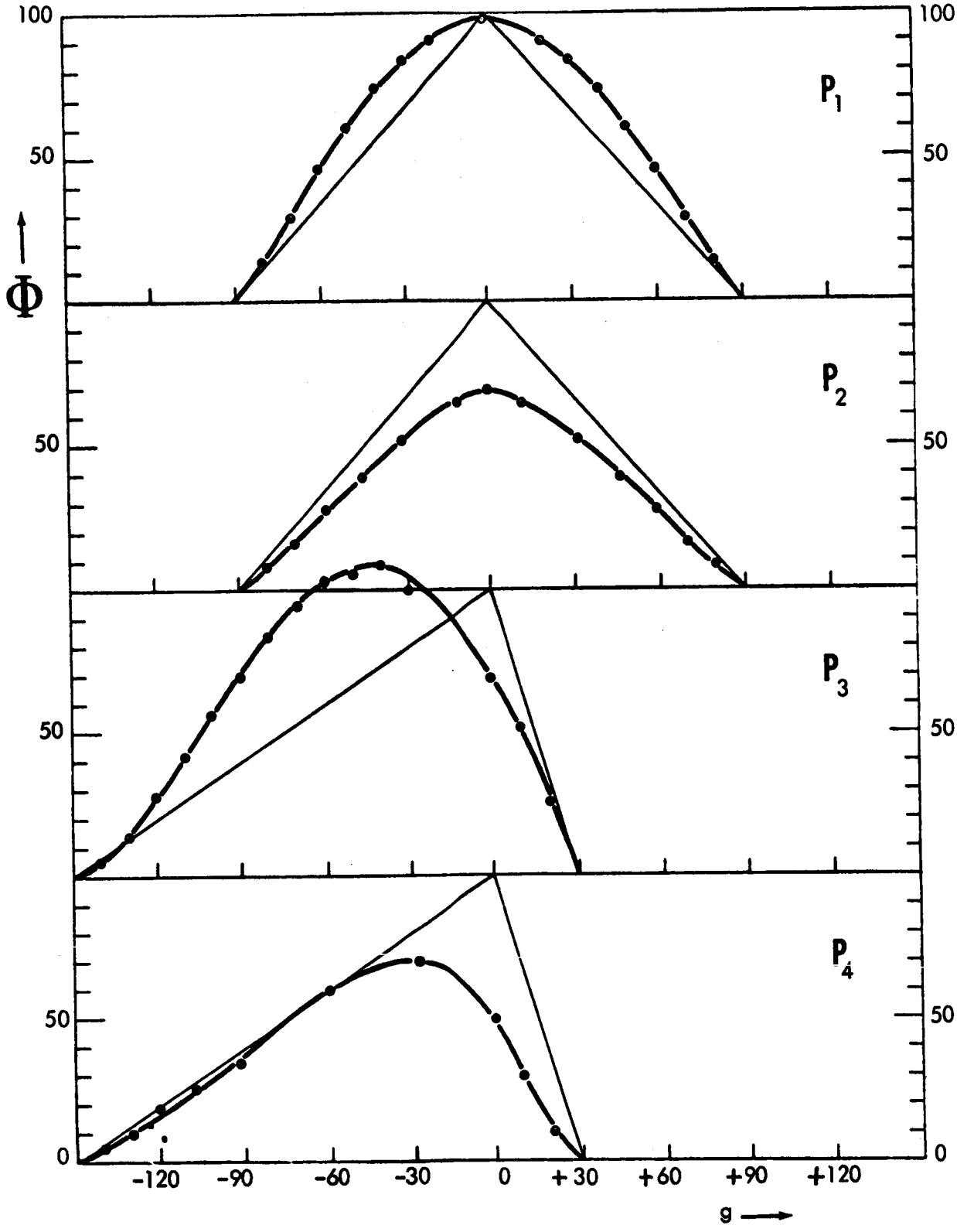

FIGURE 17 LUNATION CURVES FOR A PLATE OCCUPIED 36% WITH CUPS LOCATED AT THE FOUR STANDARD POINTS.

(after Van Diggelen, 1959)

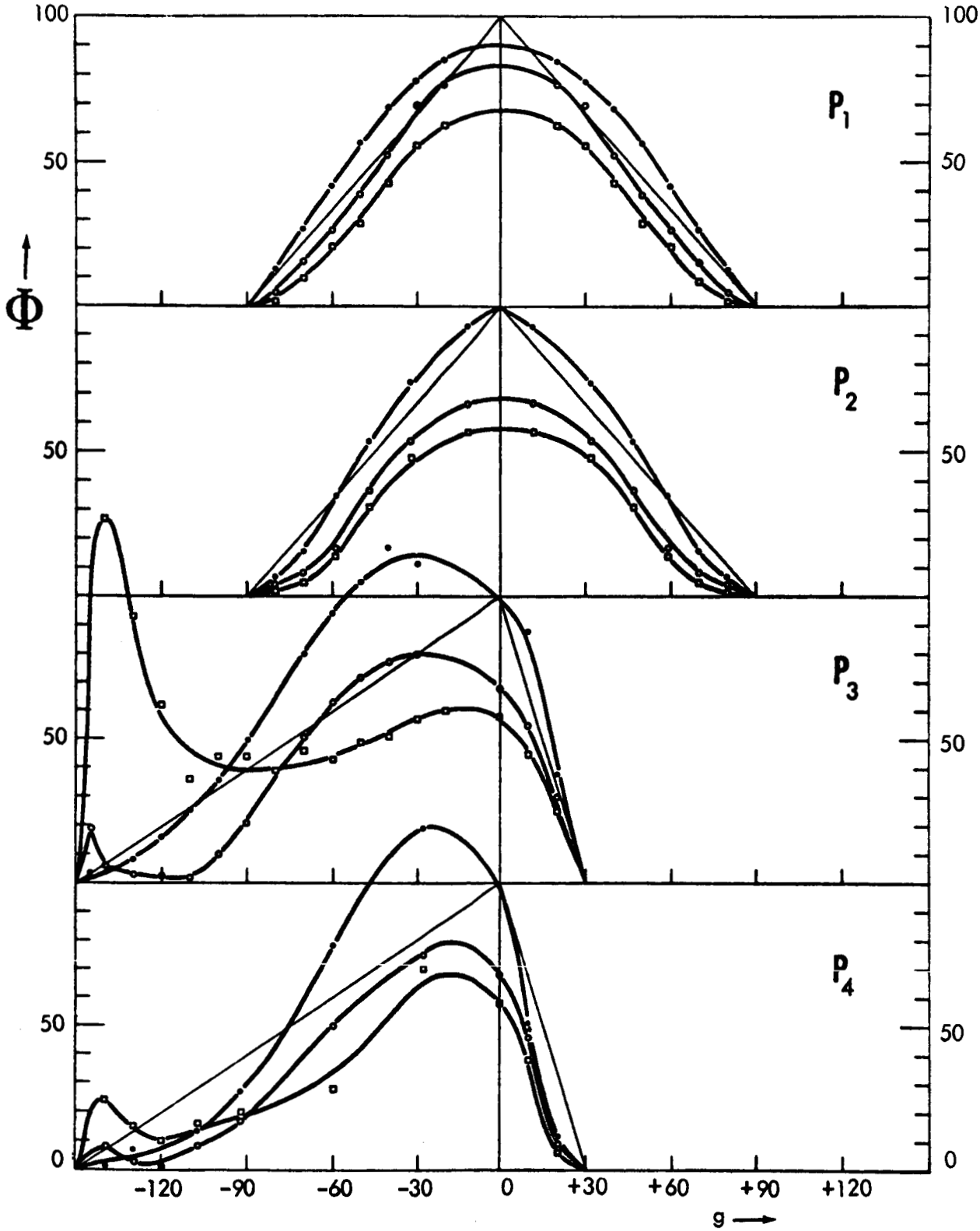

FIGURE 18 LUNATION CURVES MEASURED FOR A PLATE OCCUPIED 100% WITH CUPS AND COVERED WITH MAGNESIUM-OXIDE (Filled circles), A GRAY MIXTURE (Open circles), AND BLACK NORIT-POWDER (Squares) LOCATED AT THE FOUR STANDARD POINTS.

(after Van Diggelen, 1959)

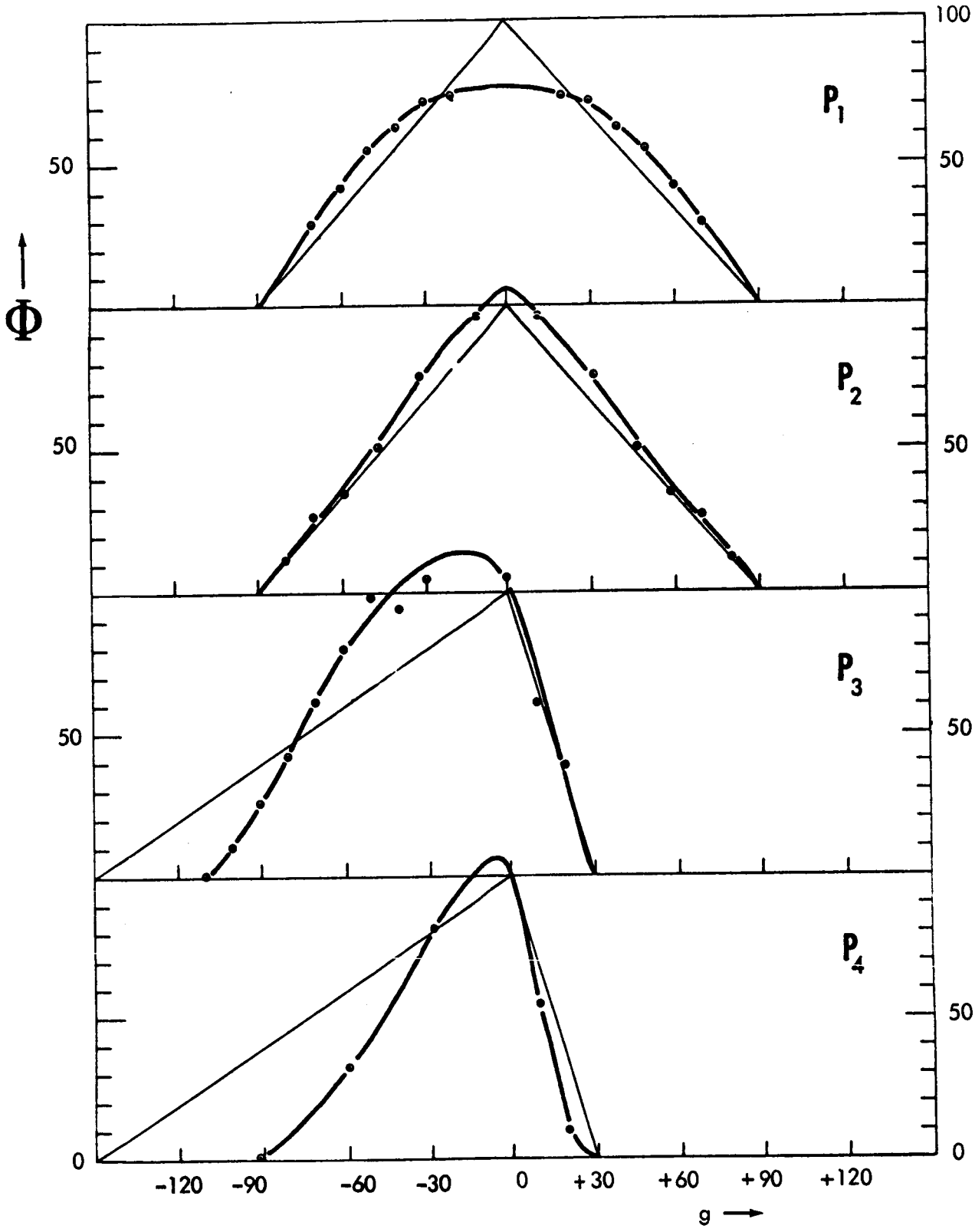

FIGURE 19 LUNATION CURVES FOR A PLATE OCCUPIED 100 % WITH HUMPS LOCATED AT THE FOUR STANDARD POINTS.
(after Van Diggelen, 1959)

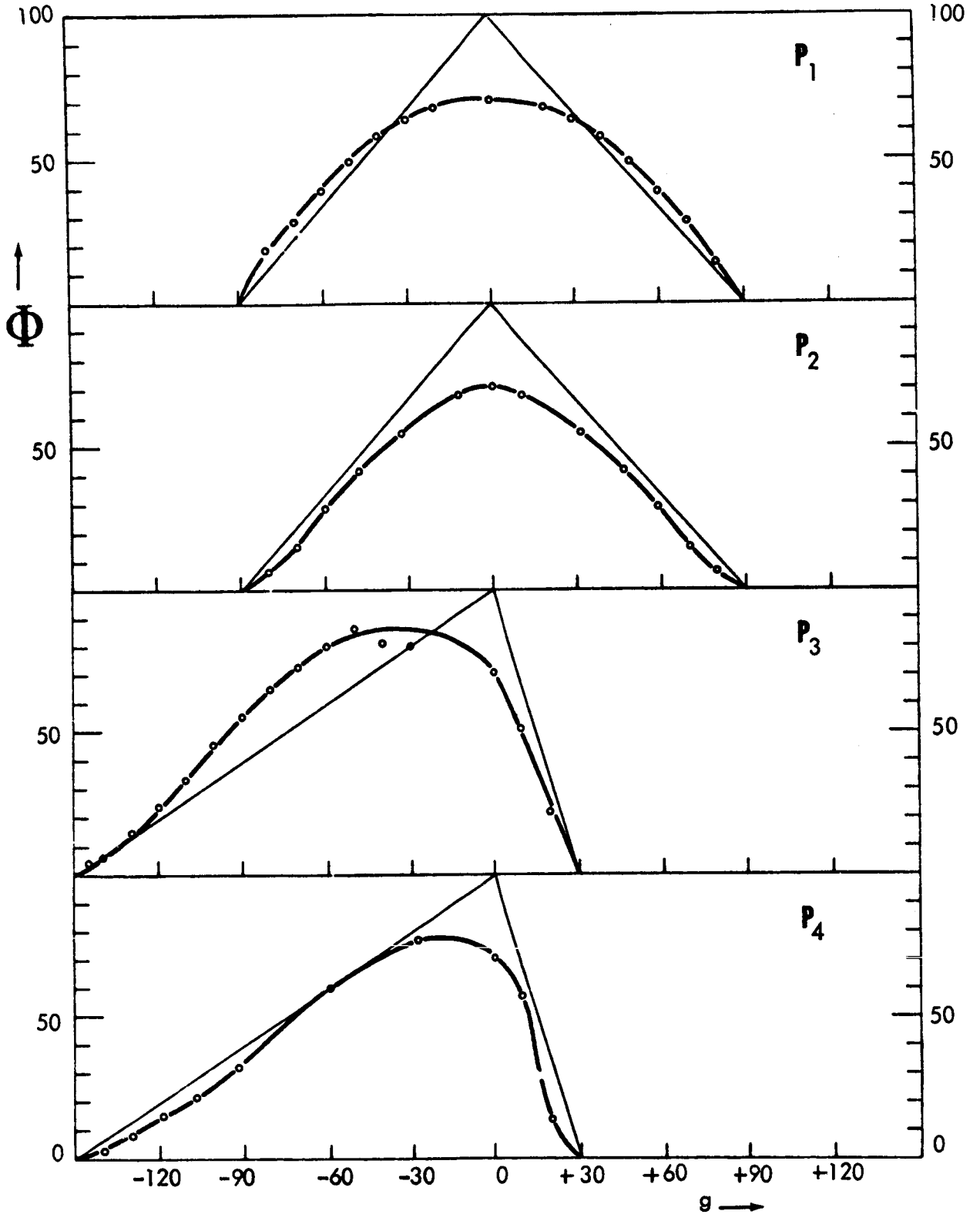

Figure 20 LUNATION CURVES OF A FLAT PLATE, COVERED BY SEEDS LOCATED AT THE FOUR STANDARD POINTS.
(after Van Diggelen, 1959)

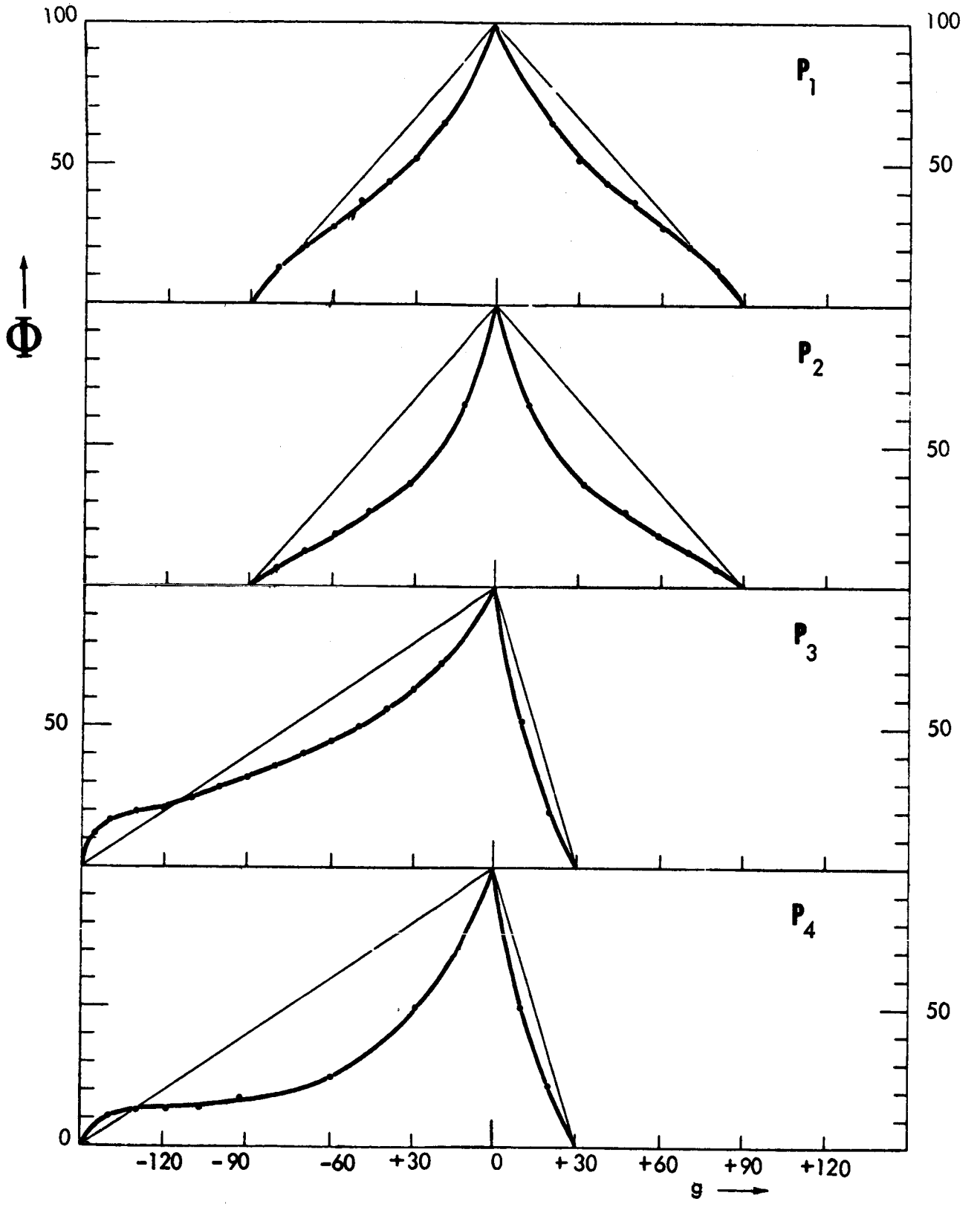

Figure 21 LUNATION CURVES FOR A LAYER OF THE LICHEN CLADONIA RANGIFERINA LOCATED AT THE FOUR STANDARD POINTS.
(Compare with Figure 6) (after Van Diggelen, 1959)

force, very loose surface formations may be formed, with properties similar to those of our model. The true structure may be intermediate between this and the hemi-ellipsoidal cup."

Of course, one should not infer from this result that the surface of the moon is made of lichen or "reindeer" moss. Rather, one has one's view strengthened that the surface of the moon is made up of a fine mesh of highly absorbing material whose structure is sufficiently interconnected to afford extensive shadowing.

VIII. A RECENT THEORETICAL PHOTOMETRIC FUNCTION

Hapke (1963) in a recent paper has derived an expression for the photometric function of a layer which is a complex interconnected matrix of particles. As a starting point he utilized the Schoenberg-Lommel-Seeliger law (see Appendix A, page 2). He chose as the particle scattering function

$$f(g) = \frac{\sin(g) + (\pi - g)\cos(g)}{\pi},$$

a function which strongly back scatters. This function was derived by Schoenberg (van de Hulst, 1957) and represents the scattering from a randomly oriented particle with rough faces.

In addition to choosing f(g) to be a strong back-scattering function, Hapke accounted for the blockage of the "line of sight" of one particle by another. The basis of this part of his analysis is the observation that a light ray which has penetrated into the matrix to a given depth before being scattered has a "preferred" direction for escaping, namely along that direction from which it entered. To quote Hapke: "A simple model which takes into account this effect can be constructed as follows: Instead of considering the idealized surface as a homogeneous, absorbing medium, let the surface layer be made up of circular tubes of radius of the same order of magnitude as the average spacing between particles and whose axes remain always parallel to the direction of the incident of radiation. Light entering the cylinder is attenuated exponentially. Light rays reflected at a given depth of the cylinder at such an angle as to pass through the walls of the cylinder in which they are reflected are also exponentially attenuated in proportion to their path length, as in Lommel-Seeliger scattering, but reflected rays which do not intersect the wall and pass out through the ends of the tube are not attenuated at all."

To account for this "preferred" direction effect, Hapke, using his model, calculated what he has called the retro-directive function, B(g,p), which is only a function of the phase angle, g, and the parameter, $p = \frac{2r}{\lambda}$ (r is the radius of a tube, and λ is just the mean-free-path as in the Schoenberg-Lommel-Seeliger Law).

Hapke's photometric function, using the nomenclature of Appendix A, and normalized to equal ρ at its maximum value, is

$$\Phi(g,p) = \frac{\rho}{1 + \frac{\cos\varepsilon}{\cos i}} \cdot \frac{\sin|g| + (\pi - |g|)\cos|g|}{\pi} \cdot B(g,p), \text{ where}$$

$$B(g,p) = \begin{cases} 2 - \frac{\tan|g|}{2p}\left(1 - e^{-p/\tan|g|}\right)\left(3 - e^{-p/\tan|g|}\right); & |g| \leq \frac{\pi}{2} \\ 1; & |g| \geq \pi/2 \end{cases}$$

where ρ is the reflectivity of a scattering particle. It will be noted that $\Phi(g,p)$ is just the Schoenberg-Lommel-Seeliger Law multiplied by B(g,p), Hapke's retrodirective function.

$\Phi(g,p)$ is plotted (after dividing by ρ) for several different values of the parameter p in Figure 22. In Figures 23 to 27 are displayed the comparisons between Hapke's photometric function (for p = 0.8) and the data for the four crescents of Van Diggelen. In Figure 28 is a comparison of Hapke's function (for p = 0.6) compared at point #123 of Fedorets, which is a mountainous region near Mare Nectaris.

As can be seen, the general agreement between the phase angle dependence of the photometric function and the experimental data is seen to be quite good. Most of these theoretical curves are characterized by p having a value of 0.8 which corresponds to a surface layer 75% of the volume of which is a void (i.e., only 25% occupied by material particles)*. This result is in agreement with results from radiometric measurements of the lunar surface emission. Troitski (1962), Salomonovich (1962), and Cudaback (1962) have found that the lunar surface must have an "effective" dielectric constant $\varepsilon < 1.5$. Since most solid materials have dielectric constant values of about 4 to 5, this result implies about an 80% void for lunar surface layer.

Hapke has also calculated the integral lunar brightness, $\mathcal{A}$, (obtained by integration of $\Phi(g,\alpha)$ over a lunar hemisphere. $\mathcal{A}$ is shown in Figure 29 compared with the experimental data of Rougier, from which the agreement is seen to be exceptionally close.

* Hapke's "best" value of p = 0.6 yields an 85% void.

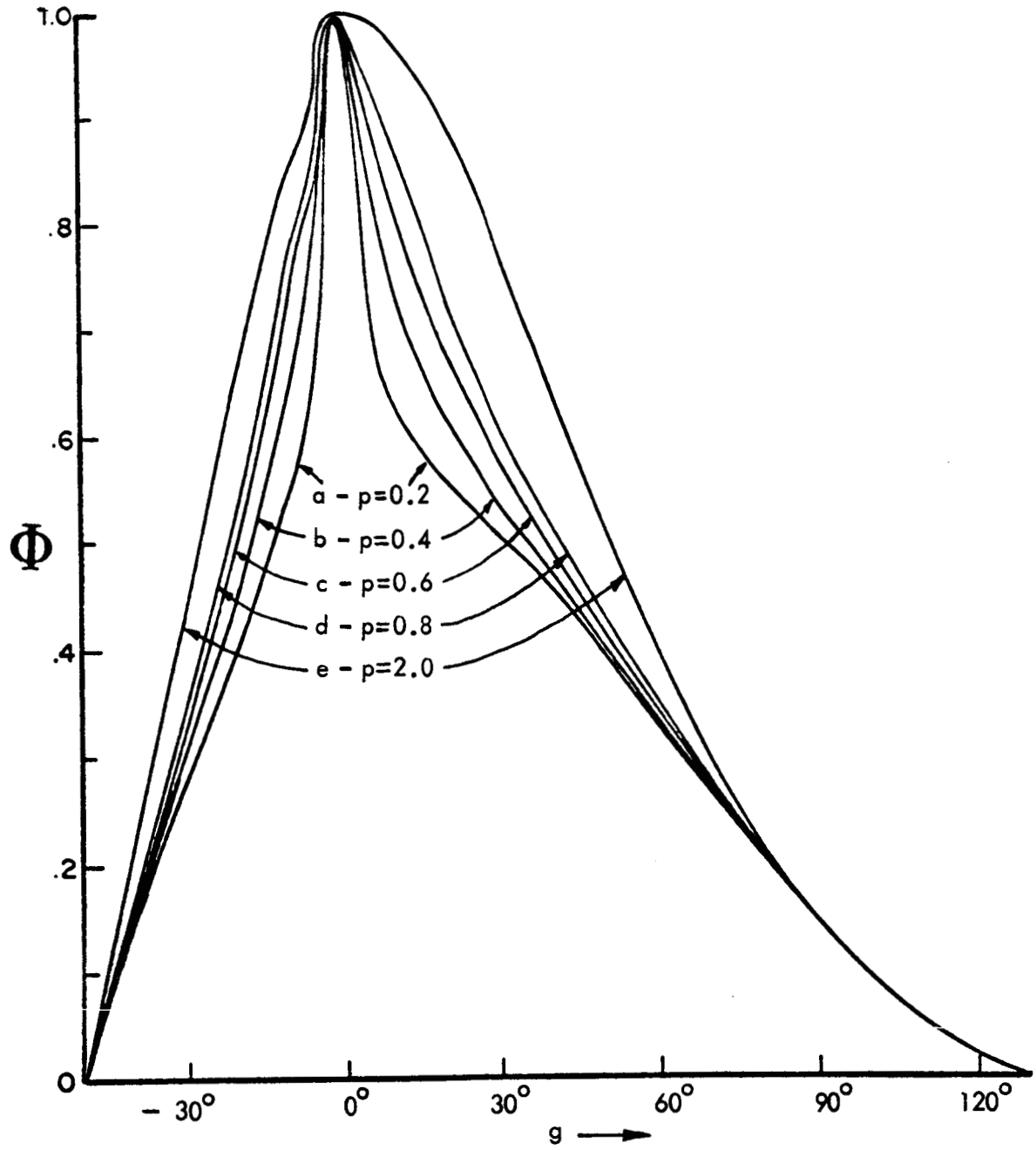

FIGURE 22 HAPKE'S THEORETICAL PHOTOMETRIC FUNCTION VERSUS g FOR $\alpha = 40^{\circ}$.

(after Hapke 1963)

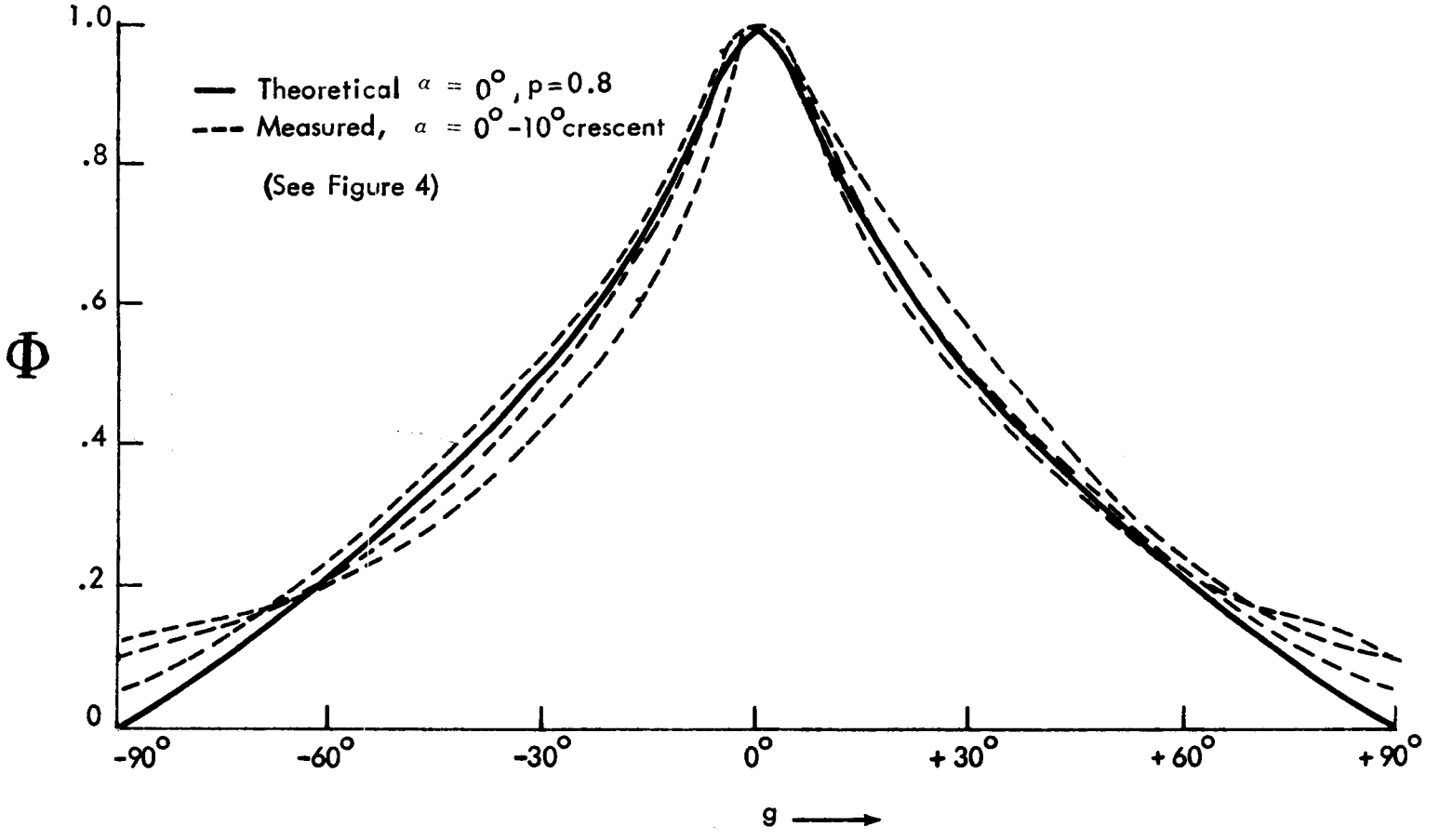

Figure 23 COMPARISON OF HAPKE'S FUNCTION WITH MEASUREMENT. (after Hapke 1963)

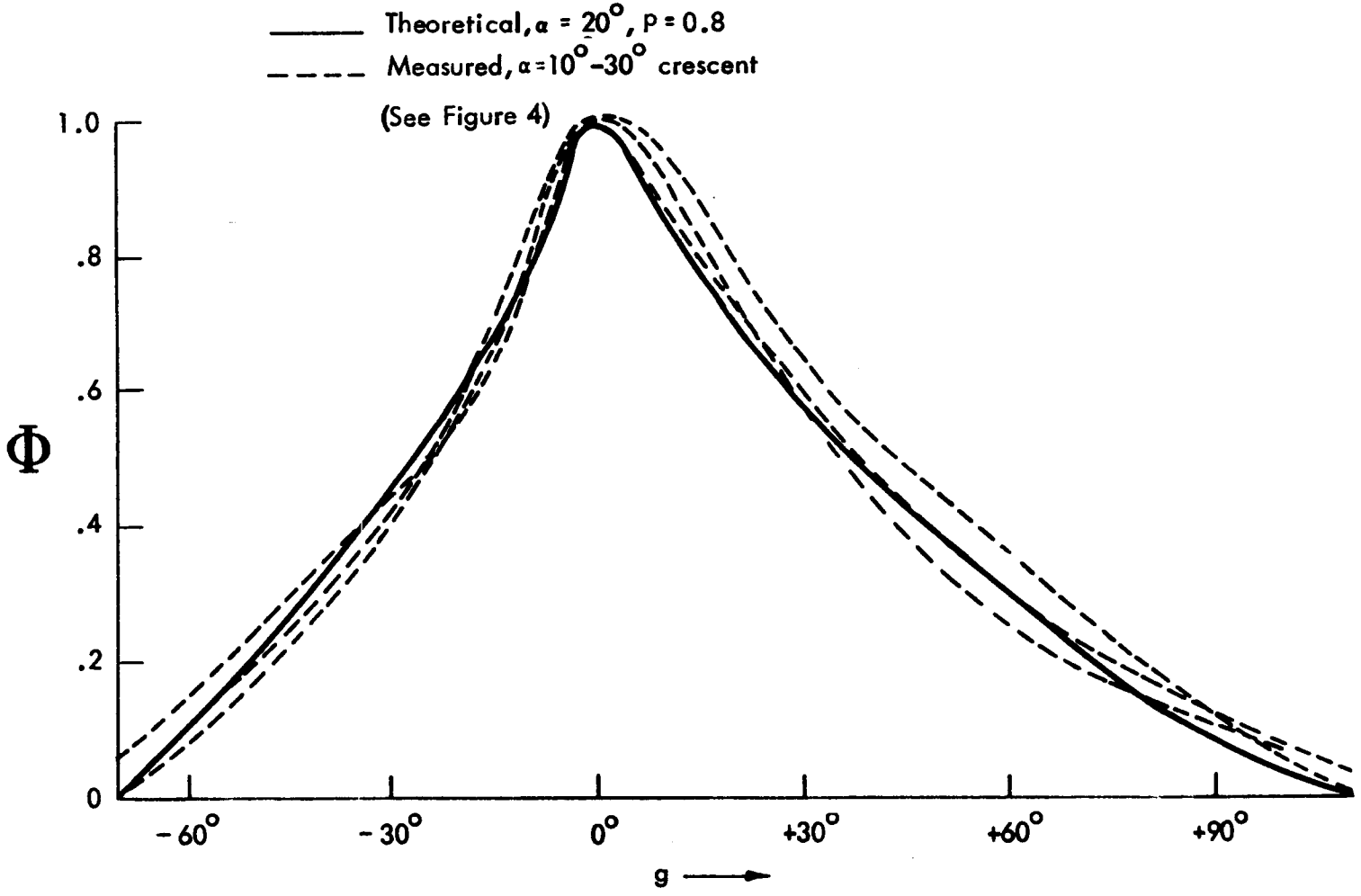

Figure 24 COMPARISON OF HAPKE'S FUNCTION WITH MEASUREMENT. (after Hapke 1963)

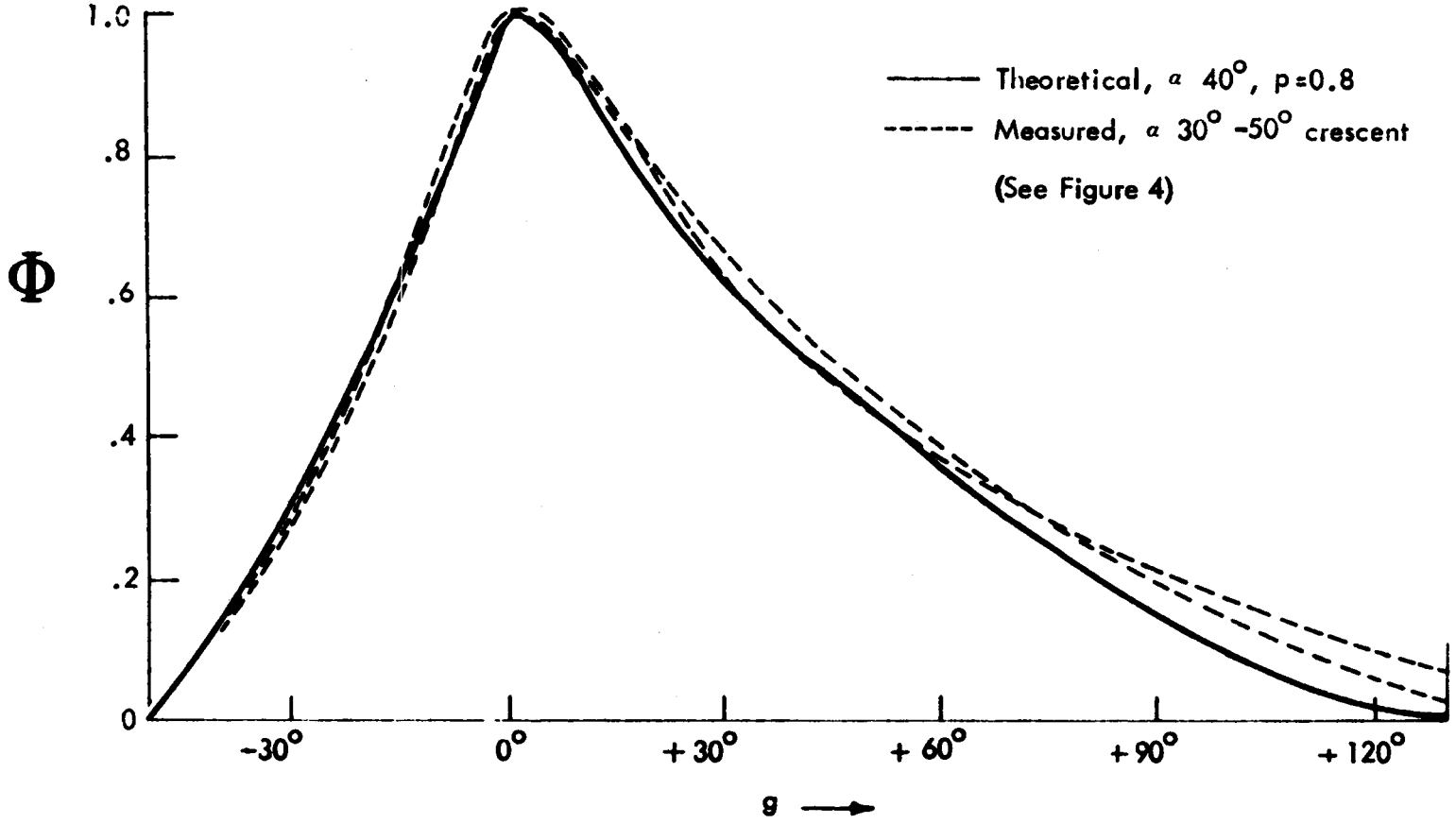

Figure 25 COMPARISON OF HAPKE'S FUNCTION WITH MEASUREMENT. (after Hapke 1963)

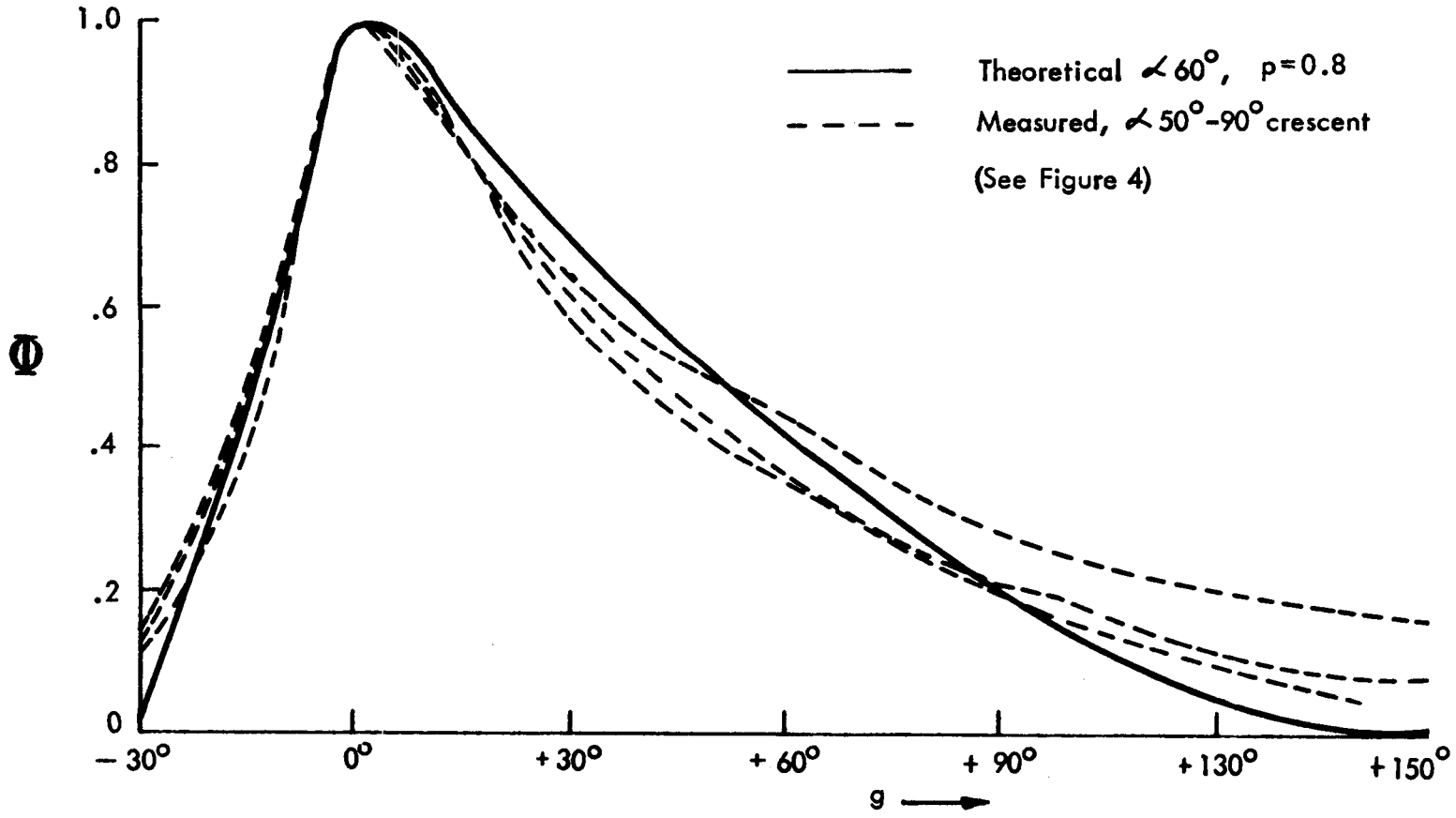

Figure 26 COMPARISON OF HAPKE'S FUNCTION WITH MEASUREMENT. (after Hapke 1963)

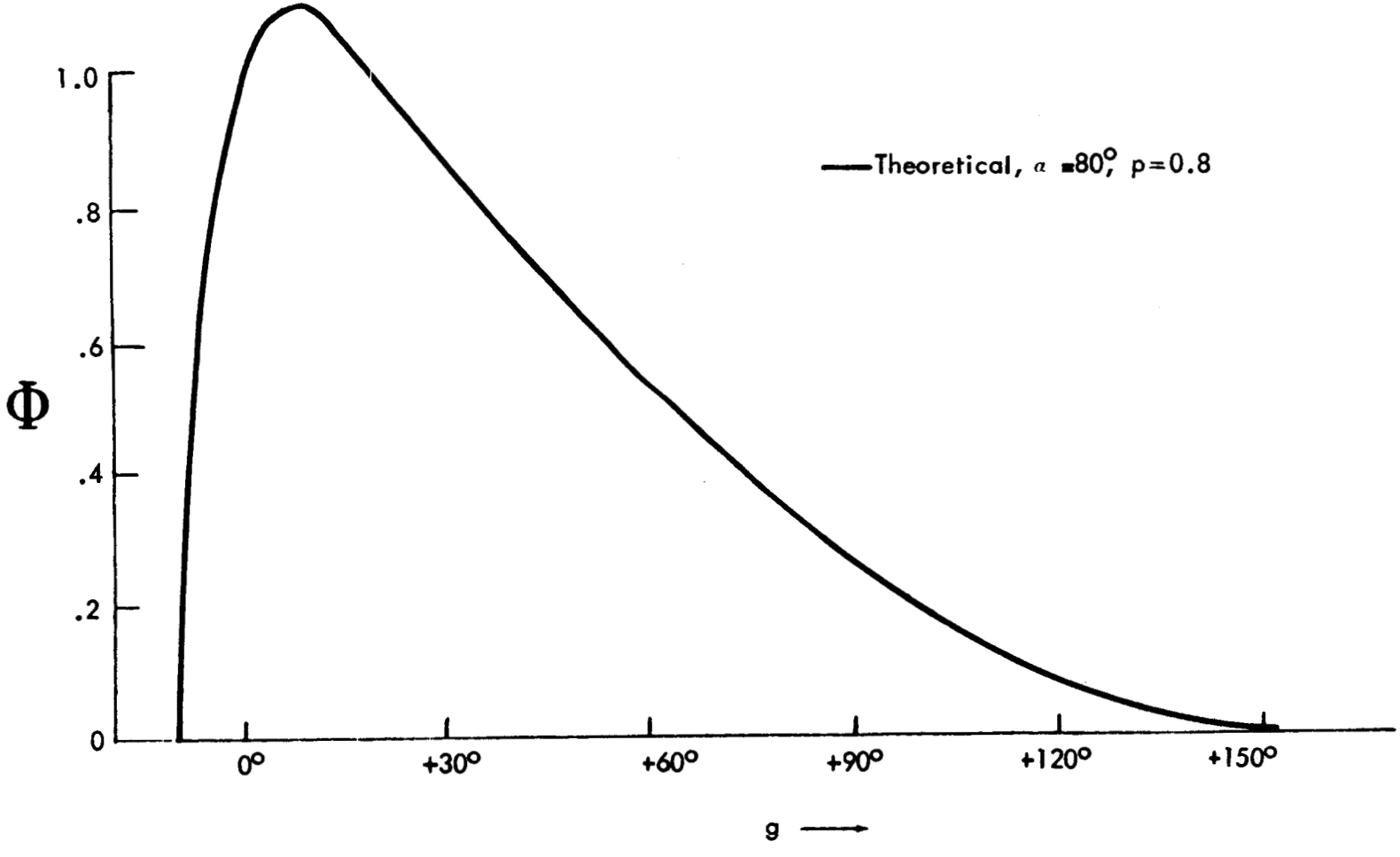

Figure 27 HAPKE'S PHOTOMETRIC FUNCTION. (after Hapke 1963)

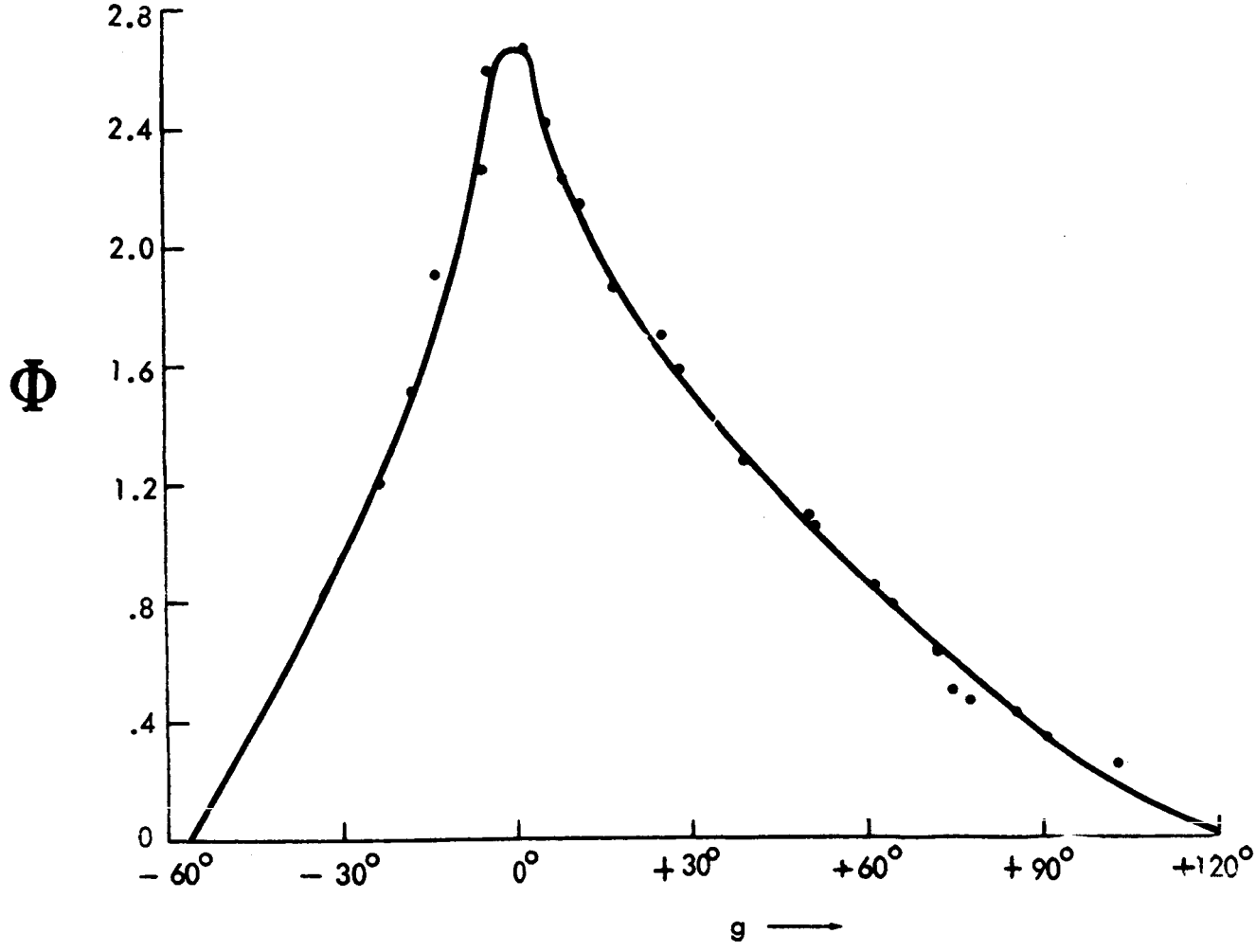

Figure 28 COMPARISON OF HAPKE'S FUNCTION WITH MEASUREMENT.
(after Hapke 1963)

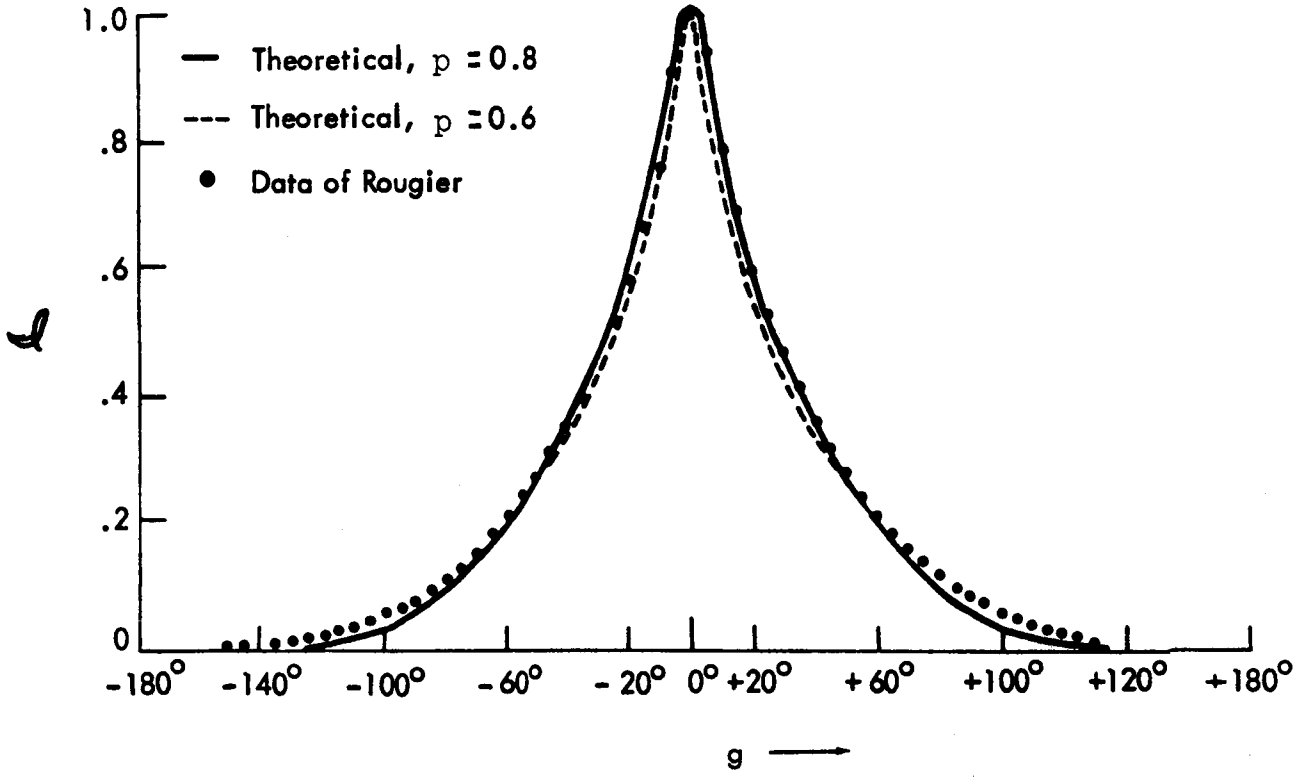

Figure 29 INTEGRAL LUNAR BRIGHTNESS (after Hapke 1963)

Byrne (Private Communication) has compared the curve of the Hapke function for g = -40° with individual data points obtained from the data of Fedorets (1952) and Orlova (1956) (Figure 30). As can be seen, one might say that there is fair agreement of the experimental data with the theoretical curve in the region between α = -40° to α = +40°, but from α = -40° to α = -90° the agreement is seen to be not satisfactory.

Hapke and Van Horn (1962) have succeeded in constructing a reflecting surface composed of what they refer to as "fairy castles" by sifting fine particulate matter, having average grain diameters of about 20 microns or 1/50 mm. They have found experimentally that the photometric behavior of these structures very closely matches that of the lunar photometric function. However, the polarization versus phase angle behavior of their "fair castle" surface has been found to not agree with lunar polarization behavior. This perhaps is not too surprising in view of the fact that they did not attempt to duplicate the agglomeration sizes (tenths of a millimeter) found by Lyot and Dollfus to give the correct lunar polarization versus phase angle behavior.

IX. LUNAR COLORIMETRIC MEASUREMENTS

Let us examine the column of Table I (following page 9) marked "Color Excess". The color excess is defined by the equation $D = C-C_o$, where C is the color index of a given object illuminated by natural or artificial sunlight, and C_o is the color index of the sun. (For definition of color index see Appendix B).

For a neutral reflecting surface D is zero. For substances which have a bluish color, D will be negative, while for yellow, brownish, and reddish materials it will be positive. In commenting on the differences in color indices of objects on a lunar surface, we shall quote Sharonov (1962) who says: "Another feature which indicates the uniformity of the outer cover of the moon is the very small differences in color according to the data in the new colorimetric catalog of lunar objects, based on visual colorimetric observations conducted by me at the Tashkent Astronomical Observatory, the extreme differences in the color index, including errors in the measurement, do not exceed 0.11. The average

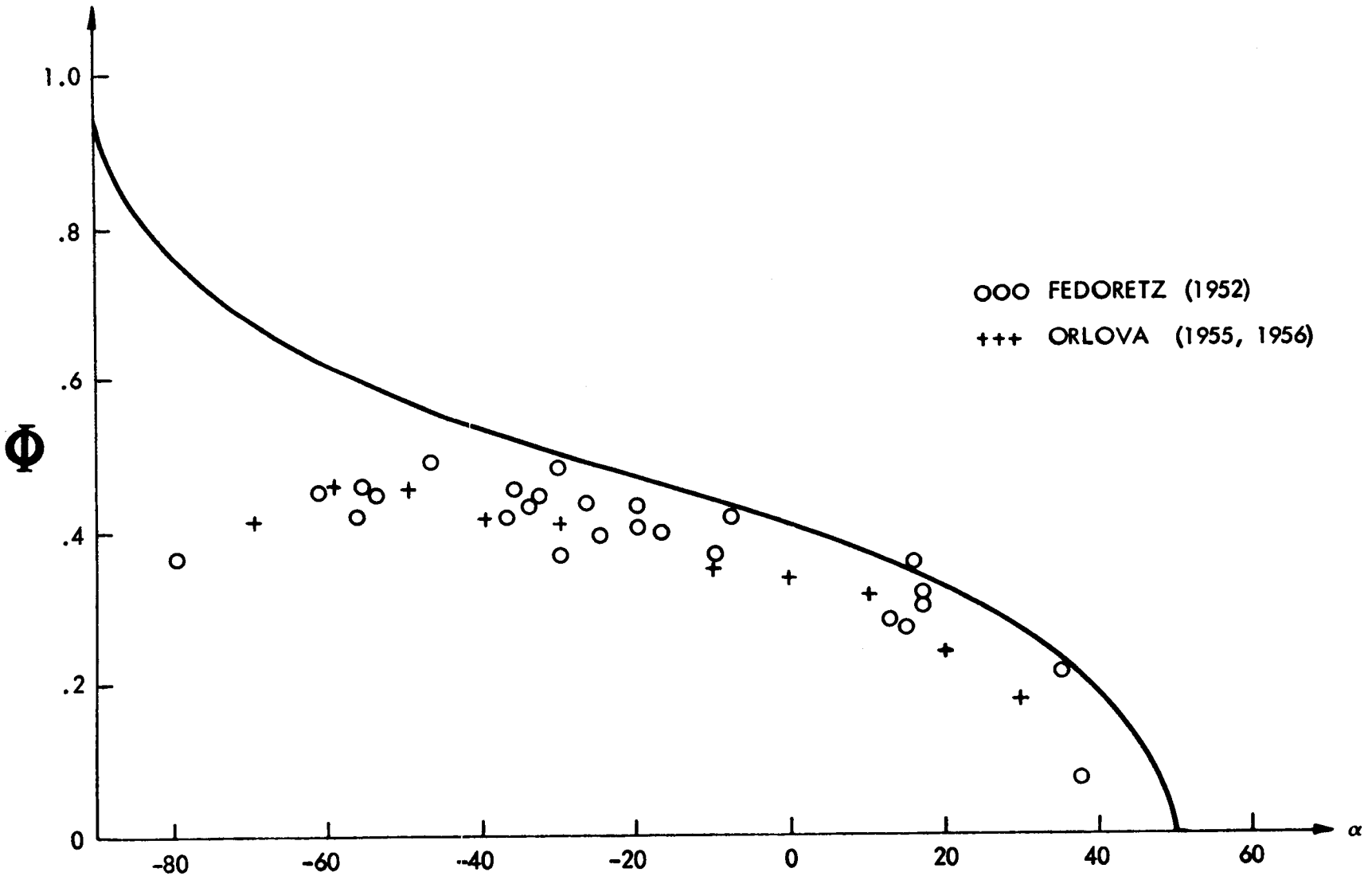

Figure 30 HAPKE'S PHOTOMETRIC FUNCTION (p=0.8 g=-40°). (AFTER BYRNE, 1963)

value for the color expressed by the difference, D, of the color indices of the moon and the sun amount to about 0.35. The continents and in general the bright parts are on the average a little redder than the maria which can be seen from the numbers given in Table I. The dispersion of the color for the maria and other dark objects was found to be somewhat larger than for the bright parts. However, a careful and repeated study of the disc of the moon conducted under great magnification with the aid of reflectors and refractors did not reveal a single small object whose color appreciably differed from that of the background."

X. EXPERIMENTAL POLARIMETRIC STUDIES

Light rays, upon being reflected from an object, may be partially polarized. The "plane of vision" is defined by the requirement that the incident ($\vec{S}$) and emergent ($\vec{O}$) direction vectors lie in it (see Figure 31). Let $|E_1|$ and $|E_2|$ be the maximum and minimum intensities of the electric vector, respectively. A third parameter, θ, is the angle between the polarization vector (i.e., electric vector maximum), $\vec{E}(\theta)$, and the normal to the plane of vision, $\vec{O} \times \vec{S}$. The polarization is then defined by $P = (|E_1| - |E_2|)/(|E_1| + |E_2|)$. The polarization curve of P versus g, the angle between the incident and emergent directions, is an important source of information concerning the light reflecting properties of a surface area.

The polarization of the light from the moon is determined essentially by the microstructure of the lunar surface and is not affected by the hills and valleys which, of course, do have an effect on the intensity of the reflected light. Polarization data reveal the fine structure of the surface, which would be seen if it were examined under a microscope. About 150 years ago, Arago first observed that lunar light was indeed polarized. In 1860, Secchi discovered the polarization vector to be perpendicular to the plane of vision (i.e., $\theta = 0°$, as would be the case for most terrestrial materials). He found the polarization to be nearly the same in regions composed of different materials but that it is in general slightly larger for the darker regions. Secchi also found that toward first quarter the polarization tends to increase. Other investigators, around the turn of the century, found approximately the same results. Barabashev (1927) obtained numerous results

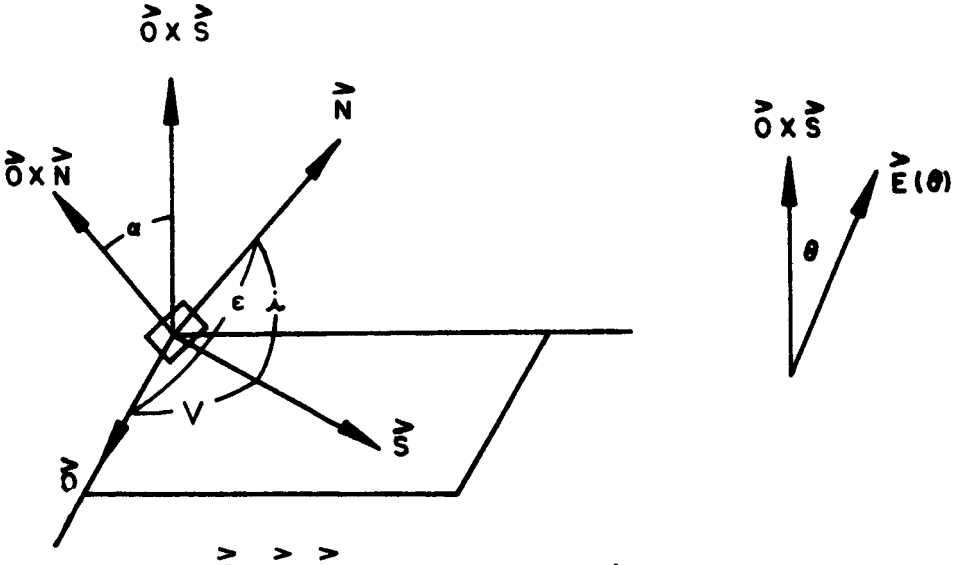

$\vec{O}$, $\vec{N}$, $\vec{S}$ are unit vectors in the directions of the observer, the surface Normal and the source respectively.

If $\alpha = 90^\circ$ $\vec{O}$, $\vec{N}$, $\vec{O} \times \vec{S}$ are coplanar $\epsilon \equiv L$ (Lateral Inclination).

If $\alpha = 0^\circ$ $\vec{O}$, $\vec{N}$, $\vec{S}$ are coplanar $\epsilon \equiv I$ (inclination in the plane of vision.)

Figure 31 Polarization Coordinate System

on the polarization of lunar light and determined that there were very few, if any, terrestrial materials which have the same polarization characteristics as the moon.

The first detailed observation and precise analysis of the polarization of the lunar light dates primarily to the investigations of Lyot (1924). This success was due essentially to his development of a very sensitive polarimeter. Lyot found that the polarization vector was almost always either perpendicular to or parallel to the plane of vision (i.e., $\theta = 0°$ or $\theta = 90°$). By characterizing the portion of polarized light with $\theta = 0°$ by a (+) sign and that with $\theta = 90°$ by a (-) sign, Lyot introduced what is now called a "curve of polarization" which fairly completely describes the polarization properties of light over all areas of the entire lunar disc. The polarization of the integrated light flux from the moon is shown in Figure 32 as obtained by Lyot (1929). By observing the curve marked A →, we find that the maximum value of the (+) polarization is about 0.088 and by following the curve marked ← A we notice that this maximum value of the polarization is about 0.066. This difference in maxima of polarization in the waning phase (→) of the moon versus the waxing phase (←) of the moon is explained by Dollfus (1962a) to be due to the fact that the maria occupy about twice as large a region in the last quarter of the moon as in the first. To further describe this curve we shall quote Lyot (1929) who says, "about two days before full moon, when the angle of vision has a value of 23°30', the polarization goes to zero and reappears, a few hours later, in a perpendicular plane. It then passes through a negative minimum of 0.012 at an angle of 11°, then bends rapidly enough toward zero so as to disappear at the same time as the angle of vision."

Dollfus has described the studies of Lyot in which he found that the polarization vectors of light from different patches and regions of the surface of the moon were found to have the same direction at each point on the disc with a precision of better than half a degree. It was found that toward the time of quadrature (i.e., $g \rightarrow 90°$) the magnitude of polarization, however, varies greatly from one point to another over the lunar disc and that it has a larger value on the dark regions and smaller value on the bright regions. It was found to vary approximately inversely with the brightness of the measured region. From first quarter to full moon the polarization of all regions diminishes and approaches that

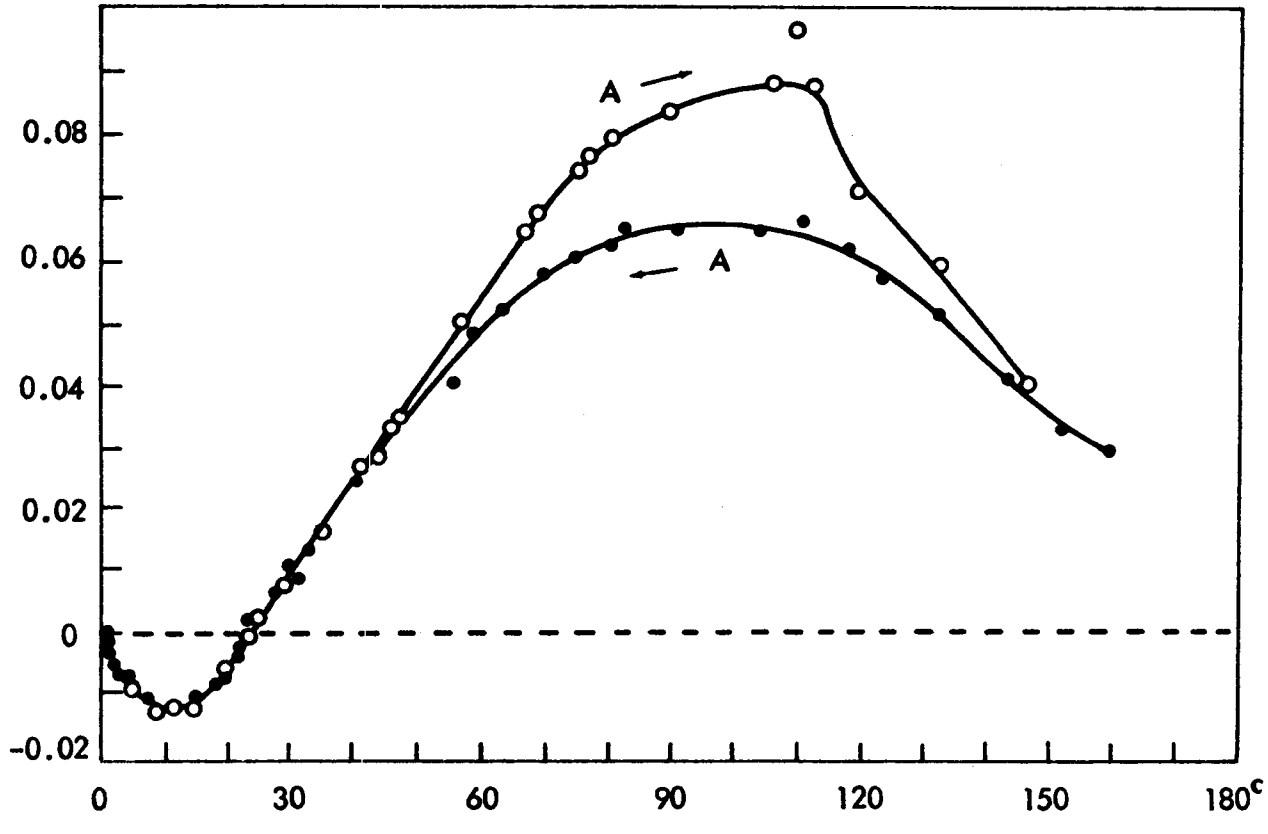

Figure 32 POLARIZATION OF THE MOON (After Lyot , 1929)

value which is obtained for the polarization of the integrated brightness. The difference between the polarization of terrae and the maria, which is quite conspicious around times of quadrature, becomes nearly undetectable. The polarization was also found to be only weakly dependent upon the angle of incidence, but it did increase somewhat toward the terminator, where the incident angle is very large.

In an attempt to understand the polarization curves obtained for the moon, Wright (1929) studied the polarization characteristics of several terrestrial materials. A very systematic continuation of this work has been carried out by Dollfus (1955, 1956). His general study allowed him to classify materials into several groups which made it possible to eliminate numerous substances in an initial attempt to understand the nature of lunar materials and the microrelief of the lunar surface.

Let us now examine the polarization properties, as found by Dollfus (1961a) for several types of materials. In Figure 33, Dollfus has plotted the polarization for milky quartz under various conditions of illumination and observation. His curve labeled (i) relates the polarization versus phase angle V for the surface when viewed normally (i.e., $\epsilon = 0$). An important point to notice is that there is no negative polarization under these conditions. In the Figure labeled (ii) he has plotted the polarization versus the angle L, lateral inclination with the phase angle V as a parameter (see Figure 31 for explanation of g, ϵ, V, L). It can be seen again that there is no negative polarization and that the polarization increases as the angle L increases as well as increases with phase angle. The curve labeled (iii) displays the polarization versus, I, the inclination of the plane of vision. It should be noted that maximum polarization occurs at the condition for specular reflection (i.e., when the angle of incidence is equal to the angle of emergence) in all cases. It should also be noted that the peak polarization values tend to increase as the phase angle increases (i.e., approaches the grazing angle).

In Figures 34 and 35 are given the polarization curves for white sugar, a granular surface, and for sandstone, both of which have a partially absorbing and rough surface. In both of these cases it may be noted that the sharpness of the curve of polarization versus I has diminished but that the peak value of the polarization is still obtained at the specular reflection angle.

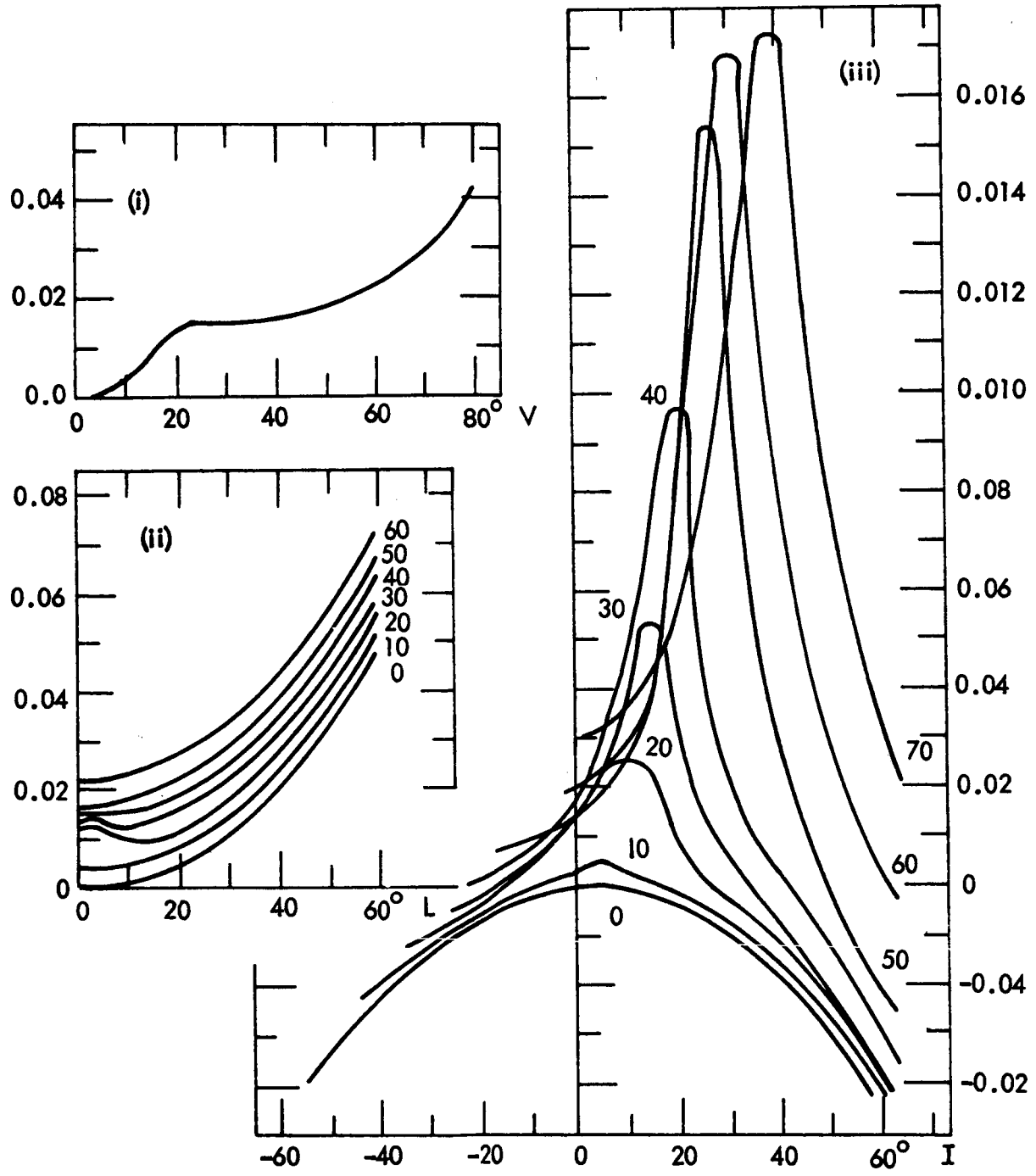

Figure 33 Polarization of light reflected from homogeneous diffusing material with an almost plane surface (milky quartz). Ordinates: polarization P. (i) L=O; (ii) and (iii), values of the phase angle V are given for each curve.
(After Dollfus, 1961 b)

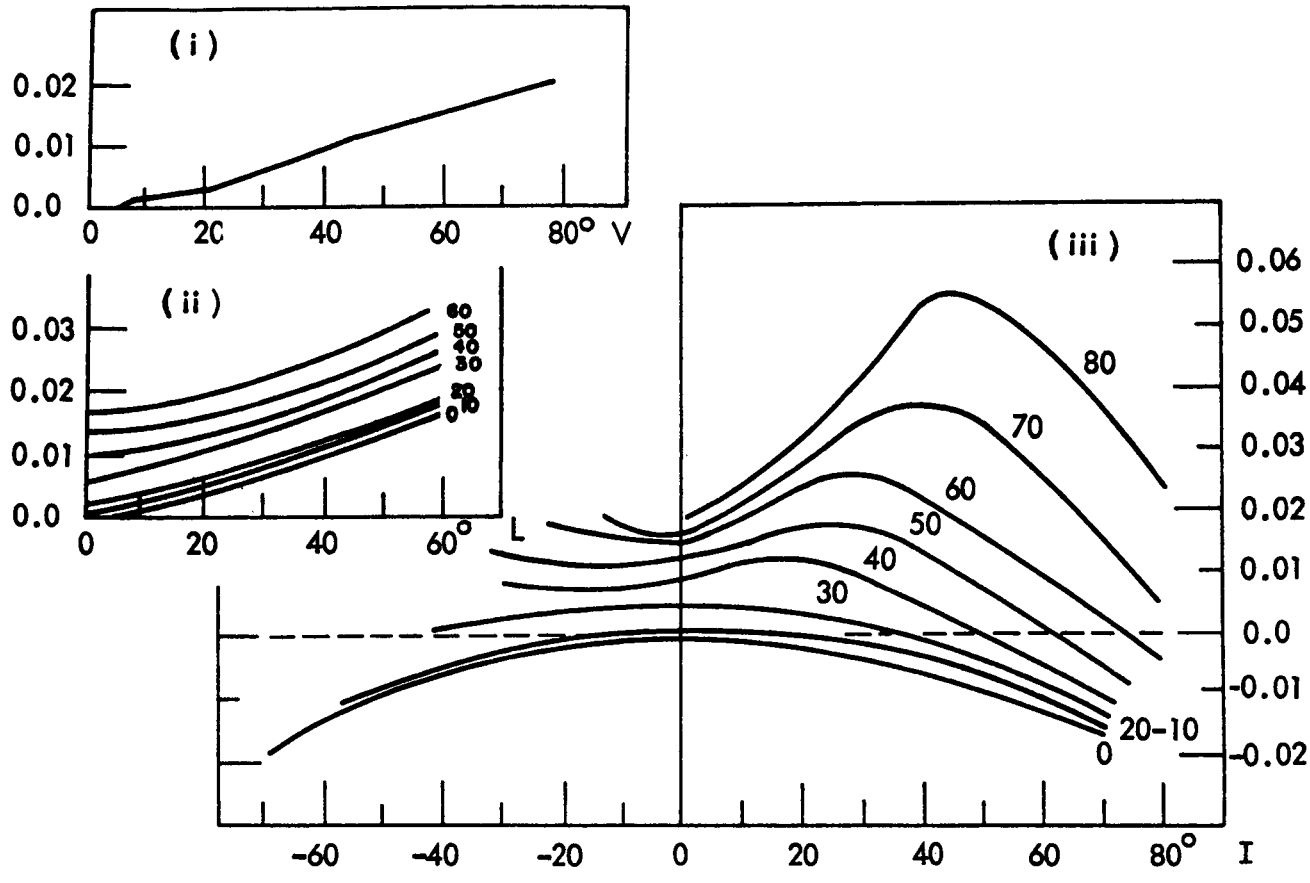

Figure 34 Polarization of light reflected from a piece of white sugar (inhomogeneous material with granular surface).
(after Dollfus, 1961 b).

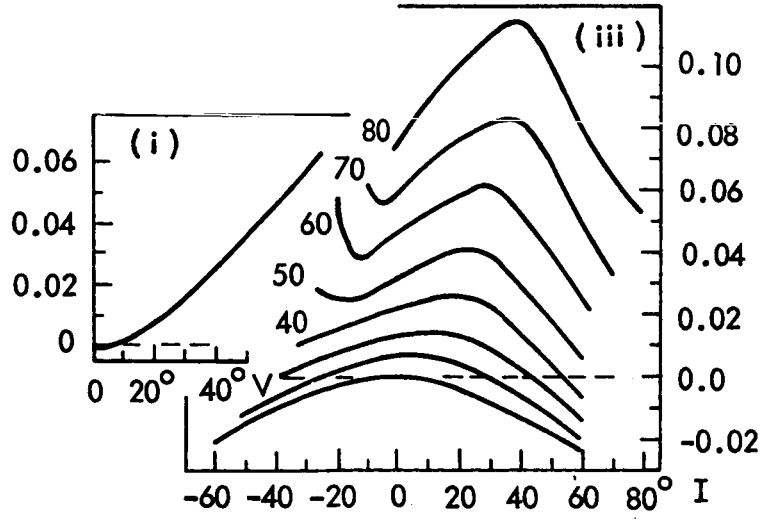

Figure 35 Polarization of light reflected from sandstone containing quartz (partially absorbing with rough surface). (after Dollfus, 1961 b).

In Figure 36 is seen the polarization curves for emery powder. It should be noticed that the polarization versus I curves are virtually flat and have very small peaking at the specular reflection angle. The polarization versus phase angle V, at normal emergence, is seen to develop a negative peak which was not true of previcus examples.

In Figure 37 is seen the polarization curve obtained for iron filings. It can be seen from this figure that, as the filing sizes go from coarse, medium to fine, the negative polarization maximum value increases and the point at which polarization changes from (-) to (+) is shifted to larger values of the phase angle V. In Figure 38 are shown the polarization curves obtained in three cases for antimony powder, carborundum and emery powder. The curves labeled (A) represent fine powders and curves labeled (B) represent agglomerated powders. It should be noted that agglomeration produces larger negative polarization.

From these experimental results we can conclude that to obtain large negative polarization one must have fine grains of material which are strongly absorbing and which are agglomerated.

As has been seen, opaque powdered materials produce a negative branch in the polarization curves, which was first discovered by Lyot (1929). The polarization of light from opaque substances, by necessity, must be due to a purely surface phenomenon (i.e., there can be no internal refraction and re-emergence of light from the particle). Dollfus (1956) found that the negative polarization branch depends strongly upon multiple scattering between grains, as can be seen from the results of a simple experiment he performed. He found that when the grains were in a free-fall stream the negative branch of polarization curve disappears.

We shall quote Dollfus (1961b) in order to describe further the behavior of the negative polarization branch of opaque powders. He says: "The greater the absorption by the powder, the deeper the negative polarization becomes. There is also a dependence on particle size. [Figure 37] shows the curves for coarse, medium, and fine iron filings, respectively, which show that the finest filings have the deepest negative branch. The branch is especially deep for opaque materials ground to very fine grains which themselves are combined into

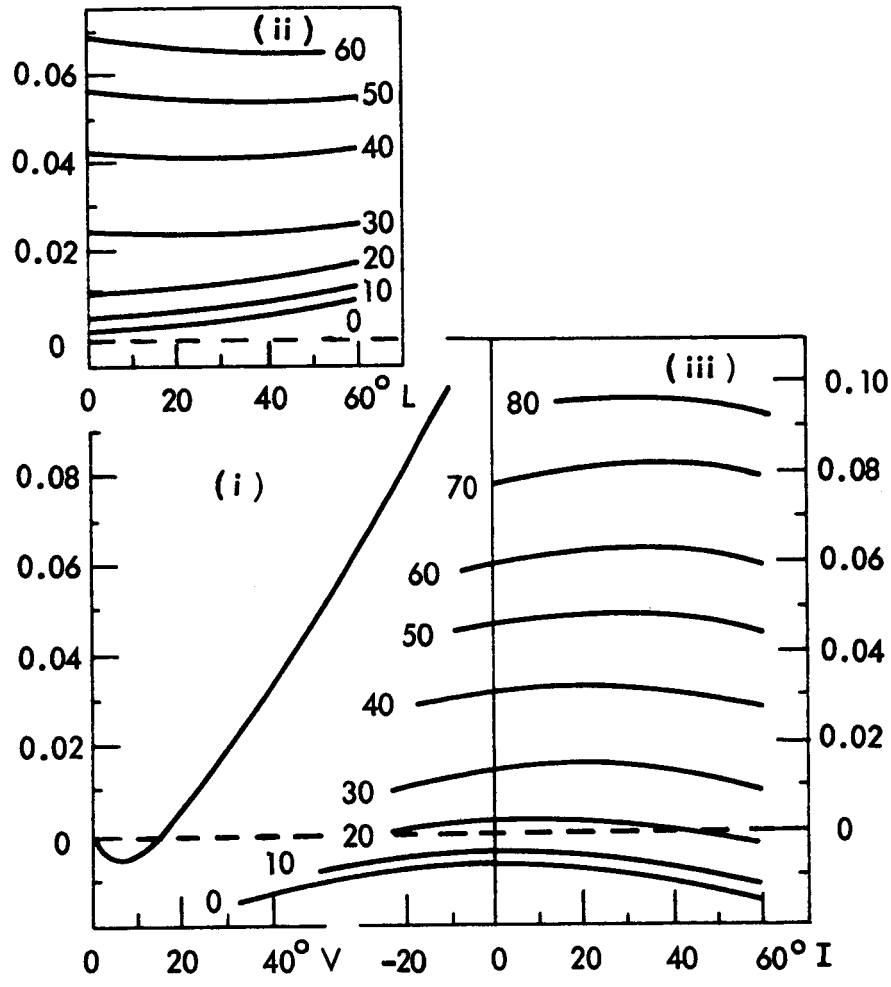

Polarization of light reflected from emery powder (small opaque grains).
Figure 36 (After Dollfus, 1961 b)

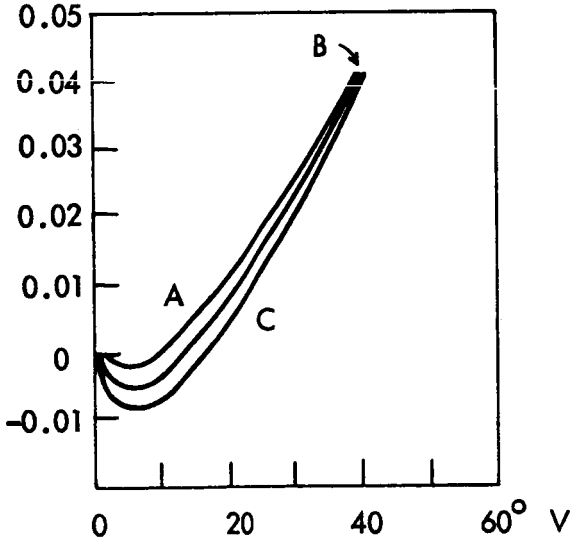

Polarization of light reflected from iron filings: A; coarse, B: medium, C: fine.
(After Dollfus, 1961 b)
Figure 37

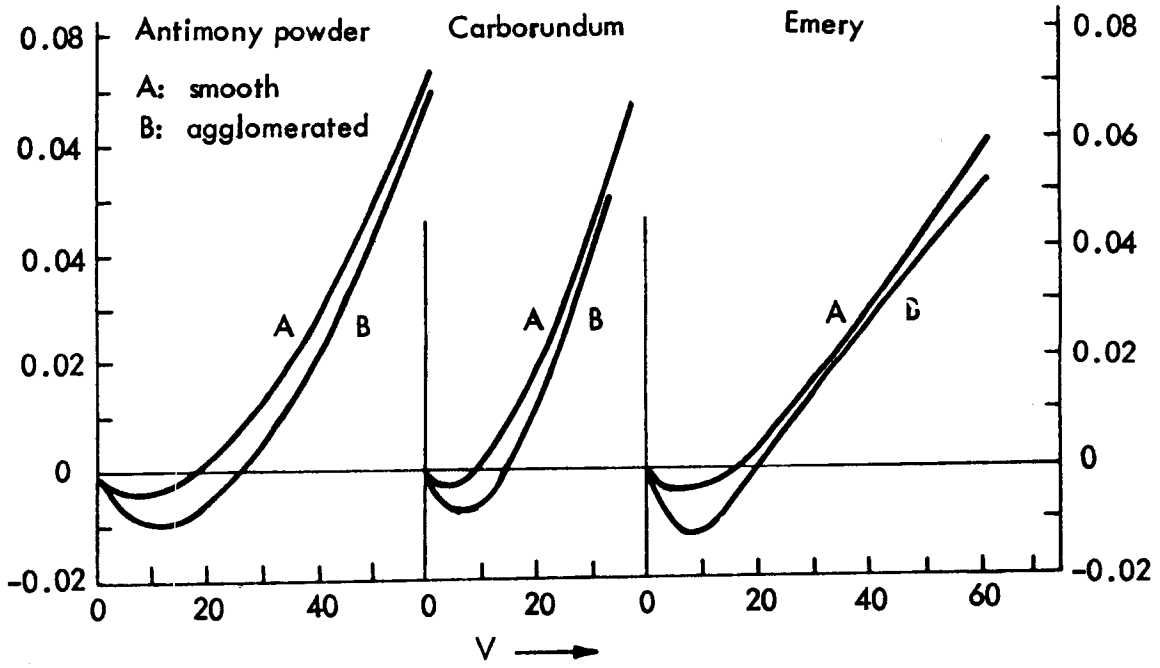

Figure 38 Polarization of light by powders consisting of small, very absorbing, grains (after Dollfus, 1956).

larger grains. This type of curve is observed for the moon, Mercury, both the bright and the dark areas on Mars, and the asteroids."

XII. INTERPRETATION OF THE POLARIZATION OF LIGHT FROM THE MOON

To obtain the French school's interpretation of the polarization of light from the moon, we shall again quote Dollfus (1962b). He says, "The polarization of light from the moon is exactly that of granular opaque substances previously studied. We must conclude therefore that the lunar surface is covered with a very absorbent powder having a constitution similar to that of volcanic ash. This powder could be spread out in a very thin layer but it apparently must cover all of the surface. Lyot has indicated this result as early as 1929. He had prepared a mixture of volcanic ash in the laboratory matching the optical properties of the lunar ground. The continuous line (Figure 39) shows the polarization of the moon. The dotted curve which is slightly raised shows that of Lyot's mixture."

The researches that followed since have completely confirmed this result (Dollfus, 1955). Figure 40 shows a microscopic view of volcanic ash having the observed polarization characteristics of the bright regions of the lunar ground.

XIII. RECENT POLARIMETRIC STUDIES

Kohan (1962) recently has investigated the polarization properties of the moon with a newly developed rotating polaroid device which permitted him to measure low values of polarization with a high degree of accuracy at phase angles close to full moon. The salient points of his results are: (a) The angle of orientation of the plane of polarization for a given phase angle does not depend upon the position of the detail on the lunar surface (i.e., it does not depend upon the angle of emergence ϵ). (b) It, however, does depend strongly upon the absolute value of the phase angle. At large values of phase angle the electric vector's maximum intensity was found to be perpendicular to the photometric equator (i.e., $\theta = 0$) and a rapid rotation of the maximum electric vector begins at about phase angle $\psi^\circ = 40^\circ$ and at $\psi^\circ = 10^\circ$ it becomes approximately equal to 90°, returning to zero once more at

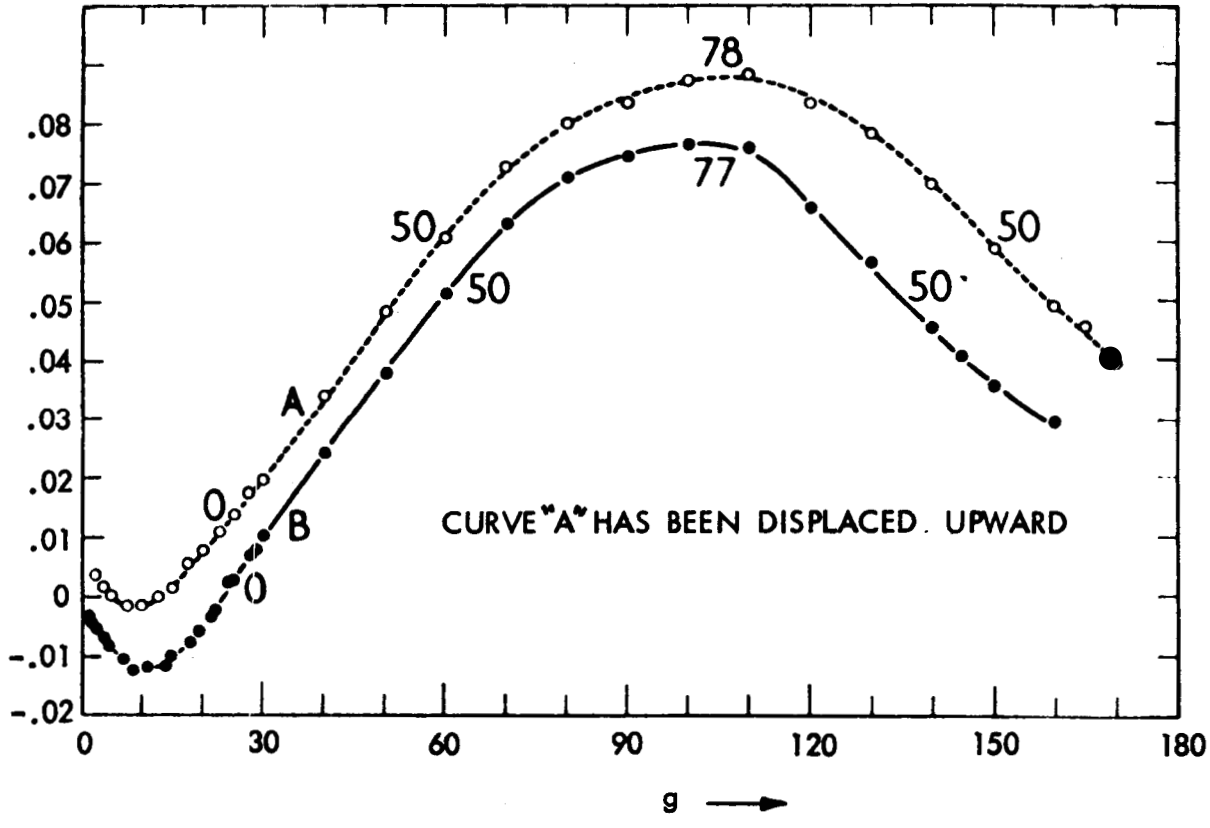

FIGURE 39 POLARIZATION OF LIGHT OF THE MOON AND OF SOME MIXTURES OF VOLCANIC ASHES (after Lyot , 1929).

A = MIXTURE OF ASHES WITH AN ALBEDO OF 0·13.
B = MEAN CURVE FOR YTHE MOON

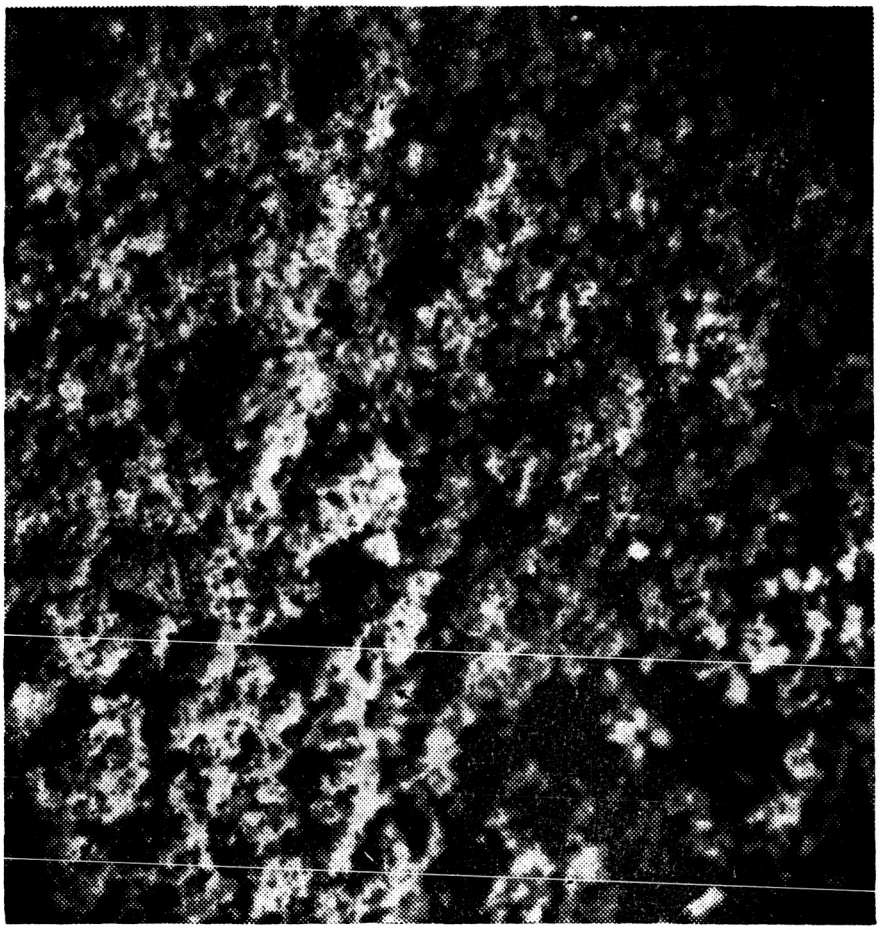

FIGURE 40 AN EXAMPLE OF ASH WITH VERY DARK GRAINS, REPRODUCING THE OBSERVED POLARIZATION PROPERTIES OF THE LUNAR GROUND. DIMENSIONS OF THE FIELD: 3 X 3 MM.

zero phase angle. The results of his measurements of the polarization angle of moonlight are found in Figure 41.

Kohan also investigated terrestrial specimens in the non-pulverized as well as in the pulverized state having grain dimensions of $0.25mm<d<1mm$; $1mm<d<3mm$ at various angles of incidence and two angles of reflection ($\epsilon = 0$ and $\epsilon = 45°$). In Figure 42 are shown the resultant angular positions of the maximum electric vector versus phase angle, $\psi°$ of four different materials. Curve number I designates the polarization curve for granite, II-for tuff, III-for ocherous limonite, IV-for slag. As can be seen from an examination of Figure 42, no one of the specimens had a polarization angle versus phase angle dependence that is nearly so steep as the moon. In specimens III and IV, it can be seen that, although they have steeper slopes than curves I and II, the breakpoint occurs at a much smaller phase angle than that of the moon. A summary of Kohan's experimental investigations is as follows. He says: "In case of terrestrial rock, the angle of orientation of the plane of polarization:

a. Does not depend upon the degree of pulverization.
b. Does not depend upon the angle of reflection at which observations are made.
c. Depends upon the phase angle $\psi°$, and at large phase angles the direction of polarization is perpendicular to the plane passing through the specimen, illuminator and electropolarimeter; a rapid rotation of the plane of polarization begins at approximately $\psi° = 28°$.
d. In the case of limonite and volcanic slag, the most rapid rotation of the polarization plane is observed, which is similar to the rotation of the polarization plane of moonlight. In other terrestrial rock, including volcanic tuff, the angle of rotation is considerably smaller. In contrast to the similar nature of the rotation of the plane of polarization of different regions of the lunar surface, the degree of polarization exhibits greater variety. The maximum degree of polarization of different lunar features decreases in the following order: maria, bays, crater maria, craters with central peaks and the continents. [Figure 43] shows the dependence of the maximum degree

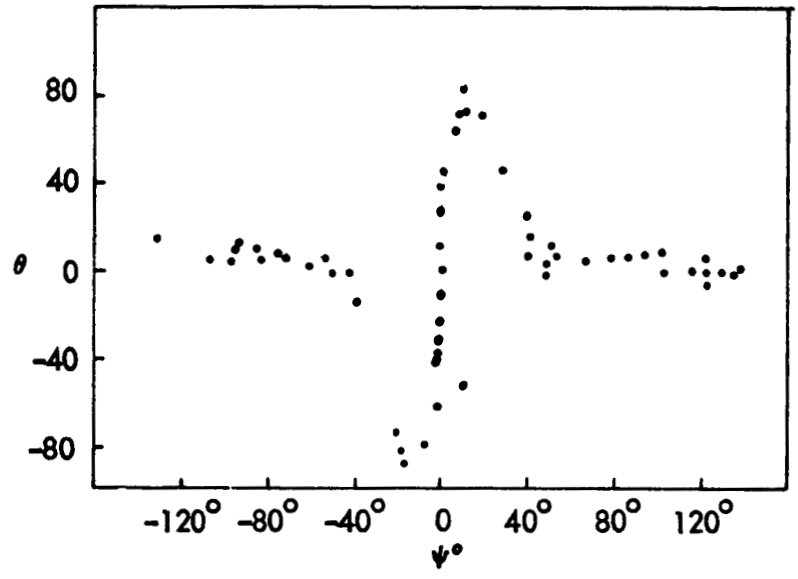

Figure 41 LUNAR POLARIZATION ANGLE θ VERSUS LUNAR PHASE ANGLE $\psi°$.

(after Kohan 1963)

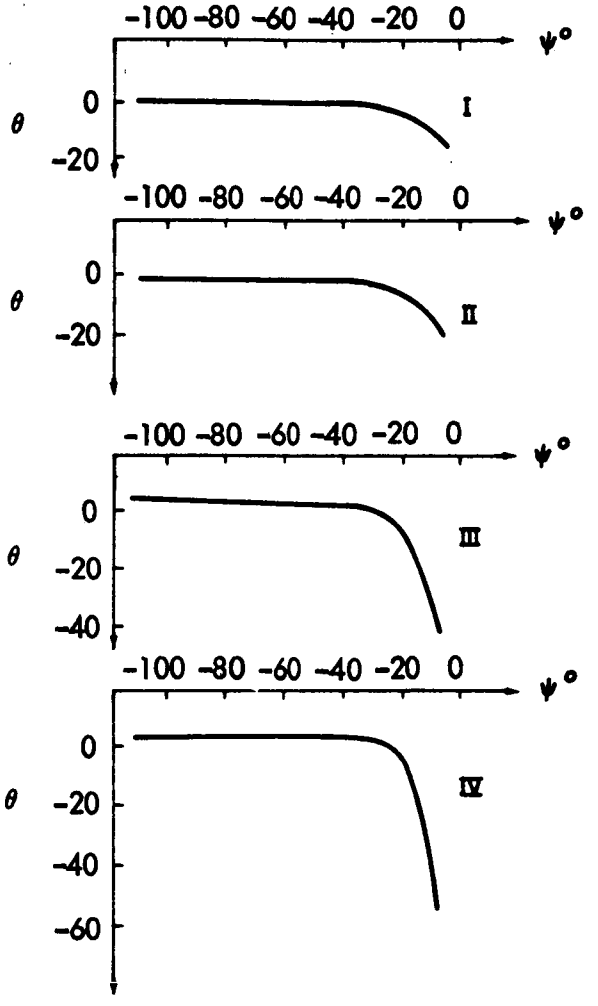

Figure 42 LUNAR POLARIZATION ANGLE θ VERSUS LUNAR PHASE ANGLE ψ° FOR GRANITE I ; TUFF i; OCHEROUS LIMONITE III; SLAG IV.

(after Kohan 1963)

of polarization, found by our measurement, on the maximum brightness of the given detail according to Fedorets. Exactly the same dependence is also obtained for the terrestrial rocks, (Figure 44), where we plotted the magnitudes of the degree of polarization at $\psi^\circ = 80^\circ$ for various degrees of pulverization, taken from the graph, which shows the dependence of the degree of polarization on the phase angle, and corresponding values of relative brightness obtained by the same instruments. From here it is evident that the darker the investigated sample, the greater the polarization. The maximum degree of polarization depends upon the pulverization of the rock, (Figure 45), i.e., the diameter of the grain; the larger the grain, the greater the degree of its polarization."

Based essentially upon the preceding information, Kohan then draws the following conclusions: "As far as change in the angle of orientation of the polarization is concerned, ocherous limonite and volcanic slag match closely the characteristics of moonlight. However, as the degree of pulverization of volcanic slag is larger than that of the moon, it becomes necessary to assume that the polarization characteristics of the lunar surface come closest to that of ocherous limonite. The degree of polarization of limonite is, on the average, equal to the degree of polarization of lunar maria. (Note: for the uninitiated, as is the author of this report, Webster defines limonite as follows: Hydrous ferric-oxide, $Fe_2O_3 \cdot nH_2O$, an important ore of iron, appearing in earthy forms as ochers, and as a yellowish brown powder; called also brown hematite.)

XIV. THEORETICAL POLARIMETRIC CONSIDERATIONS

Ohman (1955) has suggested that an adequate theoretical treatment of the negative polarization could be made by considering multiple scattering between particles. However, he has not carried these calculations far enough to be able to apply them to the experimental data.

The scattering and polarization of light by particles of size comparable to the wave length was first derived theoretically by Mie (1908). This theory has been generalized and applied to transparent and

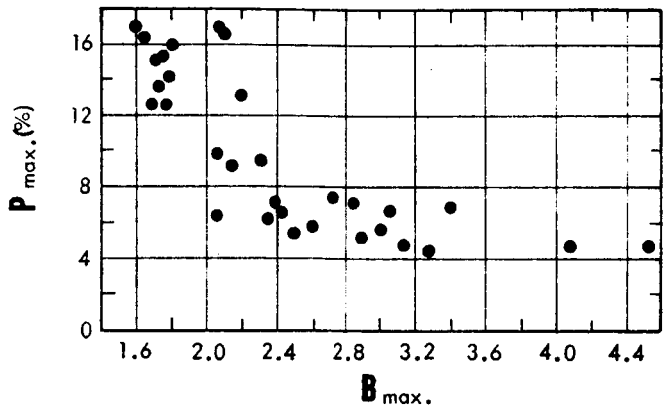

Figure 43

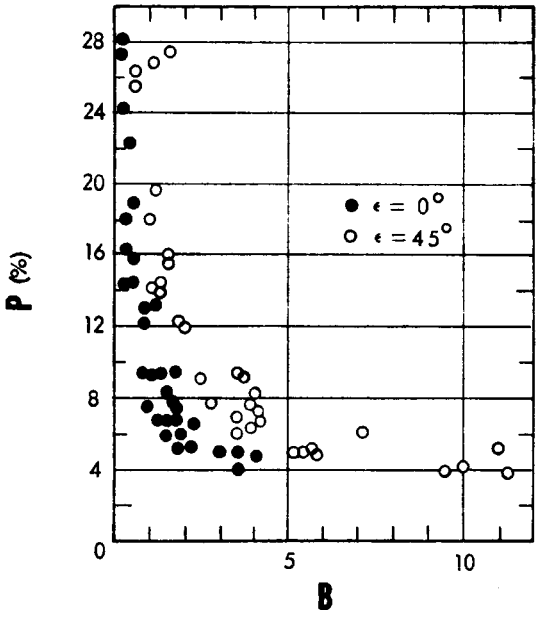

Figure 44

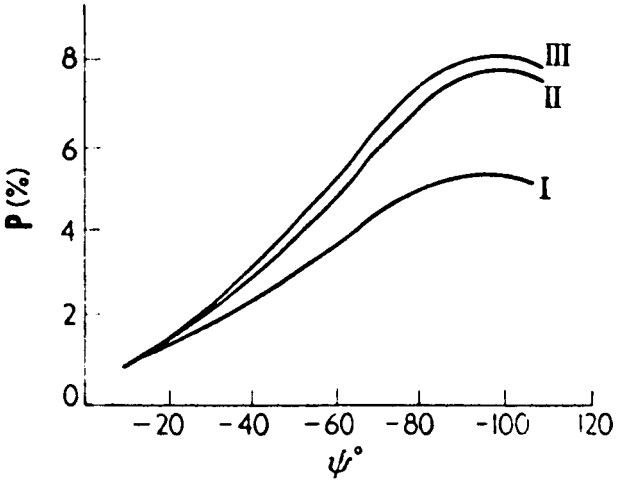

I. $\alpha < 0\text{-}25$ mm
II. $0\text{-}25\ \text{mm} < \alpha < 1\ \text{mm}$
III. $1\ \text{mm} < \alpha < 3\ \text{mm}$

Figure 45

opaque particles by Schirman (1919), Born (1933), van de Hulst (1946, 1949) and others. These considerations apply only to a single particle and take no account of multiple scattering however.

XV. PROBABLE SMALL SCALE LUNAR SURFACE CONDITIONS

From an analysis of the foregoing experimental and theoretical data one is able to draw certain conclusions based on this information with regard to probable lunar surface conditions:

(A) Analysis of experimental photometric information enables one to conclude that:
  (1) The entire lunar surface has a similar microrelief.
  (2) The microrelief of the lunar surface must be very porous and interconnected since any other topology would give a greatly different photometric function from that observed.

(B) From an analysis of the intrinsic albedo differences and colorimetric differences, one can conclude that the lunar surface is covered with a similar material over all regions with only slight local differences in composition.

(C) From the theoretical analysis of the photometric functions one finds that:
  (1) The individual scattering grains must be very irregular in shape, otherwise there would not be sufficiently large back-scatter to account for the experimental photometric functions.
  (2) Complex shadow casting is required to obtain the very sharp maximum in the photometric function at zero phase angle, as well as low surface reflectivity.
  (3) The covering layer must consist largely of a void with only about 25% of the volume occupied with scattering particles.
  (4) A lower limit of 1 micron (1/1000mm) on the particle size is necessitated by the requirement of sharp shadowing. (This criterion is based upon the assumption that a particle about 2 wave lengths across will have neglible diffraction effects).

(D) From an analysis of the polarimetric experimental information one can conclude that:
  (1) The scattering particles must be nearly opaque in order to obtain not too little (+) polarization.

(2) The surface layer must be very irregular in order that the (+) polarization peaks do not occur at the specular reflection condition (i.e., $I = \epsilon$).
(3) Agglomeration sizes of the order of tenths of a millimeter are required to obtain the correct negative polarization versus phase angle behavior.

To indicate the somewhat controversial nature of the subject as to just exactly of what the lunar surface is composed, we shall quote a statement by Kohan (1962) made recently (December 1960) at the International Astronomical Union Symposium, Leningrad. He said, "The School of Planetary Investigators at the Leningrad State University (Orlova, Sytinskaya, and Sharanov) assumes that the porous, vesicular substance resembles in structure a volcanic slag. It originated from basic rocks as a result of a transformation under the effect of explosions accompanying the impact of meteorites striking the surface of the moon. The Kharkov School of Planetary Investigators (Barabashev) considers, on the other hand, that the surface of the moon is not similar to a fused one but that it is most probably covered by finely crushed tuff rocks with grains of the order of several millimeters, and in some places large grain volcanic ashes."

At a recent Lunar Surface Materials Conference in Boston sponsored by Air Force Cambridgy Research Laboratories and Arthur D. Little, Inc., Hapke discussed his "fairy castle" structure surface. He emphasized that lunar photometric properties can furnish information concerning only the top millimeter or so of the lunar surface. Hapke stated also that finely divided powders appear to be capable of "maintaining" themselves to considerable depths on the moon.

The controversial question of how "deep" the dust layer of T. Gold is may be summarized at this time by saying that the consensus at the Boston conference was that it may be moderately (a few meters) deep at local depressions but even this is still largely conjecture.

Recent ultra-high vacuum (10^{-10}mm Hg) experiments at Arthur D. Little, Inc., indicate there are strong adhesive forces between fine silicate particles, which makes plausible that Hapke's "fairy castle structures" may be a reality on the moon, where radiation "cleaning" may provide ultra-clean contact surfaces.

XVL. APPENDIX A - PHOTOMETRIC MODELS OF OPTICALLY ROUGH SURFACES

1. Surface Scattering Function

Each element of area of an emitting or reflecting surface is completely characterized photometrically by the surface emission or scattering function $I(i,\epsilon,g)$ (see Figure 1). This function gives the amount of light energy leaving the surface per unit time, per unit area, per unit solid angle; where i is the angle of incidence of the radiation which excites the surface, ϵ is the angle of emergence of the outgoing radiation and g is the angle between the i and ϵ directions or the so-called phase-angle. If the surface element is not externally excited, but, say, is incandescent, of course, this function is a function only of the emergence angle ϵ and becomes $I(\epsilon)$. Let us consider two classical radiation laws:

2. Lambert Emission Law

Lambert's law of emission is based upon the experimental observation that most incandescent objects appear uniformly bright. Referring to Figure 2 one can formulate this statement quantitatively.

Suppose one views an incandescent surface at normal emergence (Case I) and at emergence angle ϵ (Case II) by means of a detector with an angular aperture $d\omega$, and an aperture of area da, which at the source distance subtends a solid angle $d\Omega = \frac{da}{R^2}$

The light flux in Case I is seen to be $F_I = I(0) \cdot d\Omega\, R^2 d\omega$, where $R^2 d\omega$ is the area of the surface viewed by the detector. The light flux in Case II is given by $F_{II} = I(\epsilon)\, d\Omega\, (\frac{R^2 d\omega}{\cos\epsilon})$, where now the detector views a surface area $(\frac{R^2 d\omega}{\cos\epsilon})$ because $d\omega$ is the same in the two cases. Since $F_I = F_{II}$ experimentally, we see that $I(\epsilon) = I(0) \cos\epsilon$, which is, of course, Lambert's Law of emission.

3. Lambert Reflection Law

Let us now consider a surface which, instead of being incandescent, is a "diffuse" reflector (i.e., re-radiates in accordance with Lambert's Law). If an incident parallel light beam of flux density $\mathcal{F}$ (energy/area/sec) makes an angle i with the normal to a surface element of the reflecting surface, then each unit of surface area receives a light flux of

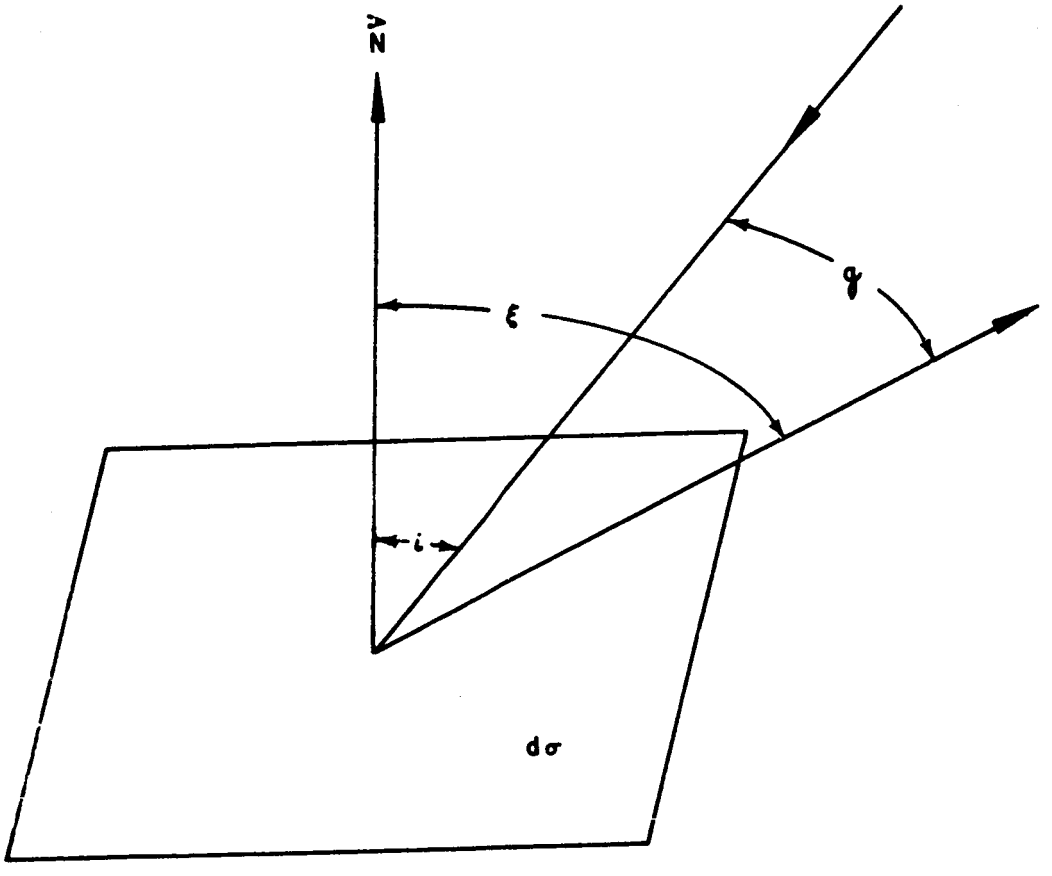

Figure 1

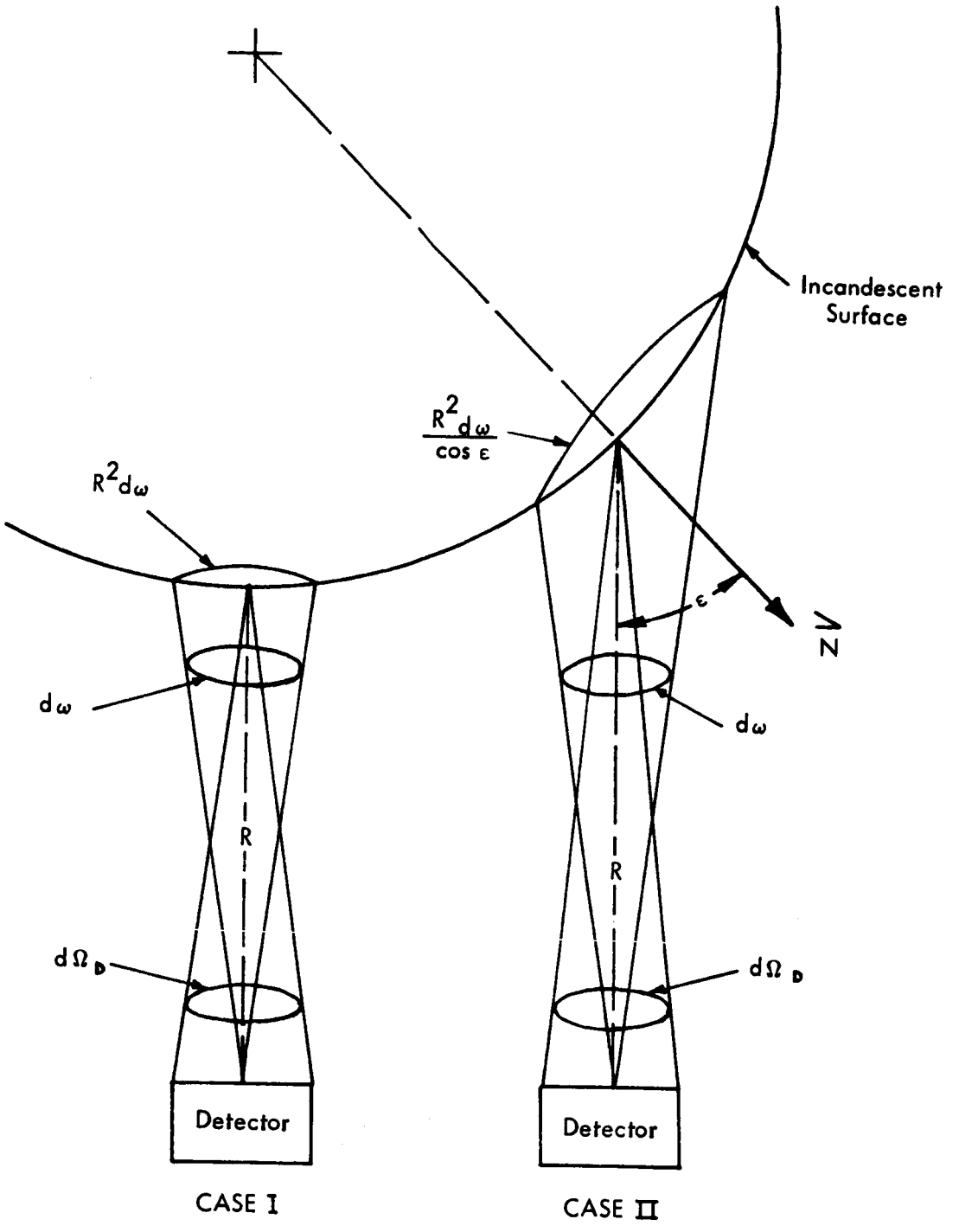
Incandescent Surface
$\frac{R^2 d\omega}{\cos \varepsilon}$
$R^2 d\omega$
ε
N
$d\omega$
$d\omega$
R
R
$d\Omega_D$
$d\Omega_D$
Detector
Detector
CASE I
CASE II

Figure 2

$\mathcal{F}\cos i$. Let us define $r\, S(\epsilon)d\Omega$ as being the fraction of the flux incident per unit area which is re-radiated in direction ϵ into a solid angle $d\Omega$, where $S(\epsilon)$ is normalized such that $\iint_{2\pi} S(\epsilon)d\Omega = 1$.

The quantity r is dimensionless and represents the ratio of the incident energy to that which is re-radiated from a surface element into 2π solid angle. We note that here the quantity $\mathcal{F}\cos i \cdot r\, S(\epsilon)$ is analogous to $I(\epsilon)$, hence we can write down the light flux received by the detector. It is

$$F_D = \mathcal{F}\cos i\ r\ S(\epsilon)\ d\Omega\ \frac{R^2 d\omega}{\cos\epsilon} = \mathcal{F}\cos i\ r\ S(\epsilon)\ da\frac{d\omega}{\cos\epsilon}$$

and since we have a Lambert surface $S(\epsilon) = \frac{\cos\epsilon}{\pi}$ so that

$$F_D = \frac{\mathcal{F}r}{\pi}\cos i\ \cos\epsilon\ da\frac{d\omega}{\cos\epsilon} = \mathcal{F}r\ da\ d\omega\frac{\cos i}{\pi}\ .$$

F_D describes the flux scattered from a Lambert surface, which is seen to be characterized by a surface scattering function of the type $I(i,\epsilon) = I_o \cos\epsilon \cos i$. It is clearly seen that the signal at the detector will be maximum with $i = 0$, so, for example, a sphere would have its brightest region directly beneath the beam and it would be limb-dark, hence the lunar surface could not be described as a Lambert Surface, as it sometimes is erroneously.

4. Schoenberg-Lommel-Seeliger Law

Let us calculate the light flux into a detector, with a viewing aperture of $d\omega$, due to a light flux $\mathcal{F}$ incident upon an apparent surface S. It is assumed the scattering body is composed of a loose aggregate of small particles, of geometrical cross-section σ and number density n, each of which may be characterized by a differential scattering cross-section $\sigma f(g)$ such that $\mathcal{F}\rho\sigma f(g)d\Omega$ is the light flux removed from the beam by a single particle and scattered into solid angle $d\Omega$ at an angle g relative to the beam direction. Here ρ is the reflectivity of a particle (i.e., the ratio of the energy incident upon a particle to that scattered into 4π solid angle) and $f(g)$ is normalized such that $\iint_{4\pi} f(g)d\Omega = 1$.

It is further assumed that multiple scattering and shading of one particle by another can be ignored with the consequence that after a light beam has traveled a distance ℓ it is attenuated in accordance with the well-known law $e^{-(\ell/L)}$, where L is the mean free-path for scattering and is equal to $\frac{1}{n\sigma}$ in this case.

Referring to Figure 3 we can write down the light flux arriving at the detector from a volume element dV at a distance x below the apparent surface. In the volume element dV there are n dV particles (n being the number density of particles) so that a light flux $dF_D = \mathcal{F}\rho n\sigma dV\, f(g)\, d\Omega$ would be received if no attenuation took place. Accounting for entrance and exit attenuation yields the expression

$$dF_D = \mathcal{F}\rho n\sigma\, dV\, f(g)\, d\Omega \cdot e^{-\frac{x}{L\cos i}} \cdot e^{-\frac{x}{L\cos\varepsilon}}$$

$$= \mathcal{F}\rho n\sigma\, dV\, f(g)\, d\Omega \cdot e^{-\frac{x}{L}\frac{\cos i + \cos\varepsilon}{\cos i \cdot \cos\varepsilon}} .$$

Let us now assume that the detector acceptance cone is sufficiently small and R is sufficiently great so that within the body it may be taken as a cylinder with cross-section $R^2 d\omega$, hence $dV \sim R^2 d\omega dq$.

Using the fact that $d\Omega = \frac{da}{R^2}$ and $q = \frac{x}{\cos\varepsilon}$, we can write

$$dF_D = \mathcal{F}\rho n\sigma\, f(g)\, d\omega\, da\, dq\, e^{-\frac{q}{L}\frac{(\cos i + \cos\varepsilon)}{\cos i}}$$

By integrating this expression for all values of q from q = 0 to some large value (and ignoring the slightly improper boundary condition at q = 0) we obtain the total flux

$$F_D = \mathcal{F}\rho f(g)\, d\omega\, da\, n\sigma \cdot \int_0^\infty e^{-q\, n\sigma \frac{(\cos i + \cos\varepsilon)}{\cos i}}\, dq =$$

$$\boxed{F_D = \mathcal{F}\rho f(g)\, d\omega da \frac{\cos i}{\cos i + \cos\varepsilon}}$$

We call this the Schoenberg-Lommel-Seeliger Law (Schoenberg, 1929) because of the presence of the function f(g). In the Lommel-Seeliger Law, it is assumed that the particles scatter isotropically; hence,

$f(g) = \text{const.} = \frac{1}{4\pi}$ because $\iint_{4\pi} f(g)\, d\Omega = 1$.

The expression for the Lommel-Seeliger Law then becomes

$$\boxed{F = \frac{\mathcal{F}\rho\, d\omega da}{4\pi} \cdot \frac{\cos i}{\cos i + \cos\varepsilon}}$$

SCHOENBERG-LOMMEL-SEELIGER LAW

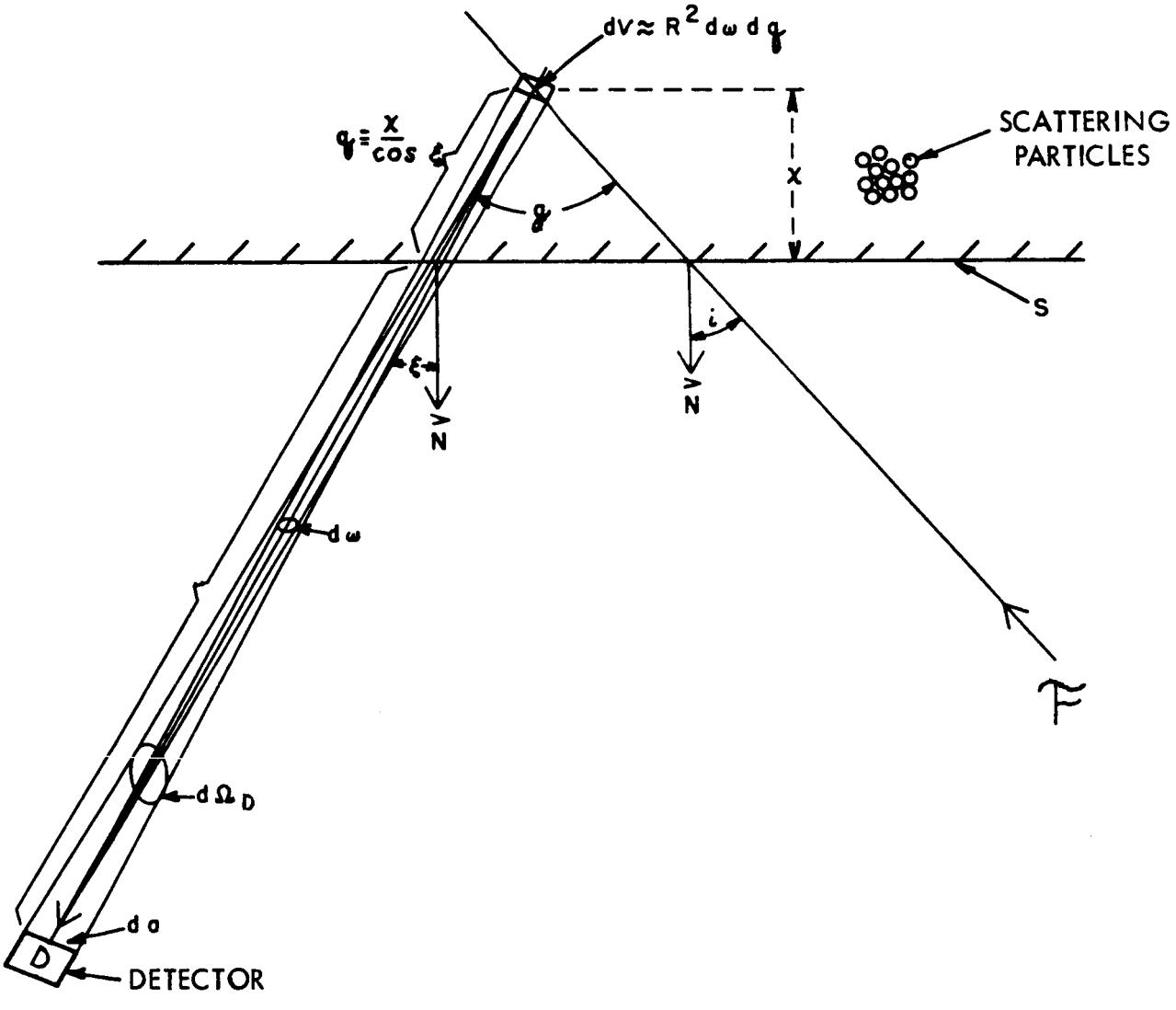

Figure 3

Note that when $i = \varepsilon$, $F_D = \frac{\mathcal{F} \rho \, d\omega da}{8\pi}$ which is independent of incident and emergence angles, so that for this viewing angle a sphere would appear uniformly bright if its surface obeyed the Lommel-Seeliger Law.

5. Surface Brightness - Photometric Function

A useful quantity called the surface brightness is defined to be the light flux received from a surface by a detector. F_D, divided by the area, da, that it presents perpendicularly to the incident direction and divided by its solid angle of view, $d\omega$. Using present nomenclature it is

$$B(i,\varepsilon,g) = \frac{F\ (i,\varepsilon,g)}{da\,d\omega}$$

The brightness of a "perfectly diffuse" reflector or "ideal white screen" surface (i.e., a Lambert surface with r = 1) is seen to be $B(i) = \frac{\mathcal{F}}{\pi} \cos i$, so that for normal incidence, one has for the "normal brightness" $B = \frac{\mathcal{F}}{\pi}$.

In general it is conventional to express the surface brightness as $B(i,\varepsilon,g) = \frac{\mathcal{F}}{\pi} a\Phi(i,\varepsilon,g)$ where a is called the albedo of the surface and Φ is called the photometric function and is ordinarily normalized to unity at its maximum value. In lunar photometry, $\mathcal{F}$ is just the solar constant E_S (about 0.14 watts/cm^2).

The normalized photometric functions for Lambert's Law and the Lommel-Seeliger Law are seen to $\Phi_L(i) = \cos i$ and $\Phi_{L\text{-}S}(i,\varepsilon) = \frac{2\cos i}{\cos i + \cos\varepsilon}$ which are compared in Figure 4 for a normal emergence angle ($\varepsilon = 0°$) with experimental photometric data obtained from a magnesium-oxide screen.

6. The Principle of Reciprocity

The requirements of the principle of reciprocity, first formulated by Helmholtz, have been emphasized with regard to photometry by Minnaert (1941). Applied to homogeneous surfaces it requires that the surface scattering function $I(i,\varepsilon,g)$ be symmetric under the interchange of the angles i and ε i.e., $I(i,\varepsilon,g) = I(\varepsilon,i,g)$. This requirement should always be kept in mind when considering the various proposed theoretical and empirical photometric functions. Very often they have failed to satisfy this requirement.

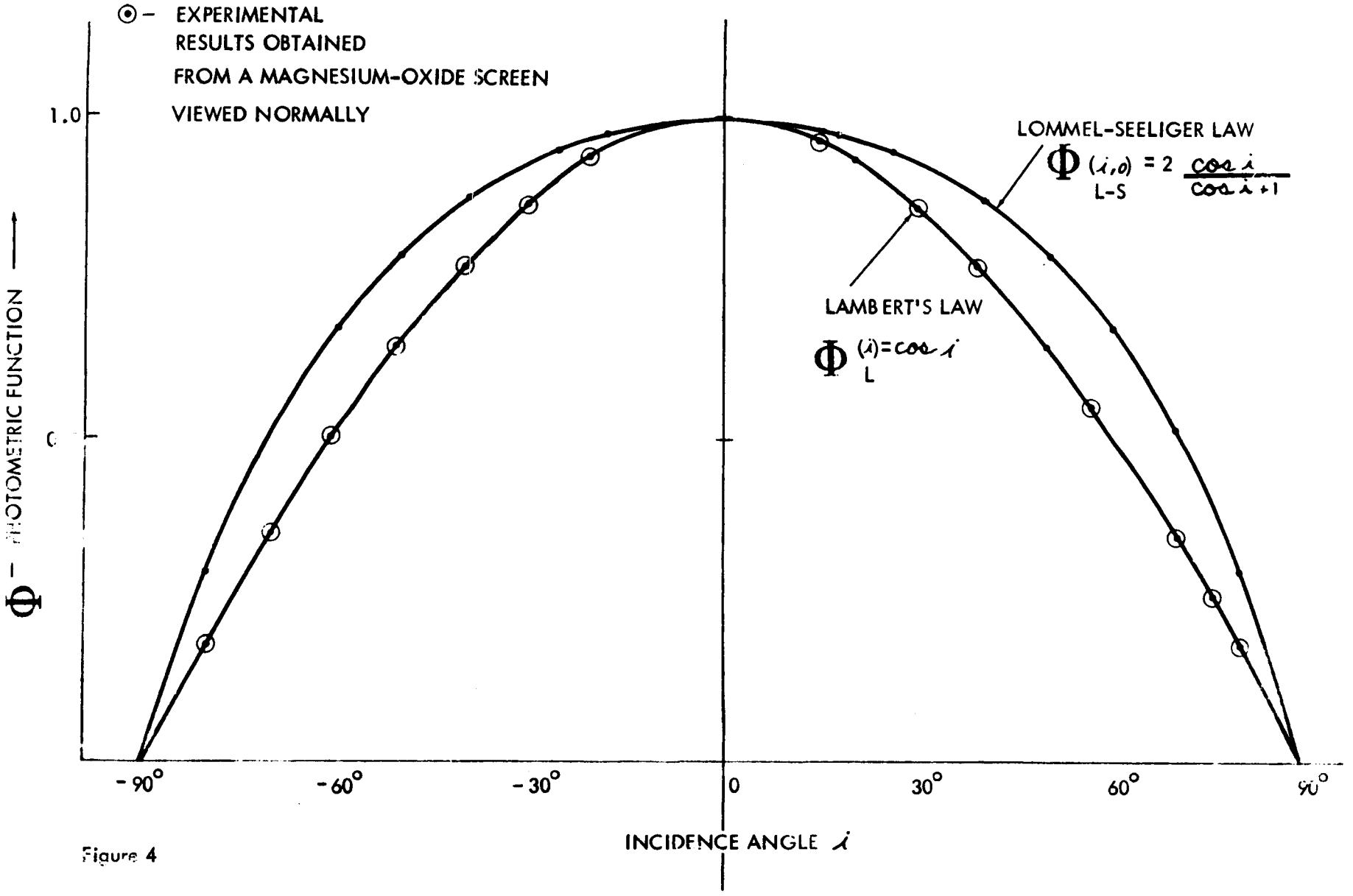
⊙ – EXPERIMENTAL RESULTS OBTAINED FROM A MAGNESIUM-OXIDE SCREEN VIEWED NORMALLY
1.0
0
Φ – PHOTOMETRIC FUNCTION
LOMMEL-SEELIGER LAW
$\Phi_{L\text{-}S}(i,0) = 2\frac{\cos i}{\cos i + 1}$
LAMBERT'S LAW
$\Phi_{L}(i) = \cos i$
-90°
-60°
-30°
0
30°
60°
90°
INCIDENCE ANGLE i

Figure 4

XVII. APPENDIX B - COLOR INDEXES AND EFFECTIVE TEMPERATURES

The stars are known to radiate to a first approximation as a black body. Radiation from an ideal black body is determined by the well known Planck law:

$$E\nu = \frac{8\pi h}{c^3} \frac{\nu^3}{\frac{h\nu}{(e^{kT} - 1)}}$$

in which ν is the frequency of radiation, c is the velocity of light, h is the Planck constant, k is the Boltzmann constant, T is the absolute temperature of the radiator, $E\nu$ is the energy radiated per unit time, per unit area, per unit frequency interval. This distribution curve is shown in Figure 5, in which the ordinate is $\log_{10} E\nu$ and the abscissa ν, the frequency and the corresponding wave length λ in angstroms, Å.

The color index of a star is defined (Johnson & Morgan, 1953) to be the difference between its astronomical magnitudes as observed in two different narrow spectral regions. The narrow regions are usually chosen to be the blue (centered on ~4480Å) and the yellow (centered on~5540Å).

In general the differences of two astronomical magnitudes is given by $\Delta m_{12} = m_1 - m_2 = -2.5 \log_{10} \frac{I_1}{I_2}$

where m_i is the magnitude and I_i is the surface intensity of radiation. From the definition of Color Index (C) of a star we may write

$$C = -2.5 \log_{10} \frac{I\ (\text{blue})}{I\ (\text{yellow})}$$

From an examination of Figure 5 it is evident that $\frac{I\ (\text{blue})}{I\ (\text{yellow})} > 1, = 1, < 1$ for the blue stars ($T > 11{,}000°K$), a "normal" star ($T = 11{,}000°K$), and red stars ($T < 11{,}000°K$) respectively.

It is seen from the expression for $C < 0$ (i.e. -) for blue stars, $C = 0$ for "normal" stars and $C > 0$ (i.e. +) for red stars.

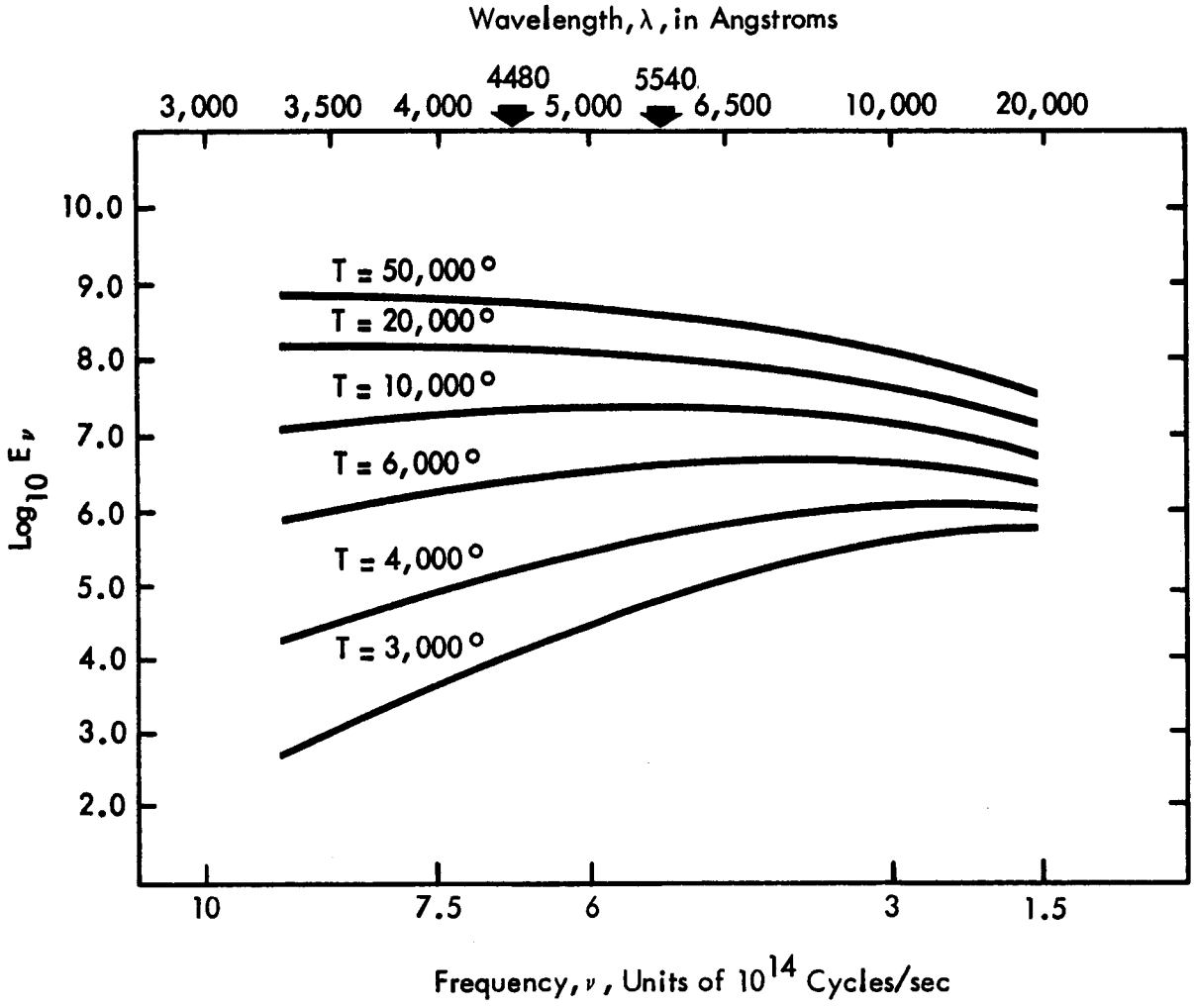

Fig. 5 Black-body curves for various temperatures as a function of frequency and wave length.

REFERENCES

Barabashev, N.P. (1922) Astr. Nachr. 217, 445.

Barabashev, N.P. (1927) Astr. Nachr. 229, 7.

Barabashev, N.P. (1945) Russ. Astro. Jour. 22, 11.

Bennet, A.L. (1938) Astro. Jour. 88, 1.

Bond, W.C. (1861) Mem. Amer. Acad. Arts Sci., NS. 8.

Born, M. (1933) Optik (Berlin; J. Springer).

Byrne, C.J. (1963) Bellcomm Report "Lunar Photographic Orbiter: Lighting and Viewing Conditions" TM6311121.

Cudabock, D.D. (1962) Stanford Electronics Laboratory Report #62-105, Stanford University.

Diggelen, Van, J. (1959) Recherches Astronomiques de l'Observatoire d'Utrecht 14, No. 2.

Dollfus, A. (1955) Ann. Astrophys. 18 (Supplement).

Dollfus, A. (1956) Ann. Astrophys. 19, 71.

Dollfus, A. (1961a) page 352, Planets and Satellites, Vol. III of The Solar System, edited by Gerald P. Kuiper and Barbara M. Middlehurst, The University of Chicago Press, 1962.

Dollfus, A. (1961b) page 356, Planets and Satellites, Vol. III of The Solar System, edited by Gerald P. Kuiper and Barbara M. Middlehurst, The University of Chicago Press, 1962.

Dollfus, A. (1962a) page 132, Physics and Astronomy of the Moon, edited by Zdenek Kapal, Academic Press, 1962.

Dollfus, A. (1962b) page 144, Physics and Astronomy of the Moon, edited by Zdenek Kapal, Academic Press, 1962.

Fedorets, V.A. (1952) Pub. Karkov Obs., Vol. II and Vch. Zap. Karkov Univ. 42, 49.

Fessenkov, V.G. (1926) Astro. Jour. USSR 3, 75.

Hapke, B.W. (1963) Center for Radiophysics and Space Research Publication #138.

Hapke, B.W. and Van Horn, H. (1962) Center for Radiophysics and Space Research Publication #127.

Herschel, F.J.W. (1947) "Results of Astronomical Observations Made at the Cape of Good Hope," London.

Herriman, A.G., Washburn, H.W., and Willingham, D.E. (1963) Jet Propulsion Laboratory Report No. 32-384 (Rev.), Calif. Inst. of Technology.

Hulst, Van de, H. (1946) Rech. Astr. Obs., Utrecht 11, Part 1.

Hulst, Van de, H. (1949) Ibid 11, Part 2.

Johnson, H.L. and Morgan, W.W. (1953) Astro. Jour. 117, 313.

Kohan, E.K. (1962) page 453 "The Moon," Report on Symposium #14 of the International Astronomical Union held at Pulkovo Observatory, December 1960, Academic Press, 1962.

Lyot, B. (1924) Compte Rendus Acad. Sci., Paris, 179, 1796.

Lyot, B. (1929) Ann. Obs. Paris, 8, Fasc. 1.

Markov, A.V. (1924) Astr. Nachr. 221, 65.

Markov, A.V. and Barabashev, N.P. (1926) Astr. Jour., USSR 3, 55.

Markov, A.V. (1948) Astr. Jour., USSR 25, 172.

Mie, G. (1908) Ann. d. Phys. (4) 25, 377.

Minnaert, M. (1941) Astr. Jour. 93, 403.

Minnaert, M. (1961) page 235, Planets and Satellites, Vol. III of The Solar System, edited by Gerald P. Kuiper and Barbara M. Middlehurst, The University of Chicago Press, 1962.

Ohman, V. (1955) Stockholm Obs. Am., 18, No. 8.

Opik, E. (1924) Pub. Astr. Obs. Tartu 26, No. 1.

Orlova, N.S. (1955) Astr. Tsirk. Akad. Nauk. USSR, No. 156, p. 19.

Orlova, N.S. Astr. Jour. USSR, 33, 93.

Rougier, M.G. (1933) Ann. Obs. Strasbourg 2, 205.

Russel, H.N. (1916) Astr. Jour. 43, 103.

Salomonovich, A.E. (1962) page 491, "The Moon," Report on Symposium #14 of the International Astronomical Union held at Pulkovo Observatory, December 1960, Academic Press, 1962.

Secchi, A. (1862) "La Luna," Rome.

Schoenberg, E. (1925) Acta Soc. Sc. Fannicae, 50, No. 9.

Schoenberg, E. (1929) page 136, Handbuch der Astrophysik 2, Vol. I.

Sharonov, V.V. (1962) page 385 of "The Moon," Report on Symposium #14 of the International Astronomical Union held at Pulkovo Observatory, December 1960, Academic Press, 1962.

Shirman, M.A. (1919) Ann. Astrophysik (4) 59, 493.

Sytinskaya, N. and Sharonov, V.V. (1952) Utch. Zap. Univ. Leningrad No. 153.

Sytinskaya, N. (1953) Astr. Jour. USSR, 30, 295.

Troitski, V.S. (1962) page 475, "The Moon," Report on Symposium #14 of the International Astronomical Union held at Pulkovo Observatory, December 1960, Academic Press, 1962.

Tschunko, H.F.A. (1949) Z. Astrophys. 26, 279.

Wisliscenus (1895) reported in Wirtz, C. (1915) Astr. Nachr. 201, 289.

Wright, F.E. (1929) Publ. Astr. Soc. Pacif. 41, 125.